6.0 SEISMIC HAZARD ANALYSIS

6.1 Introduction

Following the methodology of the DCPP Long Term Seismic Program, the seismic hazard is evaluated using both deterministic seismic hazard analysis (DSHA) and probabilistic seismic hazard analysis (PSHA) approaches.

It is important to keep in mind that the source characterizations in Section 5 and the analysis of logic trees to produce seismic hazard results in Section 6 involve using the elements of the source characterizations and logic trees in a mathematical model. The elements of the model are simplified representations of more complex faults or fault zones identified in the DCPP vicinity based on geological, geophysical, and seismological measurements and observations. In Section 5 and continuing in this section, the terminology that is used distinguishes the modeled elements as "fault sources" and the real-Earth features as "fault zones". For example, the Shoreline fault source is the model representation for the Shoreline fault zone, and the San Luis Bay East segment source is the model for the San Luis Bay East fault segment. The mathematical models are simplifications of the real world.

The source characterization described in Section 5 provides descriptions of the alternative geometries, senses of slip, and slip rates of the main fault sources in the DCPP region. Additional source characterization parameters are required for the DHSA and PSHA: the mean characteristic magnitude and the magnitude probability density function. These additional parameters are described in Sections 6.3 and 6.4.

The logic trees in Section 5 include several correlations between the four main fault sources: Shoreline, San Luis Bay, Los Osos, and Hosgri. As a result of these correlations, the full logic tree becomes very large and a simplification is needed for application to the DSHA and PSHA. The simplifications made to the logic trees are described in Section 6.2

The DCPP site conditions are described in Section 6.5 and ground motion models are described in Section 6.6. The results of the DSHA and PSHA are described in Sections 6.7 and 6.8, respectively.

6.2 Simplified Logic Trees

As described in the Section 5, the logic trees for the Shoreline and San Luis Bay fault sources are correlated through the "linked" branch (branch 12 on Figure 5-3). There are additional correlations between the other fault sources. The logic trees for the San Luis Bay and Los Osos fault sources are correlated because the San Luis Bay fault source is truncated at depth by the intersection with the Los Osos fault source (note 3 on Figure 5-5). The depth at which the Los Osos and San Luis Bay fault sources intersect depends on the depths and dips of the two fault sources. The logic trees for the Shoreline and San Luis Bay fault sources are also correlated to the logic tree for the Hosgri fault source because the San Luis Bay West segment source and Shoreline North segment source are truncated at depth by the intersection with the Hosgri fault source (note 3 on Figure 5-11 and note 2 on Figure 5-3). These truncations depend on depth to the bottom of the fault source and the dips of the three fault sources. Using the logic trees as described in Section 5 leads to over 60,000,000 alternative for the rupture geometries and slip rates of the Shoreline fault source. To reduce the logic tree for the Shoreline fault source to a manageable size, simplifications to the logic trees for the Los Osos, San Luis Bay, and Shoreline fault sources are made. The simplifications are described below.

6.2.1 Shoreline Fault Source

In the Shoreline fault source logic tree, the northern end of the North segment is truncated by the Hosgri fault source (Note 2 on Figure 5-3). This truncation is ignored and the Shoreline fault North segment source is allowed to cross the Hosgri fault source. The amount of overlap is small and will have a negligible effect on the fault source area and hazard.

For the linked case, the rupture from the Shoreline Central segment source onto the San Luis Bay East segment source has three alternative end points for the east end (Note 4, Figure 5-6). A single model in which the full length of the East segment source is used replaces these three alternatives.

For the linked case, the slip rate of the South segment source is reduced by the slip rate of the San Luis Bay East segment source (Note 8, Figure 5-6). This adds additional correlation between the San Luis Bay and Shoreline logic trees. As a simplification, a mean slip rate of 0.18 mm/yr for the San Luis Bay East segment source is removed from the South segment (linked branch only) with the constraint that the slip rate on the South segment is not less than 0.05 mm/yr.

6.2.2. San Luis Bay Fault Source

In the linked model for the Shoreline and San Luis Bay fault source logic tree (Figure 5-5), the western end of the San Luis Bay West segment source is truncated by the Hosgri fault source (Note 2 on Figure 5-5). This truncation is ignored, and the San Luis Bay West segment source is modeled as crossing the Hosgri fault source. The amount of overlap is small and will have a negligible effect on the fault source area and hazard.

In the linked model, the San Luis Bay East segment source has two alternative dips (80 and 85 degrees), is truncated by the Los Osos fault source, and has three alternative senses of slip. For linked ruptures that include the San Luis Bay East and the Shoreline Central segment sources, three simplifications are made to the logic tree. First, the dip of the San Luis Bay East segment source is modeled as 90 degrees (consistent with dip of the Shoreline fault source). The difference in the down dip fault source width for a dip of 80 degrees as compared to a dip of 90 degrees is less than 1.5 percent. Second, the truncation of the San Luis Bay East segment source by the Los Osos fault source is ignored. The logic tree models the Shoreline Central segment source as crossing the Los Osos fault source, so this simplification leads to a consistent model for the linked ruptures. Third, the sense of slip for the linked fault sources is modeled as strike-slip. The linked rupture has a mixture of strike slip on the Shoreline Central segment and reverse, reverse-oblique, or strike slip on the San Luis Bay East segment source. The ground motion models require a single sense of slip for an individual earthquake. Given that the Shoreline Central segment source is closest to the DCPP and has a weight of 1.0 for strike-slip faulting, the strike-slip sense of slip is applied to all linked ruptures, because the ground motions are most influenced by the closest portion of the rupture to the site.

In the linked model, there are also separate ruptures of the San Luis Bay East segment source by itself. For these single-segment-source ruptures, the logic tree is simplified to use a single dip of

83 degrees in place of the two values of 80 and 85 degrees. The truncation of the San Luis Bay East segment source by the Los Osos fault source is included, but the correlation with the dip of the Los Osos fault is not modeled. As this segment source has a small contribution to the hazard, ignoring the correlation will not have a significant effect on the fractiles (epistemic uncertainty) of the hazard.

6.2.3 Los Osos Fault Source

The Los Osos logic tree includes alternative for the east end of the fault (branch 1 on Figure 5-10). In the simplified model, the longer fault length (57 km) is used with a weight of 1.0. This simplification leads to a slightly larger fault source, but because the rupture lengths are fixed in branch (Figure 5-10) at 19 km and 36 km, this simplification has no effect on the deterministic analysis and only a small increase in the hazard for the probabilistic analysis.

6.2.4 Simplified Logic Tree for the Shoreline Fault Source

With the simplifications noted above, the total number of alternative models for the rupture geometries and slip rates of the Shoreline fault source is reduced to about 500,000. The simplified parts of the logic trees for the Shoreline fault source are shown on Figures 6-1 and 6-2.
The coordinates of the top edges of the fault segment sources are listed in Table 6-1a. The geometry of the San Luis Bay West segment source is more complicated due to the truncation by the Shoreline fault source. For simplicity, the west end of the intersection with the Shoreline fault was fixed at Shoreline fault coordinate S2 (Figure 5-1). The coordinates used for alternative models of the San Luis Bay West segment source are listed in Table 6-1b.

The depth of intersections of the San Luis Bay Fault source with the Los Osos Fault source are listed in Table 6-2a for the not-linked branch and in Table 6-2b for the linked branch.

6.3 Mean Characteristic Magnitude Models

For fault sources, the mean characteristic magnitude is estimated using the Wells and Coppersmith (1994) (WC) and Hanks and Bakun (2008) (HB) models. These models are listed in Table 6-3.

For the Hosgri and Shoreline fault sources, which are strike-slip, the HB model and HC strike-slip (SS) model are used with weights of 0.7 (HB) and 0.3 (WC). The HB model is preferred because it does a better job of capturing the magnitude-area scaling for large strike-slip earthquakes in California (Hanks and Bakun, 2008). For the Los Osos and San Luis Bay fault sources, which are reverse (RV) and reverse-oblique (RV/OBL), the Wells and Coppersmith "All Fault Type" (ALL) model is used with a weight of 1.0.

The epistemic uncertainty in the mean magnitude is estimated from the standard error of the estimated coefficients given by Wells and Coppersmith (1994) and shown in Table 6-3. For strike-slip earthquakes, the standard error of 0.07 is used. For the reverse and reverse-oblique earthquakes, the average of the standard errors of the ALL model and the RV model is used (0.09). These standard errors are estimates of the epistemic uncertainty of the constant term for a single model. Because two strike-slip models are used, the standard error of 0.07 for strike-slip earthquakes is reduced by 1/SQRT(2), leading to a standard error of the mean of 0.05.

For the logic tree, a three-point distribution is used with values of $-1.6\ \sigma$, $0\ \sigma$, and $1.6\ \sigma$ with weights of 0.2, 0.6, and 0.2, respectively, where σ is the standard error of the mean. For strike-slip earthquakes, this corresponds to ±0.08 magnitude units. For reverse and reverse-oblique earthquakes, this corresponds to ±0.15 magnitude units.

6.4 Magnitude Probability Density Function

The two main classes of magnitude probability density functions (pdfs) used in probabilistic seismic hazard analyses (PSHAs) are truncated exponential models and characteristic earthquake models. There are several different forms of the characteristic earthquake model, but the main feature is that the characteristic model has a higher pdf near the characteristic magnitude than the exponential model. The truncated exponential model has long been known to work well for large regions, but for individual faults, the characteristic model is preferred in most PSHA applications.

The primary reason usually given for using the characteristic model is that the truncated exponential model greatly overpredicts (by about a factor of 5) the rate of small earthquakes that occur along a fault if the maximum magnitude is determined following standard practice (e.g. based on the area of the fault) and the activity rate of a fault is typically estimated by balancing the accumulation and release of seismic moment (e.g. Geomatrix, 1993). This conclusion depends on the horizontal width of the zone around the fault that is used to determine which earthquakes occur on the fault. If wide zones (e.g. ±20 km) around the fault are included, then the fault zones become regions and the exponential distribution is applicable.

The overprediction of small magnitude earthquakes by the exponential model can be avoided by increasing the maximum magnitude about 1.5 units above the mean magnitude computed from magnitude-area scaling relations. To test the exponential model with the large maximum magnitude model, the observed distribution surface slip at a point from multiple earthquakes can be used. Hecker et al. (2010) compiled a set of paleoseismic observations of slip at sites with more than one earthquake and found that the coefficient of variation (CV) is about 0.4.

Using the Wells and Coppersmith (1994) model for average displacement with a uniform distribution of magnitudes (M 6–8) and including the effects of variability of slip along strike, the CV for the exponential model with large maximum magnitudes is about 1.0 which is much larger than the observed CV of 0.4, indicating that the exponential distribution can be rejected for use for individual faults. Some form of characteristic model should be used for individual faults.

In this report, the composite model (mixture of characteristic earthquakes with an exponential tail at smaller magnitudes) is used for the magnitude pdf for all fault sources. The most commonly used composite model is the Youngs and Coppersmith (1985) model. The form of the Youngs and Coppersmith model is shown on Figure 6-3. The model corresponds to approximately 94 percent of the seismic moment being released in characteristic and 6 percent of the moment being released in the exponential tail. Using this model, the CV for slip at a point is about 0.6, which is still larger than the observed CV of 0.4, but is much closer than the exponential model. Therefore, the composite model is adopted for individual faults.

To address the epistemic uncertainty of the composite model, the fraction of the moment that is released in characteristic earthquakes was varied in a sensitivity study using 90, 94, and 97 percent (Figure 6-3) with weights of 0.2, 0.6, and 0.2, respectively. Changing this parameter mainly affects the rate of earthquakes in the exponential tail of the distribution. The results of the sensitivity study showed that including this epistemic uncertainty changed the mean hazard by about 1 percent and changed the 10th and 90th fractiles by about 3 percent. The effect is small because the hazard at DCPP is dominated by the characteristic earthquakes. Due to the small effect, the epistemic uncertainty in the magnitude pdf is ignored and the Youngs and Coppersmith (1985) model is used with a weight of 1.0.

6.5 Site Condition

The ground motion models described in Section 6.6 use the shear-wave velocity in the top 30 m as the site parameter. This parameter, called V_{S30}, was computed for the DCPP power block using a shear-wave profile measured at the power block location in 1978 (PG&E, 1988). The estimated V_{S30} for the rock under the power block foundation is 1,200 m/s (GEO.DCPP.10.01).

The methods for measuring shear-wave velocity have improved significantly since 1978. New measurements of the shear-wave velocity profile were made at the DCPP ISFSI site as part of the ISFSI site characterization (PG&E, 2004). Because the ISFSI is located on the same geologic unit as the power block, the recent shear-wave velocity measurements for the DCPP ISFSI are used to compute the V_{S30} at the ISFSI location for comparing with the results based on the older shear-wave velocity measurements.

The V_{S30} values are listed in Table 6-4. For the measurements at the ISFSI site, the V_{S30} was measured without the top 10 m to be consistent with the embedment depth of the power block foundation. The V_{S30} values for the ISFSI are very similar to the V_{S30} based on the 1978 data. The estimate of V_{S30}=1200 m/s for the power block foundation remains applicable.

6.6 Ground Motion Prediction Equations

The Next Generation Attenuation (NGA) models represent the current state-of-practice for estimating ground motions from crustal earthquakes in active tectonic regions. The five NGA ground motion prediction equations (GMPEs) for the average horizontal component are used: Abrahamson and Silva, 2008 (AS08); Boore and Atkinson, 2008 (BA08); Campbell and Bozorgnia, 2008 (CB08); Chiou and Youngs, 2008(CY08); and Idriss, 2008 (I08).

Four of the NGA GMPEs use V_{S30} for the site classification parameter. The fifth model, that of Idriss (2008), does not use V_{S30} directly, but rather it is uses two V_{S30} ranges: 450–900 m/s and > 900 m/s. Three of the NGA models include an additional site parameter based on the depth to rock. The AS08 and CY08 models use depth to V_S=1.0 km/sec ($Z_{1.0}$), and the CB08 model uses the depth to V_S=2.5 km/sec ($Z_{2.5}$).

The five GMPE models were given equal weights for the analysis. Recent studies (EPRI, 2006; PG&E 2010c) have shown that there is no statistical basis for truncating the lognormal distribution at less than three standard deviations, but that there must be some upper limit to the ground motion based on physical limits. Therefore, a truncation of the lognormal distribution at 4 standard deviations is applied to all of the GMPEs.

6.6.1 Epistemic Uncertainty

In the past, it has been standard practice to address epistemic uncertainty in ground motion estimation by using a weighted set of applicable models under the assumption that the alternative models were developed somewhat independently, and thus capture the uncertainty in the estimation of ground motions; however, the NGA set of ground motion models were developed as part of a collaborative effort with many interactions and exchange of ideas among the developers. Therefore, the need for additional epistemic uncertainty should be considered when applying the set of NGA models. Although the models are based on the same initial data set, the NGA models differ in the subset of data used and in their functional forms. As a result, there is considerable variability in the ground motion estimates for conditions that are not well represented in the empirical data, such as on the hanging wall of dipping faults, as described in the following subsections.

Variability Among PEER-NGA Models

Youngs (2009) evaluated the differences in the median ground motions given by the NGA models for a range of source/site geometries in terms of the standard deviation of the medians for the four NGA models that use V_{S30} as a site parameter. Youngs (2009) found that, for strike-slip earthquakes, the standard deviation is larger for **M** 5.5 than for **M** 6.5 and **M** 7.5, reflecting both the small number of small magnitude events in the NGA data set and the different modeling of the depth-to-top-of-rupture scaling in the NGA models. Youngs (2009) also found that there tend to be larger standard deviations for reverse faults in the hanging wall region (R_x<20 km) for large-magnitude earthquakes, which reflects the much smaller amount of data in the NGA data set for this condition and the differences between the NGA models in the treatment of ground motions on the hanging wall.

Epistemic Uncertainty in a Single NGA Model

One approach for assessing the level of the additional epistemic uncertainty is to evaluate how well the empirical data constrain the NGA models. The U.S. Geological Survey (Petersen et al., 2008), following initial suggestions by the NGA developers, adopted the simple approach of using the square root of the sample size in specific magnitude and distance bins to define the relative epistemic uncertainty in an individual NGA ground motion model as a function of magnitude and distance; however, this approach ignores the fact that the constraints on model predictions are not based solely on the data in any one magnitude and distance interval.

Youngs (2009) used an alternative approach to estimating the epistemic uncertainty of the median for any one NGA model based on the statistics of the model fit combined with the data distribution to compute standard errors of the median estimates as a function of magnitude and distance. The asymptotic standard errors in the median ground motion were computed using this approach for the Chiou and Youngs (2008) NGA model. For strike-slip earthquakes, the epistemic uncertainty is between 0.1 and 0.18 natural log units. For reverse and normal earthquakes, the epistemic uncertainty at large distance is similar to the epistemic uncertainty for strike-slip earthquakes (0.1 to 0.18), but increases to up to 0.3 at short distances on the hanging wall. As is shown below (Figure 6-4a), this increase in the uncertainty at short distances for dipping faults is covered by the range in the five NGA models.

For this report, a simple model of the additional epistemic uncertainty of the median is developed. The Youngs (2009) model provides the estimates of the epistemic uncertainty of a single model due to data base limitations. The five NGA models provide some or all of this range depending on the magnitude, distance, and style of faulting. For the fault sources important to hazard at DCPP, the median ground motions from each of the five NGA models are computed. The epistemic uncertainty captured by the distribution of the five NGA models is measured by the standard deviation of the median ground. This is epistemic uncertainty is then compared to the Youngs (2009) uncertainty. If the standard deviation of the NGA models is less than the epistemic uncertainty from Youngs (2009), then additional epistemic uncertainty is added. The need for additional epistemic uncertainty was evaluated separately for the four nearby faults sources.

For each fault source, the range of the median ground motions from the five NGA models is evaluated for representative scenario earthquakes. The magnitude of the representative scenario is taken as the median (50th fractile) of the mean characteristic earthquake (see Section 6.7.1) and distance is the taken as the closest distance to the site. The representative scenario earthquakes are M=6.8 for the Hosgri, M=6.5 for the Los Osos, M=6.1 for the San Luis Bay, and M=6.2 for the Shoreline. The standard deviations of the median ground motions for each of the representative scenarios earthquakes are shown on Figure 6-4a. These standard deviations of the medians are compared to the Youngs (2009) minimum epistemic uncertainty in this figure. For sites located on the hanging wall for reverse earthquakes, there is a large range of the median ground motions in the NGA models, whereas, for sites located close to large strike-slip earthquakes, the range of the median ground motions is much smaller.

The additional epistemic uncertainty required to reach the Youngs (2009) standard deviations is shown on Figure 6-4b. The key frequency range for DCPP is in the intermediate frequency range (3–8.5 Hz). In this range, the additional epistemic uncertainty required for the four scenarios separates into two groups: the Shoreline, San Luis Bay, and Los Osos fault sources require a small additional epistemic uncertainty; the Hosgri fault source requires a large additional epistemic uncertainty. For simplicity, smoothed models of the additional epistemic uncertainty were developed for these two groups as shown on Figure 6-4b.

Epistemic Uncertainty Model

The epistemic uncertainty in the median NGA models is modeled using a three-point discrete approximation to a normal distribution. This approach places a weight of 0.6 on the median model and weights of 0.2 on the 5th and 95th percentiles (±1.6 standard deviations). This approach is implemented by developing three alternative models for each NGA relationship: one model equal to the original relationship, and two models with $\pm 1.6\sigma_E$ added to the constant term, each with weight 0.2. A smoothed model of the period dependence of the epistemic factor, F_E, for the Hosgri fault is given in Eq. (6-1):

$$F_E = \begin{cases} 0.20 & for\, T \le 1.0 \\ 0.20 + 0.20\left(\frac{T-1}{4}\right) & for\, 1.0 < T < 5.0 \\ 0.40 & for\, T \ge 5.0 \end{cases} \quad (6\text{-}1)$$

The smoothed model for the period dependence of the epistemic factor for the San Luis Bay, Shoreline, and Los Osos faults is given in Eq. (6-2):

$$F_E = \begin{cases} 0.10 & for\, T \le 1.0 \\ 0.10 + 0.20\left(\frac{T-1}{4}\right) & for\, 1.0 < T < 5.0 \\ 0.30 & for\, T \ge 5.0 \end{cases} \quad (6\text{-}2)$$

The logic tree for the median ground motion is shown on Figure 6-5.

6.6.2 Hard-Rock Site Effects

As described in Section 6.5, the DCPP power block foundation has a V_{S30}=1200 m/s which corresponds to a hard-rock site. Although the NGA models can be used for this type of hard-rock site, a V_{S30} of 1200 m/s is outside of the range of V_{S30} that is well constrained by the empirical data used to derive the NGA models. To address this hard-rock condition, an alternative approach is considered using the NGA models to estimate the ground motion for V_{S30}=760 m/s for which they are well constrained. Amplification factors based on generic site response analyses for hard-rock sites are used to scale the V_{S30}=760 ground motions to the DCPP hard-rock conditions.

As part of the PEER NGA project, Silva (2008) developed a suite of amplification factors for a range of generic site conditions based on kappa in the range of 0.038–0.04 seconds for rock sites. Kappa is an empirically derived site parameter that is usually interpreted as a measure of the amount of damping in the rock beneath a site (the Fourier spectrum is scaled by $\exp(-\pi k f)$, where f is frequency). Silva (2008) provides amplification factors relative to a V_{S30}=1100 m/s for 64 cases with different velocity profiles including rock profiles. For this application, two cases are relevant: Case 61 provides amplification factors for V_{S30}=760 m/s for a depth to rock ranging from 9 to 55 m (30 to 180 ft) and Case 64 provides amplification factors for hard rock with V_{S30}=3150 m/s. A comparison of the amplification for these two cases shows that the site amplification is close to linear. Therefore, the amplification from V_{S30}=760 m/s to V_{S30}=1100 m/s can be used to extrapolate to V_{S30}=1200 m/s. The raw and smoothed values of the log amplification, $a_1(T)$, are shown on Figure 6-6 and the smoothed values are listed in Table 6-5.

A key issue related to the use these generic amplification factors for hard-rock sites is the impact of the site-specific kappa value. For generic soft-rock sites in California used in the NGA data sets, the kappa value is about 0.04 seconds (Silva, 2008). For hard-rock sites, the kappa values can be much smaller (kappa values of 0.01–0.02 seconds) leading to an increase in the high frequency content of the ground motions for hard-rock sites.

For DCPP, the site-specific kappa was estimated based on DCPP free-field recordings from the 2003 Deer Canyon earthquake (Appendix L). The recordings from the Deer Canyon earthquake are well suited for evaluating kappa because they are rich in high frequency content due to the short distance to the fault and the small magnitude of the earthquake (high corner frequency). The analysis of the DCPP free-field ground motions from the Deer Canyon earthquake showed that the kappa at DCPP is 0.042 seconds, consistent with typical soft-rock sites in California (Figure 6-7). The relatively high kappa value for the hard-rock DCPP site is interpreted to be due to fractures in the bedrock in the Franciscan. Given this kappa value, the V_{S30} dependence of the site amplification developed by Silva (2008) for a kappa of 0.04 sec can be applied to DCPP without requiring an additional modification for kappa. Using this approach, the site-specific effects of V_{S30} and kappa at the DCPP site are incorporated in the ground motion model rather than extrapolating the NGA models to high V_{S30} values.

Applying these amplification factors, the ground motion for V_{S30}=1200 m/s is computed using the following equation:

$$SA_{1200}(T) = SA_{760}(T)\exp(a_1(T)) \qquad (6\text{-}3)$$

where $Sa_{760}(T)$ is the median spectrum from the NGA model and $a_1(T)$ is the amplification term listed in the third column of Table 6-5. An example of the effect of using the site-specific method in place of the V_{S30} scaling in the NGA models is shown on Figure 6-8 for an M=7.1, strike-slip earthquake at a distance of 4.9 km. The ground motions based on using V_{S30}=1200 m/s directly into the NGA models are shown by the dashed lines on Figure 6-8, and the ground motions computed using the eq. (6-3) are shown by the solid lines. Using the site-specific approach (solid lines) leads to a narrower range of the ground motion than extrapolating the V_{S30} scaling (dashed lines), indicating the site-specific method is more robust than using extrapolating the V_{S30} scaling in the NGA models.

6.6.3 Average Spectral Acceleration from 3–8.5 Hz

The DCPP fragilities used in the probabilistic risk analyses are based on the average spectral acceleration from 3 to 8.5 Hz. The NGA models, as published, only provide for spectral acceleration at single frequencies. To estimate the 3-8.5 Hz spectral acceleration using the NGA models, the 5 Hz spectral values are computed and then adjustment terms are applied to scale the 5 Hz spectral values to estimate the 3–8.5 Hz spectral accelerations.

The factors to adjust the 5 Hz spectral acceleration to the 3–8.5 Hz spectral acceleration are derived from the NGA data base (Chiou et al., 2008). Using the NGA data for $M \geq 6$, rupture distance ≤ 20 km, and $V_{S30} \geq 450$ m/s, the average difference between the ln(Sa(5 Hz)) and the ln(Sa(3–8.5hz)) is 0.04 with the 3–8.5 Hz values being slightly lower. In addition to the change in the median value, the use of the spectral acceleration averaged over a frequency band also results in a reduction of the standard deviation. Using the same subset of the NGA data, the variance for the 3–8.5 Hz value is 0.058 lower than the variance for the 5 Hz value.

6.6.4 Single-Station Sigma and Site-Specific Site Effects

Empirical GMPEs describe both the median and the standard deviation of the ground motion. In most empirical ground motion models, the standard deviation is computed from data sets that include recordings at a broad range of sites and from earthquakes located in different regions. By using the observed standard deviation from global models in a seismic hazard analysis, there is an assumption that the variability seen in typical strong motion data sets containing recordings at multiple sites from earthquakes in multiple regions will be the same as the variability seen in the ground motion at a single site from multiple future earthquakes at a single location. This is referred to as the ergodic assumption (Anderson and Brune, 1999).

If recordings at a single site from multiple earthquakes are available, then the variability of the ground motion will be smaller than the variability from typical empirical GMPEs based on global data because the global GMPEs include the effects of variability due to different site conditions that are systematic and repeatable for a single site.

Several recent studies have estimated the reduction in the standard deviation for single sites: Chen and Tsai (2002), Atkinson (2006), Anderson (2010), and Lin et al. (2010). These studies have found that the aleatory variability of ln(PGA) can be reduced by about 10–15 percent for single sites. This reduced standard deviation is called "single-station sigma."

Using the NGA data extended to small magnitudes (Chiou et al, 2010), a preliminary model for the single-station sigma, σ_{SS}, was derived for the NGA models (BCHydro, 2010):

$$\sigma_{SS}(T,M) = (\,0.87 + 0.0037\ln(T)\,)\,\sigma(T,M) \qquad (6\text{-}4)$$

where $\sigma(T,M)$ is the standard deviation given by the NGA models. For PGA, the value at T=0.01 sec is used. Following the notation of Al-Atik et al. (2010), the total standard deviation, σ, can be separated into the single-station sigma and the site-to-site sigma:

$$\sigma(T.M)=\sqrt{\sigma_{SS}^2(T,M)+\sigma_{S2S}^2(T)} \qquad (6\text{-}5)$$

The $\sigma_{S2S}^2(T)$ term, called the site-to-site uncertainty, is the variance of the epistemic uncertainty due to systematic differences in the site amplification between sites with the same V_{S30}.

The single-station sigma approach was first proposed by Atkinson (2006). Its implementation is rapidly developing and is gaining broad acceptance. Two ongoing major projects to update ground motion models in the United States have adopted the single-station sigma approach. The update of the NGA models applicable to the western United States (NGA-west2), being conducted through the Pacific Earthquake Engineering Research Center (PEER, 2010a), will provide single-station sigma values as well as the traditional ergodic sigma values. Similarly, the NGA-east project, sponsored by the NRC and also being conducted through the PEER center (PEER, 2010b), has also adopted the single-station sigma approach.

For the use of the single-station sigma approach, estimates of the median site-specific factor and its epistemic uncertainty are needed (e.g., how does the site-specific site amplification differ from the global average model for the given V_{S30}?). Observations from earthquakes at the site can be used to constrain the site-specific effects. At DCPP, there are observations of past earthquakes that allow estimates of the site-specific site amplification to be made. These allow the development of GMPEs that are calibrated to the site-specific effects at DCPP.

To use ground motion data recorded at the site in a single-station sigma approach, the within-event residuals need to be computed (Al-Atik et al., 2010) to avoid source-specific effects being mixed in with the site-specific effects. To allow the event term to be reliably estimated requires earthquakes with recordings at multiple sites (5 or more). For DCPP, there are recordings from two recent earthquakes that meet this requirement: the 2003 San Simeon and 2004 Parkfield earthquakes.

The ground motion data and metadata from these two earthquakes are part of the NGA-west2 database (PEER, 2010a). The distribution of the data from these two earthquakes in terms of rupture distance and V_{S30} is shown on Figure 6-9. Most of the data are for $V_{S30} < 450$ m/s so there is not enough data to use with Idriss model which is only for sites with $V_{S30} > 450$ m/s. For the other four NGA models, the total residuals were computed for each earthquake. These total residuals are used to estimate the event terms as described below.

For the San Simeon earthquake, the residuals for 5 Hz and 1 Hz for each NGA model are shown on Figures 6-10a and 6-10b. The rupture distance for the DCPP site is 35 km. The residuals show a slope with distance for large distances. The average residual from sites at distances of 0–100 km is used as the event term representative of mean residual at 35 km. This average residual is shown by the horizontal lines on Figures 6-10a and 6-10b.

For the Parkfield earthquake, the residuals for 5 Hz and 1 Hz for each NGA model are shown on Figures 6-11a and 6-11b. The rupture distance for the DCPP site is 85 km. Again, the residuals show a slope with distance for large distances. The average residual from sites at distances of 40–170 km is used as the event term representative of mean residual at 85 km. This average residual is shown by the horizontal lines on Figures 6-11a and 6-11b.

This process was repeated for the suite of spectral frequencies. The resulting event terms are given in Table 6-6 for the four NGA models.

Next, the event term adjusted median ground motions for the DCPP site are computed using each of the four NGA models for V_{S30}=760 m/s, and the ground motions are then scaled to the V_{S30} for the free-field site condition. The free-field site at DCPP has a V_{S30}=1100 m/s as compared to the V_{S30}=1200 m/s for the embedded power block. Using the same method as described in Section 6.6.2, the Silva (2008) amplification factors are applied to account for the scaling from V_{S30}=760 to V_{S30}=1100 m/s. These factors are listed in Table 6-5.

The median spectra for the free-field site, including the event terms, are shown for the four NGA models on Figures 6-12 and 6-13 for the San Simeon and Parkfield earthquakes, respectively. The small range of the NGA models is a result of applying the model-specific event terms. The average of the event-term adjusted median ground motions is shown by the black lines in Figures 6-12 and 6-13.

Figure 6-14 shows the residuals of the observed free-field ground motion at DCPP computed relative to the event-term corrected NGA median spectrum. The two earthquakes show a consistent trend in the residuals with negative residuals in the 5-10 Hz range and positive residuals in the 0.5-3 Hz range. A smoothed model of the mean residual is also shown in Figure 6-14. The mean residual represents the systematic differences in the site amplification effects at the DCPP site as compared to the average for sites with the same V_{S30} and kappa. (Kappa is included as a known parameter for DCPP because the site amplification model from V_{S30}=760 m/s to V_{S30}=1100 m/s included the effects of a known kappa.) The values of the smoothed mean residuals, called a_2, are listed in Table 6-7.

The $a_2(T)$ site terms represent the site-specific amplification observed at the DCPP site. The site terms show that the DCPP site has increased amplification of low frequency ground motions and reduced amplification of high frequency ground motions as compared to average sites with the same V_{S30} and kappa.

The consistency of the results for the San Simeon and Parkfield earthquakes indicates that this site-specific site amplification is a robust feature, but it is based on only two earthquakes. The uncertainty of the estimate of the mean has a variance of $\frac{\sigma^2_{S2S}(T)}{N}$ where N is the number of observations. Given two earthquakes recorded at the site, N=2, and the epistemic uncertainty in the a_2 values has a variance of $\frac{\sigma^2_{S2S}(T)}{2}$.

For ease of application, this additional epistemic uncertainty is combined with the single-station aleatory variability to provide an equivalent total standard deviation for use in computing the ground motion hazard at the DCPP site. This is a common simplification used in PSHA which yields the correct mean hazard, but the median fractile is biased high and the range of the fractiles is reduced.

From eq. (6-6), the standard deviation of the site-to-site uncertainty is given by:

$$\sigma_{S2S}(T.M)=\sqrt{\sigma^2(T,M)-\sigma^2_{SS}(T,M)} \qquad (6\text{-}6)$$

Three of the five NGA models include a magnitude-dependent standard deviation. To capture standard deviation for the magnitudes relevant for the DCPP site, the standard deviation of the site-to-site uncertainty is averaged over M6, M6.5, and M7. The σ_{S2S} term is then averaged over the five NGA models. The site-to-site variance, $\sigma^2_{SS}(T,M)$, is listed in Table 6-7.

The equivalent total standard deviation is given by

$$\sigma_{EQ\,Total}(T.M)=\sqrt{\sigma^2(T,M)-\left(1-\frac{1}{N}\right)\sigma^2_{S2S}(T,M)} \qquad (6\text{-}7)$$

The term $-\left(1-\frac{1}{N}\right)\sigma^2_{S2S}(T,M)$ in eq. (6-7) is the adjustment to the variance given by the NGA models. These variance adjustment terms, for N=2, are listed in the last column of Table 6-7.

The estimation of the median and standard deviation of the ground motion using the single-station approach is summarized as follows. For 5 percent damped spectral acceleration at a single frequency, the median is given by

$$\ln\left(SA_{DCPP}(M,R,T)\right)=\ln\left(SA_{DCPP}(M,R,T)\right)+a_1+a_2 \tag{6-8}$$

where $\hat{S}a_{760}(M,R,T)$ is the median spectral acceleration from the NGA models for a V_{S30} of 760 m/s, a_1 is the average amplification (in natural log units) from V_{S30}=760 m/s to V_{S30}=1200 m/s, and a_2 is the site-specific amplification (in natural log units) from an average site with V_{S30}=1200 m/s and kappa=0.04 seconds to the DCPP site. The standard deviation is given by eq. 6-7.

For 5 percent damped spectral acceleration averaged over 3-8.5 Hz, the median is adjusted by the scaling from 5Hz to 3-8.5 Hz and given by

$$\ln\left(\hat{S}a_{DCPP}(M,R,3-8.5Hz)\right)=\ln\left(\hat{S}a_{760}(M,R,5Hz)\right)+a_1+a_2-0.04 \tag{6-9}$$

The standard deviation is also adjusted by the difference between the variance for 5 Hz and the variance for 3–8.5 Hz and is given by

$$\sigma_{EQ\,Total}(3-8.5Hz,M)=\sqrt{\sigma^2(T,M)-\left(1-\frac{1}{N}\right)\sigma^2_{S2S}(T,M)-0.058} \tag{6-10}$$

6.6.5 Directivity

There are two parts of the directivity effect: scaling of the average horizontal component and systematic differences between the fault normal and fault parallel components (Somerville et al., 1999). Recently, a directivity model for the scaling on the average horizontal component was developed by Spudich and Chiou (2008) based on the residuals from NGA GMPEs. As part of the NGA project, this directivity model was reviewed by the NGA developers to evaluate its applicability to their NGA GMPEs. The Spudich and Chiou (2008) directivity model has a stronger seismological basis than of Somerville et al. (1999) because it includes a radiation pattern term. An issue with this model is that it is not centered on zero for average directivity conditions, implying a change in the median ground motion for average directivity conditions. The NGA developers were unsure of the cause for this shift and how the Spudich and Chiou (2008) directivity models should be applied to the NGA GMPEs.

Watson-Lamprey (2007) evaluated the within-event residuals from the NGA GMPEs following the same approach as used by Somerville et al. (1999). Watson-Lamprey found that the directivity effect was about one-half as strong as in the Somerville et al. (1999) model. This was not consistent with the strong directivity effects given in the Spudich and Chiou (2008) model.

As a result, the NGA developers did not make recommendations with regard to the applicability of the new directivity models to the NGA GMPEs. Rather, a follow-on project to further evaluate the directivity effect was recommended. This follow-on project began in 2010 and should be completed in 2012. As part of this follow-on project, Abrahamson and Watson-Lamprey developed an update of the Abrahamson (2000) model based on numerical simulations of ground motions conducted as part of the NGA project. This updated model is described in Appendix K. The key feature of this updated model is the use of nonnormalized lengths of rupture toward the site in place of the normalized length parameter, X. The saturation of the directivity is on the nonnormalized lengths. A main change using this revised parameterization is that relative to the NGA model, the directivity effects are strongest for backward directivity (rupture away from the site). That is, the main effect of the new directivity model is that this is a significant reduction of the long period ground motion for sites locate close to the epicenter (backward directivity) but only a small increase for sites in the forward directivity direction.

In ground-motion models, the primary effect of directivity is to increase the variability of the long period ground motion at short distances. The 84th percentile ground motion includes much of the effect of directivity through the standard deviation of the ground motion because the current larger ground-motion data sets better sample the range of directivity conditions in the data. That is, forward directivity leads to an above average ground motion at long periods, and the use of the 84th percentile is addressing this above-average ground motion case.

Given that the directivity models are under review and revision and will only affect the low frequencies that are not critical for nuclear power plants, directivity effects are not included in this analysis. They will be considered in the next full update of the PSHA as part of the LTSP Update.

6.6.6 Effect of New Ground Motion Models

The NGA ground motion models lead to significant changes in the ground motion scaling as compared to GMPEs developed prior to the year 2000. In general, for sites located close to large strike-slip earthquakes, there is a reduction of the median ground motion, but an increase in the standard deviation. For example, Figure 6-15 shows the 84th percentile spectra for the Hosgri fault source from the 1991 LTSP/SSER34 (PG&E, 1988; NRC, 1991) and the 1977 HE design spectrum. The 1991 LTSP/SSER34 spectrum and the 1977 HE design spectrum are similar, but there is a large difference between these two spectra and the Hosgri fault source spectrum computed using the NGA models: using the NGA models, the 84th percentile spectrum is reduced, indicating that previous ground motion models, based on sparse near-fault ground motions, had overestimated the ground motion at short distances.

For reverse faults, the effects are different. Figure 6-16 shows the 84th percentile spectra for the Los Osos fault source based on the 1988 LTSP (PG&E, 1988) ground motion model. The spectrum based on the NGA models is shown with and without hanging wall effects. Excluding hanging wall effects, there is a reduction for the NGA models as compared to the 1988 LTSP model, similar the reduction for strike-slip earthquakes, but a key feature of the NGA models is an increase in the high frequency ground motion for sites located at short distances on the hanging wall side of the rupture. When the hanging wall effects are included, the spectrum is increased to a level that is similar to the spectrum based on the 1988 LTSP ground motion model. The DCPP is on the hanging wall side of both the Los Osos and San Luis Bay fault sources so the hanging wall effect applies to both fault sources.

These changes in the ground motion affect the relative contribution of strike-slip and reverse faults to the seismic hazard at DCPP. Given the reduction in the near-fault ground motions from strike-slip earthquakes and only small changes in the near-fault ground motions for sites on the hanging wall of reverse earthquakes, the two nearby reverse fault sources (Los Osos and San Luis Bay) will have a larger contribution to the hazard at DCPP relative to the strike-slip Hosgri fault source as compared to the 1988 LTSP (PG&E, 1988).

6.7 Deterministic Ground Motions

The 84th percentile deterministic ground motions for the average horizontal component are computed for each of the four nearby fault sources: Hosgri, Los Osos, San Luis Bay, and Shoreline.

6.7.1 Earthquake Magnitudes

The selection of earthquake magnitude to use in deterministic evaluations involves judgment. In this report, the range in the mean characteristic earthquake magnitude resulting from the source characterization logic tree is considered. The magnitude corresponding to the 90th fractile of the mean characteristic magnitude is selected as a reasonably conservative value for use in the deterministic analysis.

The cumulative distributions of the epistemic uncertainty for the mean characteristic magnitudes for the four fault sources are shown in Figure 6-17. For the Hosgri fault source, the median magnitude is 6.8 and the 90th fractile is magnitude 7.1. This is consistent with the M7.2 magnitude selected for the determinsitic analysis of the Hosgri earthquake in the 1988 LTSP (PG&E, 1988). For the Los Osos fault the median magnitude is M 6.5 and the 90th fractile corresponds to M 6.8.

For the San Luis Bay and Shoreline fault sources, the evaluation is more complicated because the source characterization logic tree includes a branch in which these two faults are linked. For the Shoreline fault, the distribution shown in Figure 6-17 only includes the rupture scenarios that include rupture of the Central segment (e.g. rupture past the DCPP site) from either the independent or linked models. That is, rupture of just the South or just the North segments of the Shoreline fault is not included in the distribution of mean characteristic magnitudes for the development of the deterministic scenario earthquake for the Shoreline fault source. For the Shoreline fault source (including rupture of the Central segment source), the median magnitude is M 6.2 and the 90th fractile corresponds to M 6.4 to M 6.5, which is rounded up to M 6.5.

For the San Luis Bay fault source, the distribution shown in figure 6-17 is for the non-linked case (East and West segments together). The median magnitude is 6.1 and the 90th fractile corresponds to magnitude of 6.3.

The selected deterministic magnitudes for the four fault sources are listed in Table 6-8. The range of dip angles from the logic trees is also listed in this table for each fault source.

6.7.2 Deterministic Ground Motions

The 84th percentile ground motions are computed using the single-station sigma approach with the median given by eq. 6-8 and the standard deviation given by eq. 6-7. For the median from the NGA relations, $Sa_{760}(M,R<T)$,the weighted geometric mean of the spectra from the five NGA models is used. For the standard deviation from the NGA relations, $\sigma(T,M)$, the weighted average (arithmetic mean) from the NGA models is used.

The sensitivity of the ground motion to the dip is shown in Figures 6-18a-c for the Hosgri, Los Osos, and San Luis Bay fault sources, respectively. For all three cases, the lowest dip leads to the largest ground motions at the DCPP site. The uncertainty in the dip of the Los Osos fault source has the largest effect.

For this study, the lowest dip for each fault source is conservatively selected to produce the largest deterministic ground motions at the DCPP site. The geometric mean of the 84th percentile spectra for each of the four fault sources are shown on Figure 6-19. The spectral have a peak at 2.5 Hz that reflects the site-specific amplification shown in Figure 6-14. These 84th percentile spectra are compared to the 1991 LTSP/SSER34 spectrum in Figure 6-19. The 84th percentile spectra based on updated ground motion models and updated source characterizations fall below the 1991 LTSP/SSER34 spectrum.

For comparison, Figure 6-19 also shows the deterministic ground motions computed using the traditional ergodic approach. Accounting for the site-specific amplification observed at DCPP shifts the spectrum to the lower spectral frequencies as compared to the ergodic approach.

6.8 Probabilistic Seismic Hazard Analysis

The probabilistic seismic hazard analysis follows the standard approach first developed by Cornell (1968). This approach has been expanded to more fully treat both the randomness (i.e., aleatory variability) and the scientific uncertainty (i.e., epistemic uncertainty).

6.8.1 Additional Sources

For completeness, additional regional faults are included in the PSHA. The parameters used for these additional faults are listed in Table 6-9. As these faults have a small impact on the hazard, the fault source models are not described in detail.

6.8.2 Hazard Results

The hazard is computed using the program HAZ43 (GEO.DCPP.10.04). The minimum magnitude considered in the hazard calculation is M5.0. This is a commonly used value based on the assumption that earthquakes less than M5.0 will not damage engineered structures.

Figures 6-20a–c show the hazard curves for PGA, 5 Hz, and 1.0 Hz spectral acceleration. The individual contributions to the total hazard from the fault sources are shown on the figures. These plots show that the main contribution to the total hazard is from the Hosgri fault for all hazard levels. The Los Osos, San Luis Bay, and Shoreline faults are similar in terms of their contribution to the hazard. The Uniform Hazard Spectra for hazard levels of 1E-3, 1E-4, and 1E-5 are shown on Figure 6-21.

The deaggregations for the 1E-4 hazard level are shown on Figure 6-22a-c for the PGA, 5 Hz, and 1 Hz spectral acceleration. The deaggregations indicate that the earthquakes with magnitudes between 6.5 and 7.0 at short distances (i.e., 3–5 km) control the hazard at all three spectral periods.

The fragility used in the PRA for DCPP is based on the spectral acceleration averaged over the frequency band of 3–8.5 Hz. The hazard curve for this ground motion parameter is shown on Figure 6-23. To show the impact of the Shoreline fault source, the hazard is shown with and without the Shoreline fault source. The addition of the Shoreline fault source increases the hazard by 20–35 percent for hazard levels of 1E-4 to 1E-5. The epistemic uncertainty in the hazard is shown on Figure 6-24. The epistemic uncertainty in the hazard leads to about a factor of 4 difference between the 10th and 90th fractile. Compared to most sites, this is a tight range, indicating that the hazard at DCPP is relatively well constrained due to the dominance of the Hosgri fault.

Figure 6-25 compares the mean 3-8.5 Hz hazard for the 1988 LTSP (PG&E, 1988) with the mean hazard from this study. The updated hazard curve is lower than the 1988 LTSP hazard curve for spectral acceleration less than about 3g but is higher than the 1988 LTSP hazard curve for spectral accelerations greater than 3g. This figure also compares the mean hazard as computed using the traditional approach with the ergodic standard deviation and ignoring the site-specific amplification with the updated hazard. The traditional approach leads to higher hazard because it does not account for the lower standard deviation and the negative site-specific amplification term.

The epistemic uncertainty of the 3-8.5 Hz hazard from the 1988 LTSP study is compared the epistemic uncertainty from the current study in Figure 6-26. The updated mean hazard curve falls within the 10–90th fractiles from the 1988 LTSP except at very large ground motions (> 3g).

6.9 Seismic Hazard Conclusions

For the deterministic analysis, the new estimates of the 84th percentile ground motion fall below the 1991 LTSP/SSER34 (NRC 1991) deterministic spectrum, indicating that the deterministic seismic margins for the new estimates of the ground motion are at least as large as found during the LTSP (PG&E, 1988, 1991).

For the probabilistic analysis, the hazard for 3–8.5 Hz spectral acceleration is lower than the 1988 LTSP hazard for spectral acceleration less than 3.0 g and is greater than the 1988 LTSP for spectral accelerations greater than 3.0 g. This change in the hazard curve is primarily due to the change in the ground-motion models. The NGA models result in lower median ground motions for sites close to large earthquakes, but with an increased standard deviation. The flattening of the new hazard compared to the 1988 LTSP hazard curves is due to the larger standard deviation.

Because the updated hazard curve is not enveloped by the 1988 LTSP hazard curve, the seismic core damage frequency (CDF) has been reevaluated. The seismic CDF estimated as part of the 1988 LTSP (PG&E, 1988) was 3.8E-5. Using the revised source characterization and ground motion models and with the 1988 LTSP fragility curves, the seismic CDF decreases to about

2.1E-5. The reduction is mainly due to the use the NGA ground motion models with the single-station sigma approach incorporating the site-specific amplification.

Table 6-1a. Coordinates of Fault Sources

Flt	Pt_name	Long	Lat
LosOsos	O1	-120.4590	35.1270
LosOsos	O2	-120.5230	35.1670
LosOsos	O3	-120.6720	35.2220
LosOsos	O4	-120.7090	35.2720
LosOsos	O5	-120.7910	35.3050
LosOsos	O6	-120.9000	35.2990
LosOsos	O7	-120.9950	35.3620
Hosgri	H1	-120.6403	34.6702
Hosgri	H2	-120.8162	35.0443
Hosgri	H3	-121.0177	35.3860
Hosgri	H4	-121.0584	35.4403
Hosgri	H5	-121.0958	35.4961
Hosgri	H6	-121.1381	35.5528
Shoreline	S1	-120.7420	35.1318
Shoreline	S2	-120.7990	35.1769
Shoreline	S3	-120.8740	35.2130
Shoreline	S5	-120.9060	35.2350
Shoreline	S4	-120.9370	35.2563
N40W	S6	-120.9263	35.2642
N40W	S7	-120.9079	35.2418
SLB_East	L6	-120.7142	35.1732
SLB_East	L5	-120.7390	35.1800
SLB_East	L4	-120.7510	35.1790
SLB_East	L3	-120.7690	35.1810
SLB_West	L2	-120.7988	35.1769
SLB_West	L1	-120.8885	35.1953

Table 6-1b. Coordinates of San Luis Bay West Segment Source Models for the Linked Branch

Dip	Crustal Thickness (km)	Top of Fault	Bottom of fault
70	10	S2: -120.799, 35.177, Z=0.0 km	S2: -120.799, 35.177, Z=1.0 km
		L1: -120.889, 35.195, Z=0.0 km	S3: -120.874, 35.213, Z=7.1 km
80	10	S2: -120.799, 35.177, Z=0.0 km	S2: -120.799, 35.177, Z=1.0 km,
		-120.905, 35.191, Z=0.0 km	-120.890, 35.204, Z=10.0 km
		L1: -120.889, 35.195, Z= 0.0 km	S3: -120.874, 35.213, Z=10.0 km
85	10	S2: -120.799, 35.177, Z=0.0 km	S2: -120.799, 35.177, Z=1.0 km
		-120.932, 35.184, Z=0.0 km	-120.913, 35.190, Z=10.0 km
		L1: -120.889, 35.195, Z= 0.0 km	S3: -120.874, 35.213, Z=10.0 km
70	12	S2: -120.799, 35.177, Z=0.0 km	S2: -120.799, 35.177, Z=1.0 km
		L1: -120.889, 35.195, Z= 0.0 km	S3: -120.874, 35.213, Z=7.1 km
80	12	S2:-120.799, 35.177, Z=0.0 km	S2: -120.799, 35.177, Z=1.0 km
		-120.897, 35.193, Z=0.0 km	-120.882, 35.208, Z=12.0 km
		L1: -120.889, 35.195, Z= 0.0 km	S3: -120.874, 35.213, Z=12.0 km
85	12	S2: -120.799, 35.177, Z=0.0 km	S2: -120.799, 35.177, Z=1.0 km
		-120.932, 35.184, Z=0.0 km	-120.913, 35.190, Z=12.0 km
		L1: -120.889, 35.195, Z= 0.0 km	S3: -120.874, 35.213, Z=12.0 km
70	15	S2: -120.799, 35.177, Z=0.0 km	S2: -120.799, 35.177, Z=1.0 km
		L1: -120.889, 35.195, Z= 0.0 km	S3: -120.874, 35.213, Z=7.1 km
80	15	S2: -120.799, 35.177, Z=0.0 km	S2: -120.799, 35.177, Z=1.0 km
		L1: -120.889, 35.195, Z= 0.0 km	S3: -120.874, 35.213, Z=14.7 km
85	15	S2:-120.799, 35.177, Z=0.0 km	S2: -120.799, 35.177, Z=1.0 km
		-120.923, 35.186, Z=0.0 km	-120.905, 35.195, Z=15.0 km
		L1: -120.889, 35.195, Z= 0.0 km	S3: -120.874, 35.213, Z=15.0 km

Table 6-2a. Depth Limits of the San Luis Bay Fault Source

Depth to the Bottom of the Fault Source (km)	San Luis Bay Fault Source Dip	Los Osos Fault Source Dip	Depth of Intersection of San Luis Bay and Los Osos Fault Sources (km)
10	50	45	5.1
10	70	45	6.8
10	80	45	7.9
10	50	60	6.6
10	70	60	9.9
10	80	60	10
10	50	75	8.4
10	70	75	10
10	80	75	10
12	50	45	5.1
12	70	45	6.8
12	80	45	7.9
12	50	60	6.6
12	70	60	9.9
12	80	60	12
12	50	75	8.4
12	70	75	12
12	80	75	12
15	50	45	5.1
15	70	45	6.8
15	80	45	7.9
15	50	60	6.6
15	70	60	9.9
15	80	60	12.3
15	50	75	8.4
15	70	75	14.7
15	80	75	15

Table 6-2b. Depth Limits of the San Luis Bay East Segment Source

Depth to the Bottom of the Fault Source (km)	San Luis Bay Fault Source Dip	Los Osos Fault Source Dip	Depth of Intersection of SLB and Los Osos Fault Sources (km)
10	83	45	8.2
10	83	60	10
10	83	75	10
12	83	45	8.2
12	83	60	12
12	83	75	12
15	83	45	8.2
15	83	60	13.3
15	83	75	15

Table 6-3. Magnitude-Area Scaling Relations

	Sense of Slip	Model	Standard error of constant coeff
Hanks and Bakun (2008)	SS	$M = 3.98 + 1.0 \log(A)$ for $A<537\ km^2$ $M = 3.07 + 4/3 \log(A)$ for $A>537\ km^2$	Not given
Wells and Coppersmith (1994)	SS	$M = 3.98 + 1.02 \log(A)$	0.07
	RV	$M = 4.33 + 0.90 \log(A)$	0.12
	ALL	$M = 4.07 + 0.98 \log(A)$	0.06
Wells and Coppersmith (1994)	ALL	$\log(\text{Area}) = 0.91M - 3.49$ (σ=0.24)	
		$\log(\text{Width}) = 0.32\ M - 1.01\ \sigma$=0.15)	

Table 6-4. Computed V_{S30} Values (for 10 m Embedment) for the Power Block and the ISFSI Borehole Sites

	V_{S30} (m/s) for 10 m Embedment (Applicable to the Power Block)
Power Block	1210
ISFSI 98BA-1&4	1225
ISFSI 98BA-3	1214

Table 6-5. Smoothed Coefficients for the Amplification from V_{S30}=760 m/s to V_{S30}=1200 m/s

Period (sec)	Freq (Hz)	a_1 for V_{S30}=1200 m/s	a_1 for V_{S30}=1100 m/s
0.01	100.00	-0.35	-0.28
0.02	50.00	-0.35	-0.29
0.03	33.33	-0.35	-0.28
0.05	20.00	-0.26	-0.21
0.075	13.33	-0.26	-0.19
0.10	10.00	-0.27	-0.26
0.15	6.67	-0.29	-0.33
0.20	5.00	-0.31	-0.21
0.25	4.00	-0.34	-0.28
0.30	3.33	-0.37	-0.36
0.40	2.50	-0.4	-0.37
0.50	2.00	-0.42	-0.44
0.75	1.33	-0.42	-0.34
1.0	1.00	-0.36	-0.22
1.5	0.67	-0.27	-0.17
2.0	0.50	-0.21	-0.28
3.0	0.33	-0.130	-0.12
4.0	0.25	-0.080	-0.07
5.0	0.20	-0.045	-0.04
10.0	0.10	0	0
	3-8.5 Hz	-0.33	

Table 6-6. Event terms for the 2004 Parkfield and 2003 San Simeon Earthquakes.

			Parkfield Eqk, R40-170 Km, Event Terms			
T (sec)	Freq (Hz)	Nb Rec.	AS08	BA08	CB08	CY08
0.01	100	18	-0.2971	-0.7524	-0.7688	-0.1765
0.02	50	18	-0.2898	-0.7530	-0.7675	-0.1702
0.03	33.33	18	-0.2941	-0.7690	-0.7907	-0.1849
0.05	20	18	-0.2776	-0.7911	-0.8289	-0.2049
0.075	13.33	18	-0.2766	-0.8499	-0.8573	-0.2390
0.1	10	18	-0.2232	-0.7846	-0.7911	-0.1942
0.15	6.67	18	-0.2741	-0.7841	-0.7964	-0.2434
0.2	5	18	-0.3236	-0.8568	-0.7760	-0.2476
0.3	3.33	18	-0.3315	-0.8572	-0.7160	-0.2539
0.4	2.5	18	-0.2717	-0.7147	-0.5960	-0.2082
0.5	2	18	-0.1896	-0.6215	-0.5083	-0.1361
0.75	1.33	18	-0.0639	-0.4461	-0.3200	-0.0195
1	1	18	-0.0139	-0.3819	-0.2253	0.0092
1.5	0.67	18	0.1138	-0.3449	-0.1050	0.0694
2	0.5	18	0.1144	-0.3242	-0.0415	0.0856

			San Simeon, R0-100 Km, Event Terms			
T (sec)	Freq (Hz)	Nb Rec.	AS08	BA08	CB08	CY08
0.01	100	8	-0.3698	-0.4583	-0.8430	-0.1708
0.02	50	8	-0.3657	-0.4589	-0.8459	-0.1680
0.03	33.33	8	-0.3672	-0.4622	-0.8662	-0.1796
0.05	20	8	-0.3762	-0.5076	-0.9557	-0.2495
0.075	13.33	8	-0.4395	-0.6169	-1.0644	-0.3716
0.1	10	8	-0.5304	-0.6978	-1.1368	-0.4773
0.15	6.67	8	-0.6755	-0.7932	-1.1882	-0.5938
0.2	5	8	-0.6961	-0.8702	-1.1355	-0.5252
0.3	3.33	8	-0.6590	-0.8379	-1.0289	-0.4165
0.4	2.5	8	-0.4285	-0.5533	-0.7384	-0.1767
0.5	2	8	-0.3993	-0.5396	-0.6892	-0.1470
0.75	1.33	8	-0.1099	-0.2415	-0.3086	0.1410
1	1	8	0.0627	-0.0472	-0.0589	0.2835
1.5	0.67	8	0.1122	0.0918	0.0450	0.2448
2	0.5	8	0.1367	0.1403	0.1198	0.3423

Table 6-7. Site-specific site amplification terms and total variance reduction for the single-station sigma approach.

Frequency (Hz)	Smoothed a_2	σ_{S2S} (ln units)	Var Added to NGA Models (ln units)
100	-0.06	0.080	-0.040
50	-0.06	0.079	-0.040
34	-0.06	0.081	-0.041
20	-0.24	0.084	-0.042
13.33	-0.24	0.087	-0.044
10	-0.24	0.089	-0.045
6.67	-0.20	0.090	-0.045
5	-0.18	0.092	-0.046
4	-0.07	0.092	-0.046
3.33	0.05	0.093	-0.047
2.5	0.34	0.094	-0.047
2	0.43	0.096	-0.048
1.33	0.55	0.099	-0.050
1	0.40	0.103	-0.051
0.67	0.40	0.106	-0.053
0.5	0.40	0.109	-0.065
3-8.5	-0.11	0.093	-0.047

Table 6-8. Selected Deterministic Earthquake Scenarios

Fault Source	Magnitude	Dip	Smallest R_{Rup} (km)	Smallest RJB (km)	Rx	Sense of Slip	Hanging Wall or Foot Wall
Hosgri	7.1	80	4.9	2.3	4.9	SS	HW N/A for 90
		85	4.9	3.6	4.9		
		90	4.9	4.9	4.9		
Los Osos	6.8	45	7.6	0.0	9.9	RV/OBL	HW
		60	8.9	2.6	9.9		
		75	9.7	6.5	9.9		
San Luis Bay (not linked)	6.3	50	1.9	0.0	2.5	RV	HW
		70	2.4	0.0	2.5		
		80	2.5	0.0	2.5		
Shoreline	6.5	90	0.6	0.6	0.6	SS	N/A

Table 6-9. Source Parameters for Other Regional Fault Sources

Fault Source	Dip	Depth to Bottom of the Fault Source (km)	Slip-Rate (mm/yr)	Mean Characteristic Magnitude	Sense of Slip
Oceanic	35 (0.3) 45 (0.4) 55 (0.3)	10 (1.0)	0.1 (0.25) 0.3 (0.50) 0.6 (0.25)	6.4 (0.3) 6.8 (0.4) 7.0 (0.3)	RV/OBL (1.0)
West Huasna	90 (1.0)	10 (1.0)	0.5 (0.25) 1.0 (0.50) 2.0 (0.25)	6.6 (0.3) 6.9 (0.4) 7.2 (0.3)	SS (1.0)
Wilmar Ave	45 (1.0)	10 (1.0)	0.1 (0.25) 0.2 (0.50) 0.3 (0.25)	6.4 (0.3) 6.7 (0.4) 7.0 (0.3)	RV (1.0)
Oceano	45 (1.0)	10 (1.0)	0.1 (0.25) 0.2 (0.50) 0.3 (0.25)	6.6 (0.3) 6.9 (0.4) 7.2 (0.3)	RV (1.0)
San Andreas 1857	90 (1.0)	12 (1.0)	31 (0.25) 34 (0.50) 37 (0.25)	7.7 (0.3) 7.8 (0.4) 7.9 (0.3)	SS (1.0)
San Andreas Parkfield	90 (1.0)	12(1.0)	3* (0.25) 4* (0.50) 5* (0.25)	5.9 (0.3) 6.0 (0.4) 6.1 (0.3)	SS (1.0)

* Equivalent slip-rate for mean recurrence intervals of 25, 30, and 40 years

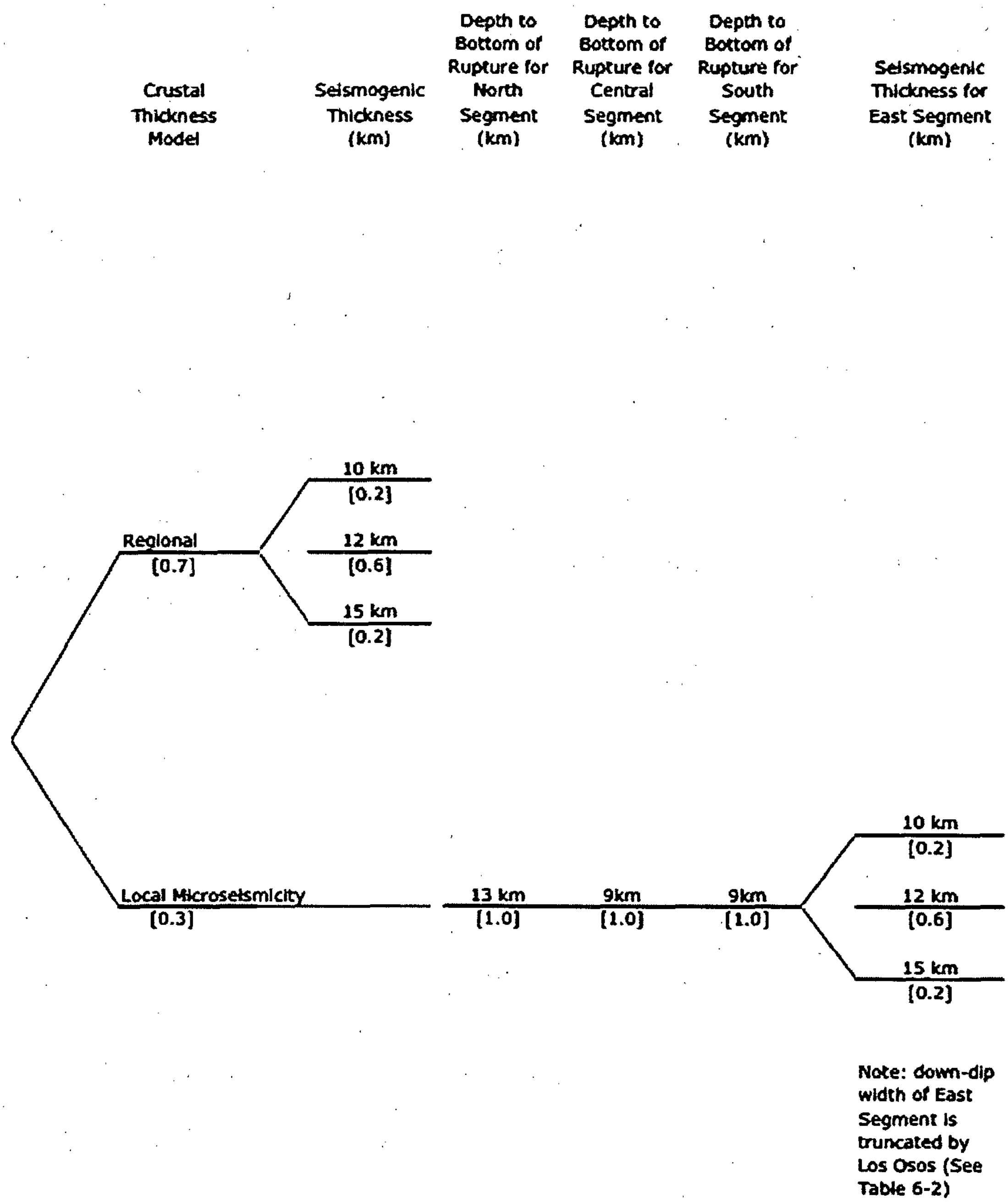

Figure 6-1. Simplified logic tree for the Shoreline fault source

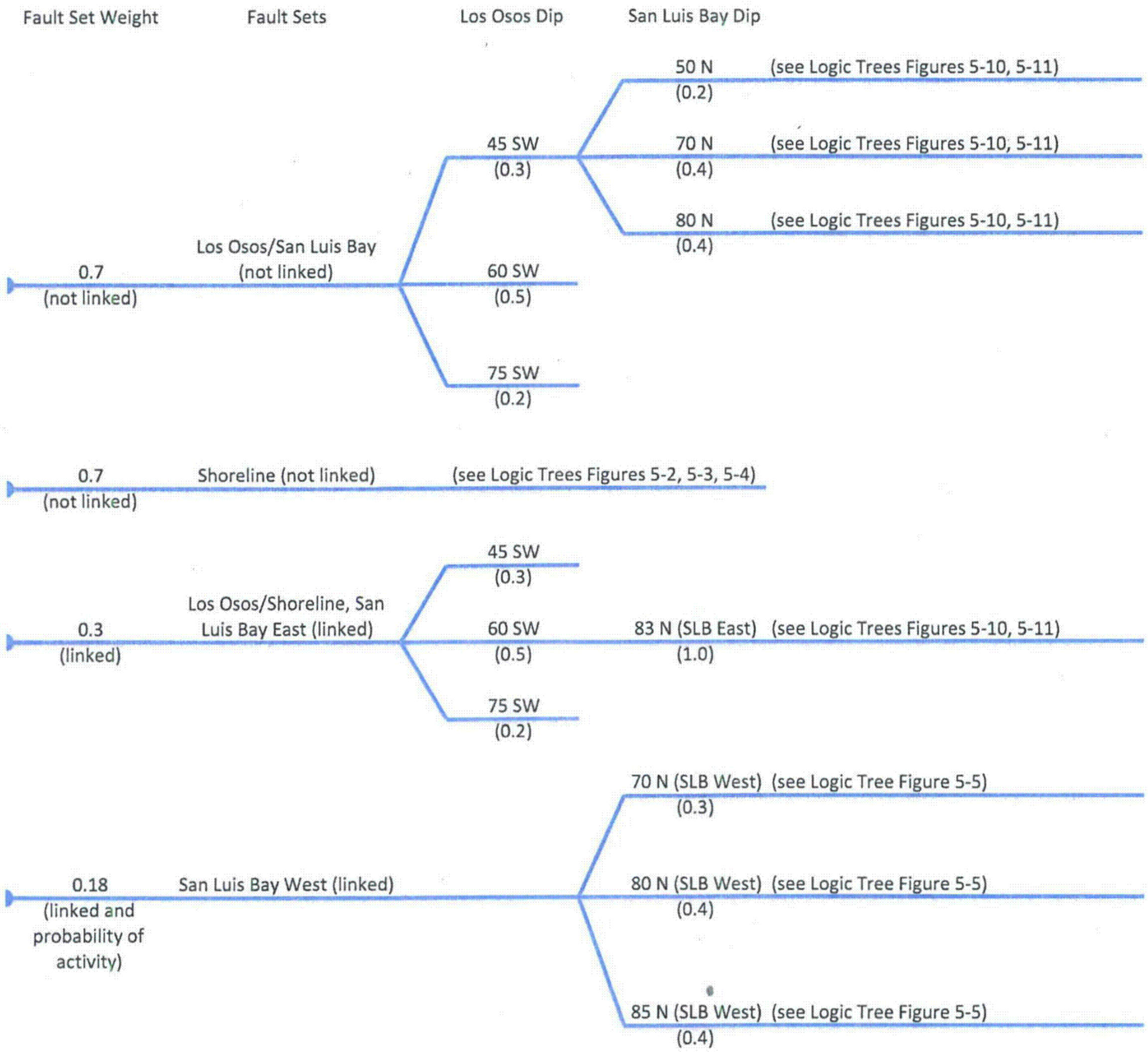

Figure 6-2. Logic tree for ruptures for Shoreline and San Luis Bay fault sources

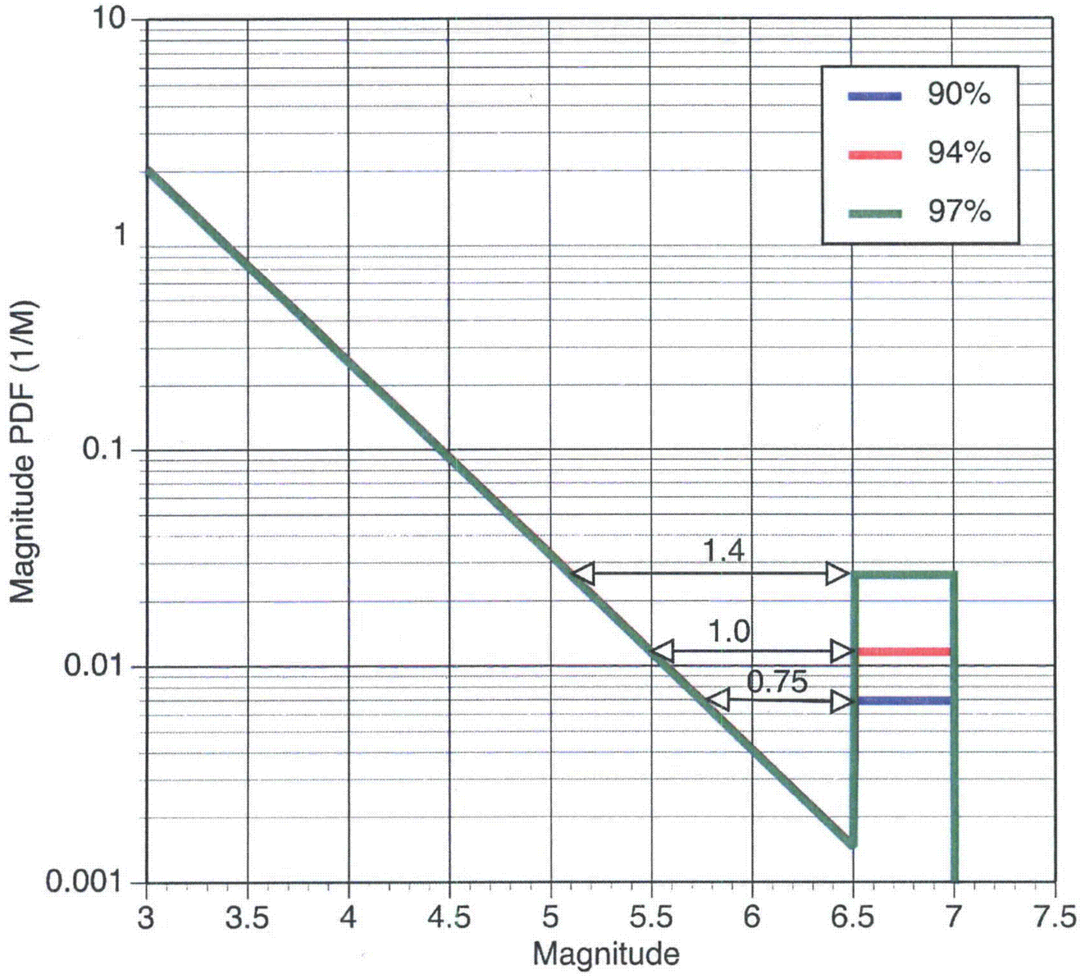

Figure 6-3. Magnitude probability density functions for difference percentages of the seismic moment being released in characteristic earthquakes. The Youngs and Coppersmith (1985) model corresponds to the case with 94% of the moment in characteristic earthquakes (red curve).

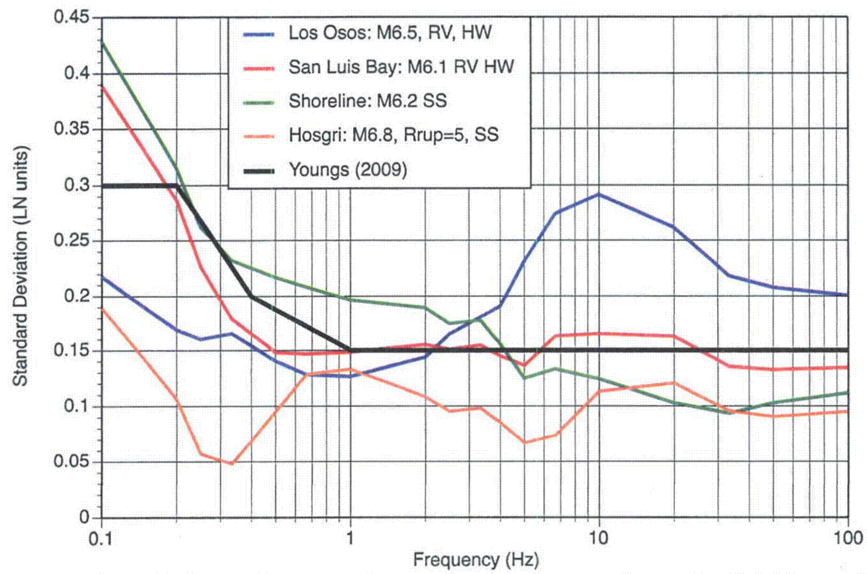

Figure 6-4a. Standard deviation of the median ground motion from the NGA models for representative earthquakes for the four nearby fault sources.

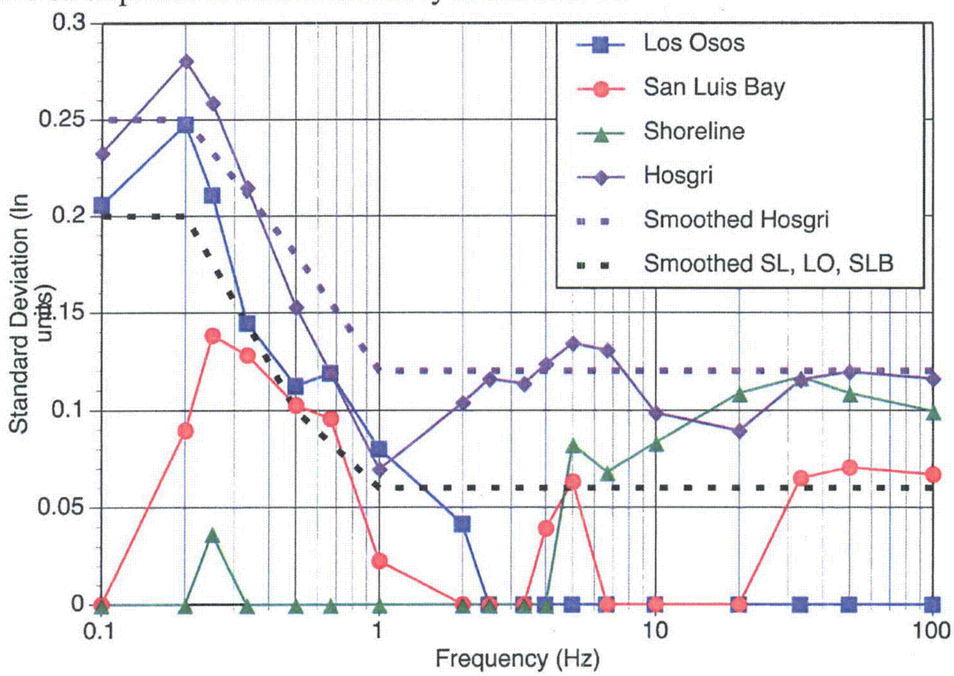

Figure 6-4b. Standard deviation of the addition epistemic uncertainty for the NGA models. The smoothed models for the two groups of fault sources are shown.

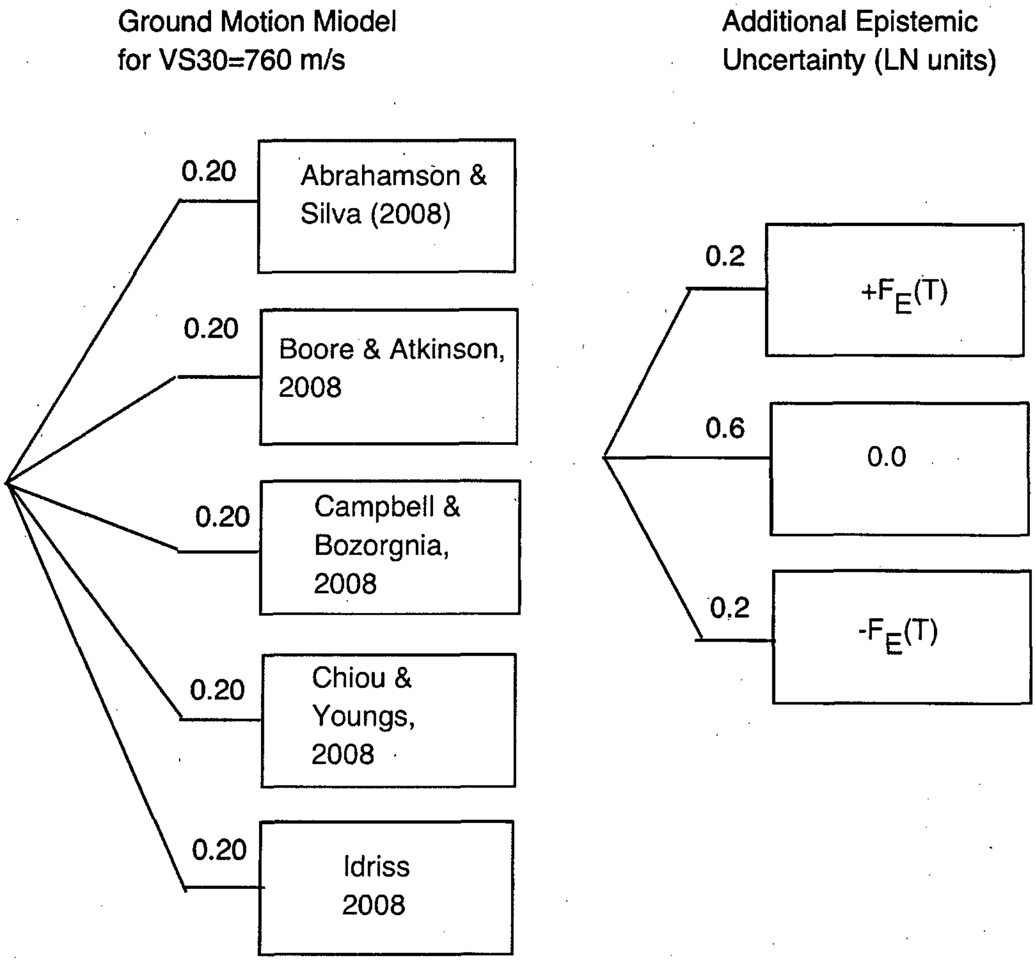

Figure 6-5. Logic tree for ground motion models for crustal earthquakes

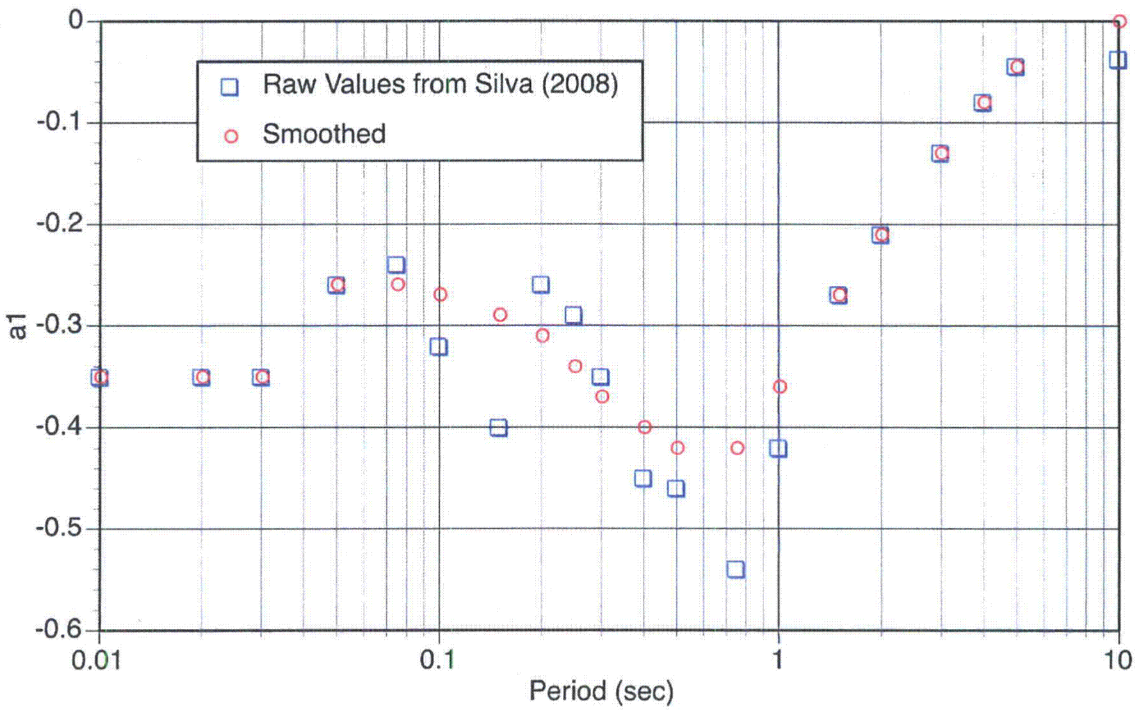

Figure 6-6. Smoothed model of the coefficient for the amplification from V_{S30}=760 m/s to V_{S30}=1200 m/s

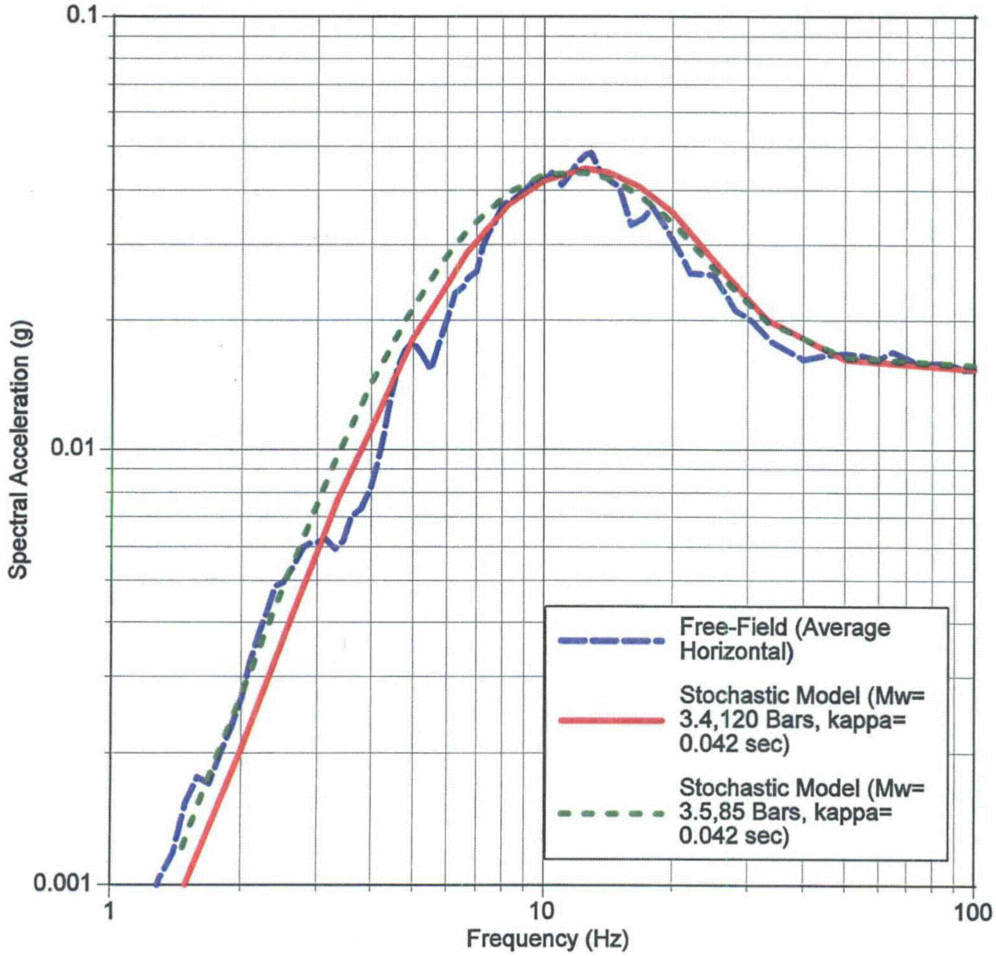

Figure 6-7. Comparison of the average horizontal response spectrum at 5% damping for the free-field recording with the expected California rock site spectrum from a moment magnitude 3.4 earthquake at a distance of 7.8 km with a stress-drop of 120 bars and kappa of 0.042 sec based on the stochastic point source model (red curve). The green curve shows the spectrum if the moment magnitude is 3.5 with a stress-drop of 85 bars. (From Appendix L-1).

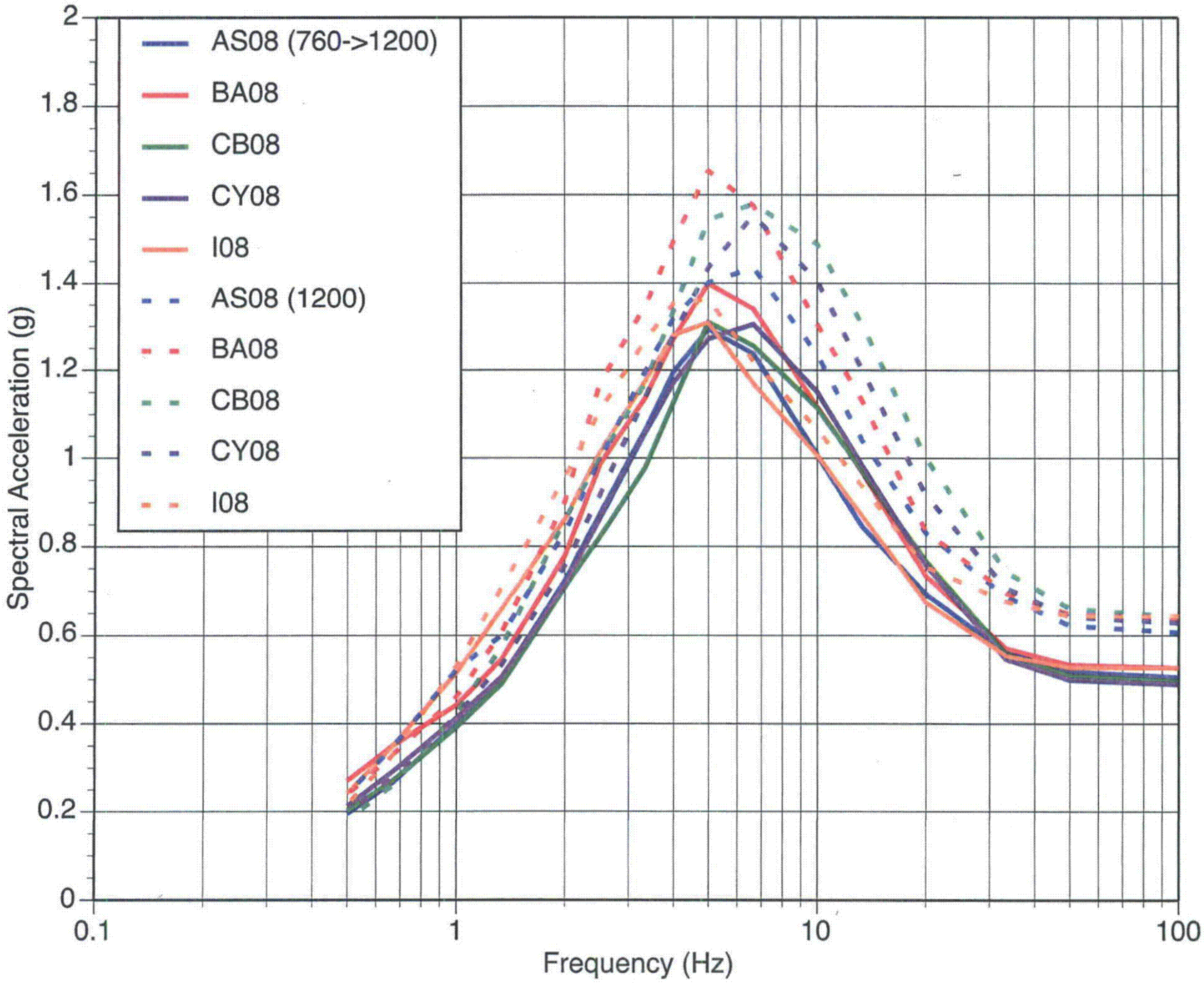

Figure 6-8. Example of effect of the site-specific hard-rock approach (solid lines) versus extrapolating the V_{S30} scaling (dashed lines) for the five NGA models. This example is for a M7.1 SS earthquake at a distance of 4.9 km.

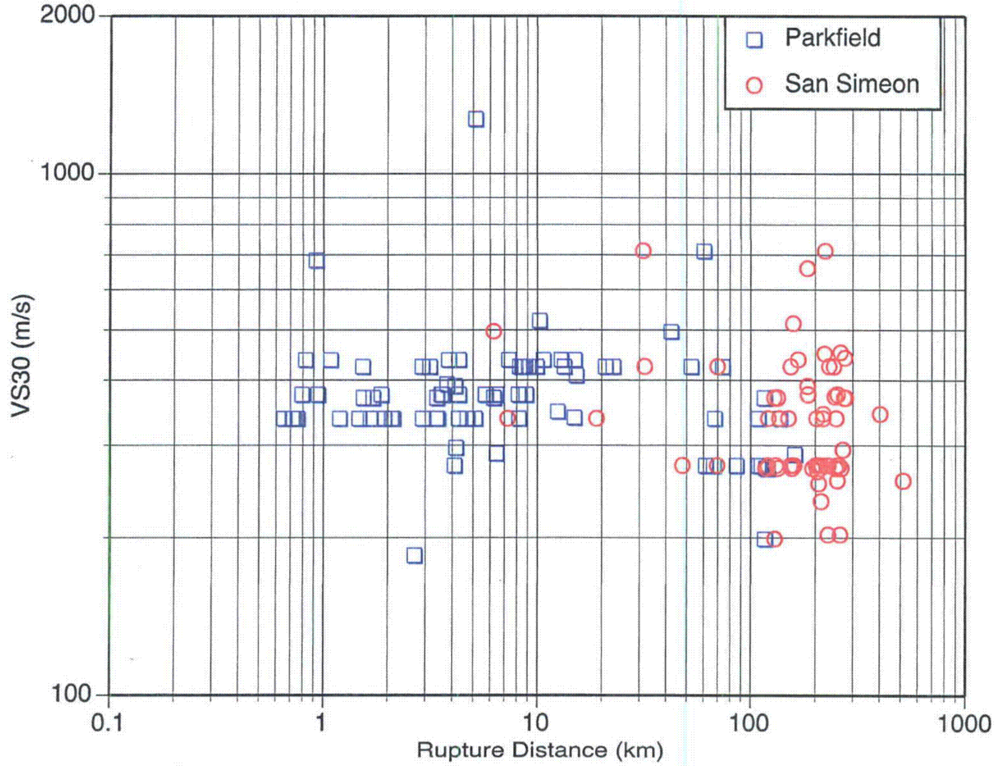

Figure 6-9. Distribution of distances and site conditions for the 2003 San Simeon and 2004 Parkfield earthquakes.

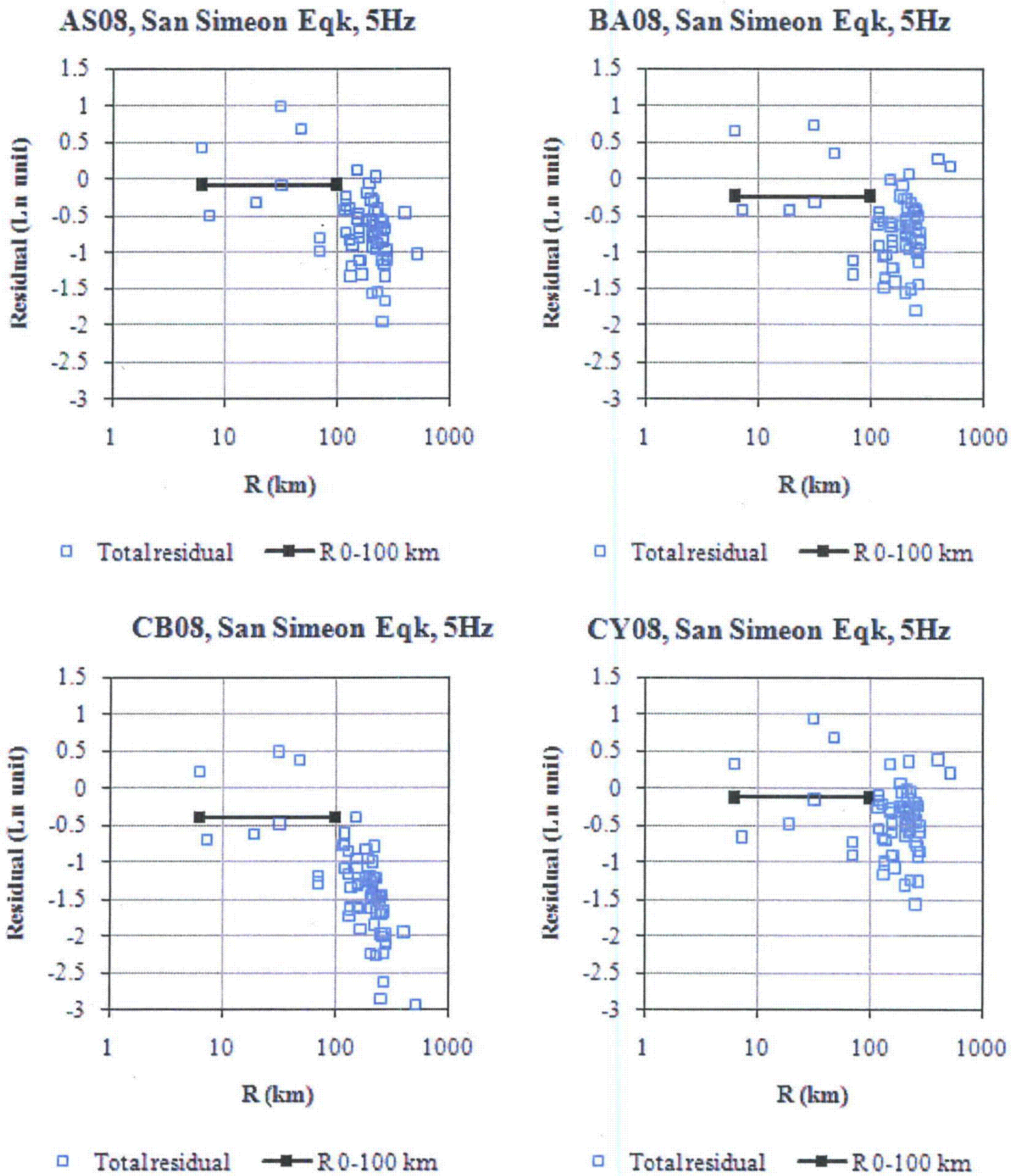

Figure 6-10a. Residuals from the 2003 San Simeon earthquake for 5 Hz spectral acceleration. The rupture distance to DCPP is 35 km. The average residual for stations at distance of 0 to 100 km is shown by the black line.

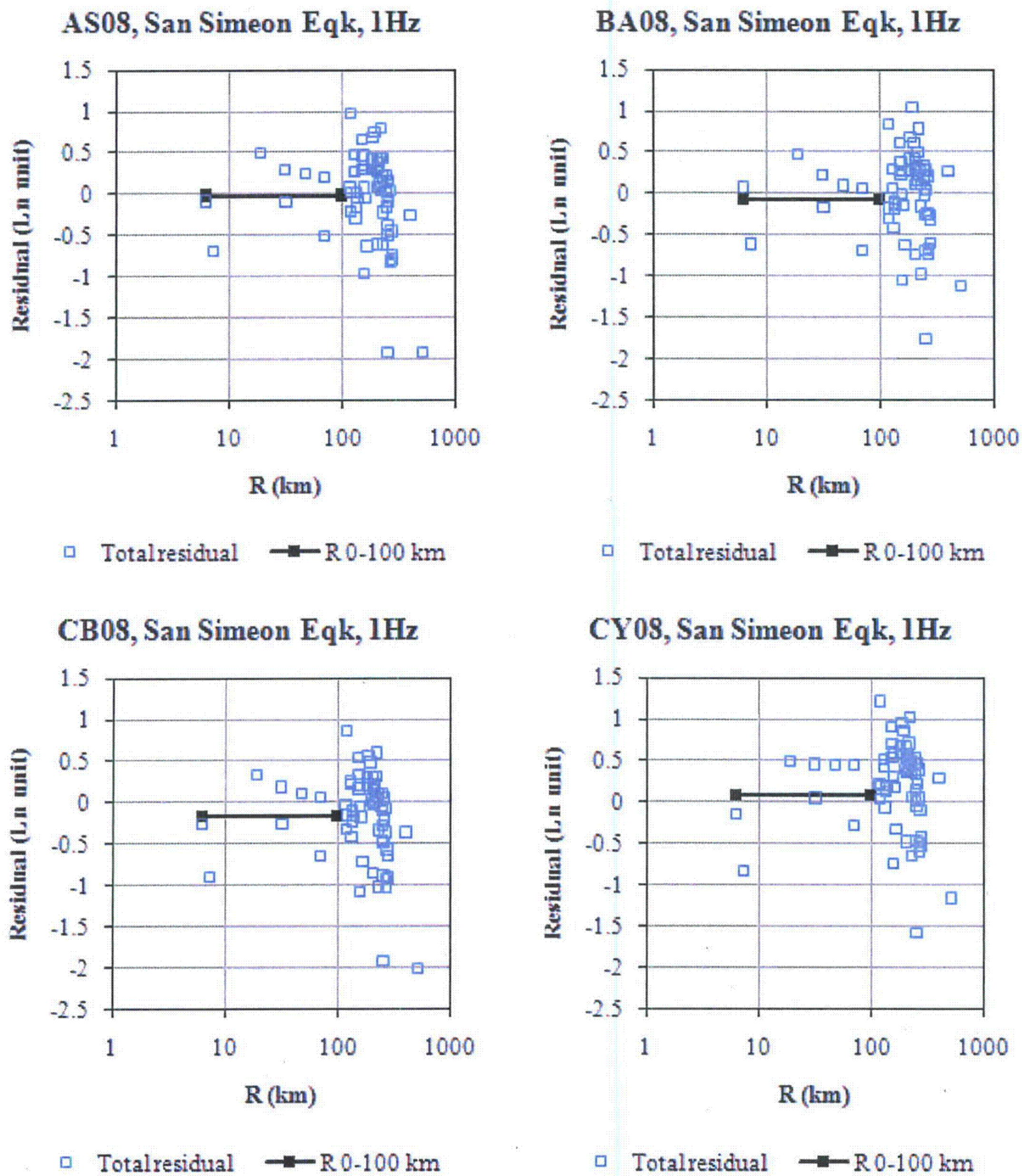

Figure 6-10b. Residuals from the 2003 San Simeon earthquake for 1 Hz spectral acceleration. The rupture distance to DCPP is 35 km. The average residual for stations at distance of 0 to 100 km is shown by the black line.

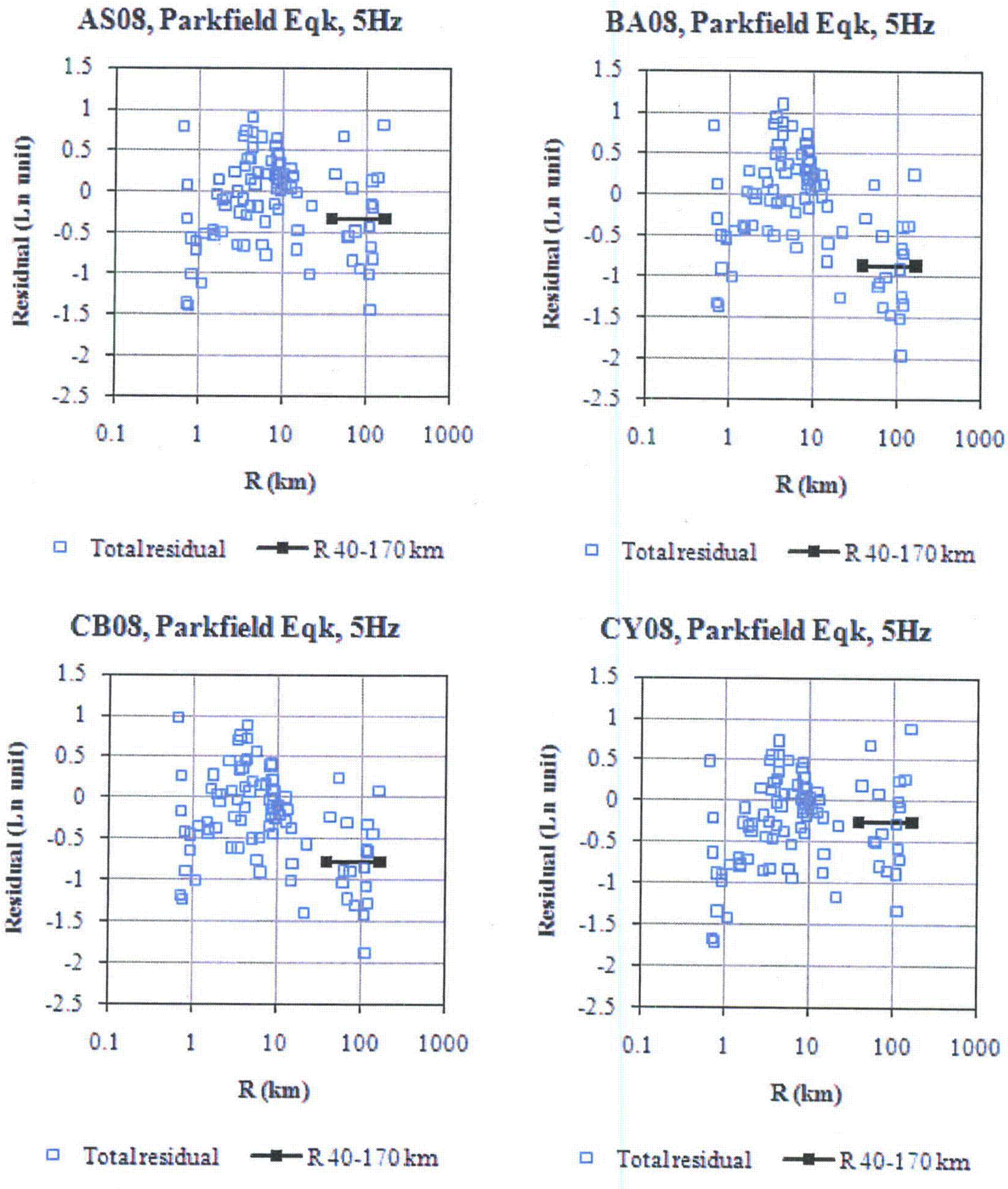

Figure 6-11a. Residuals from the 2004 Parkfield earthquake for 5 Hz spectral acceleration. The rupture distance to DCPP is 85 km. The average residual for stations at distance of 40 to 170 km is shown by the black line.

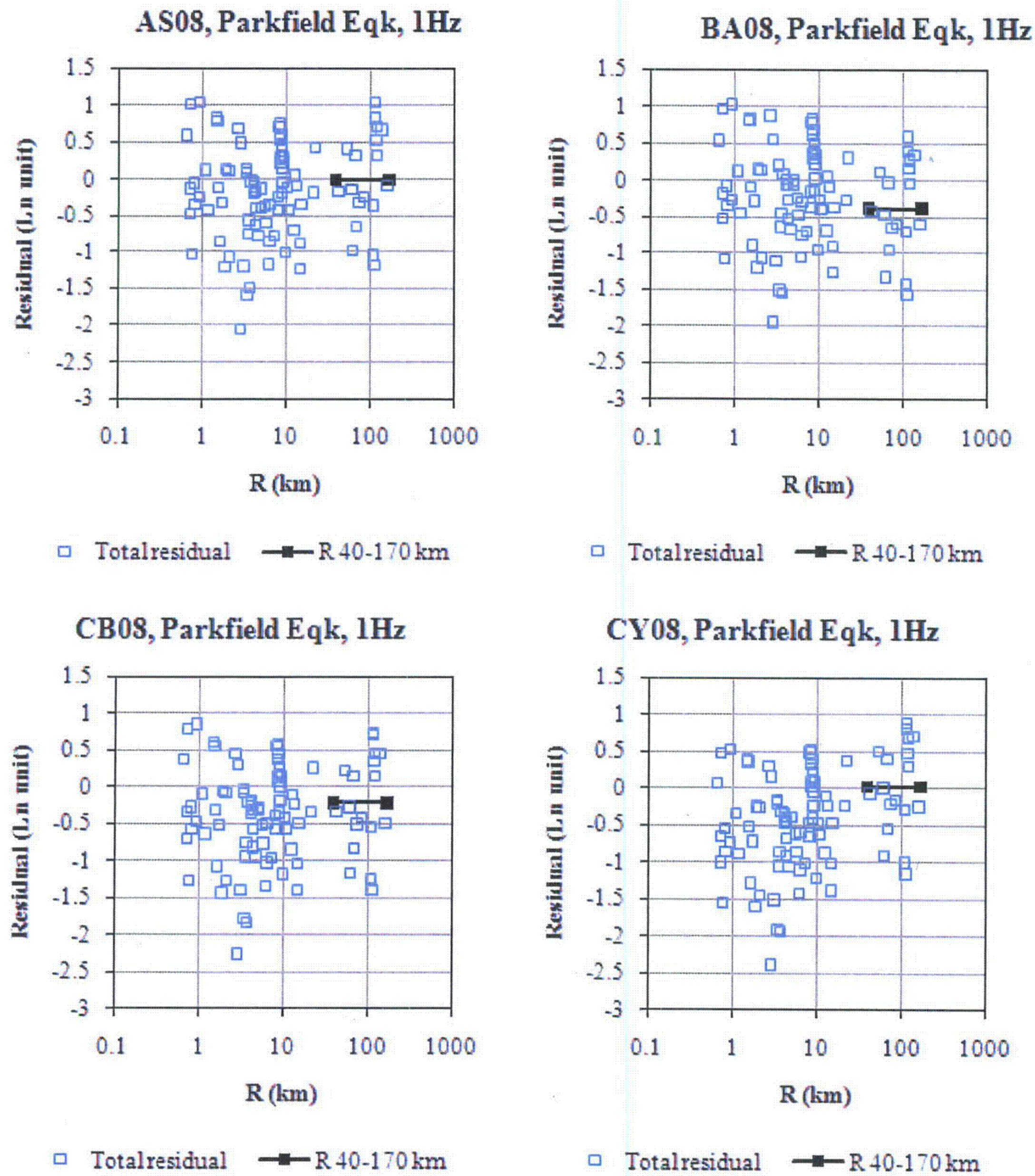

Figure 6-11b. Residuals from the 2004 Parkfield earthquake for 1 Hz spectral acceleration. The rupture distance to DCPP is 85 km. The average residual for stations at distance of 40 to 170 km is shown by the black line.

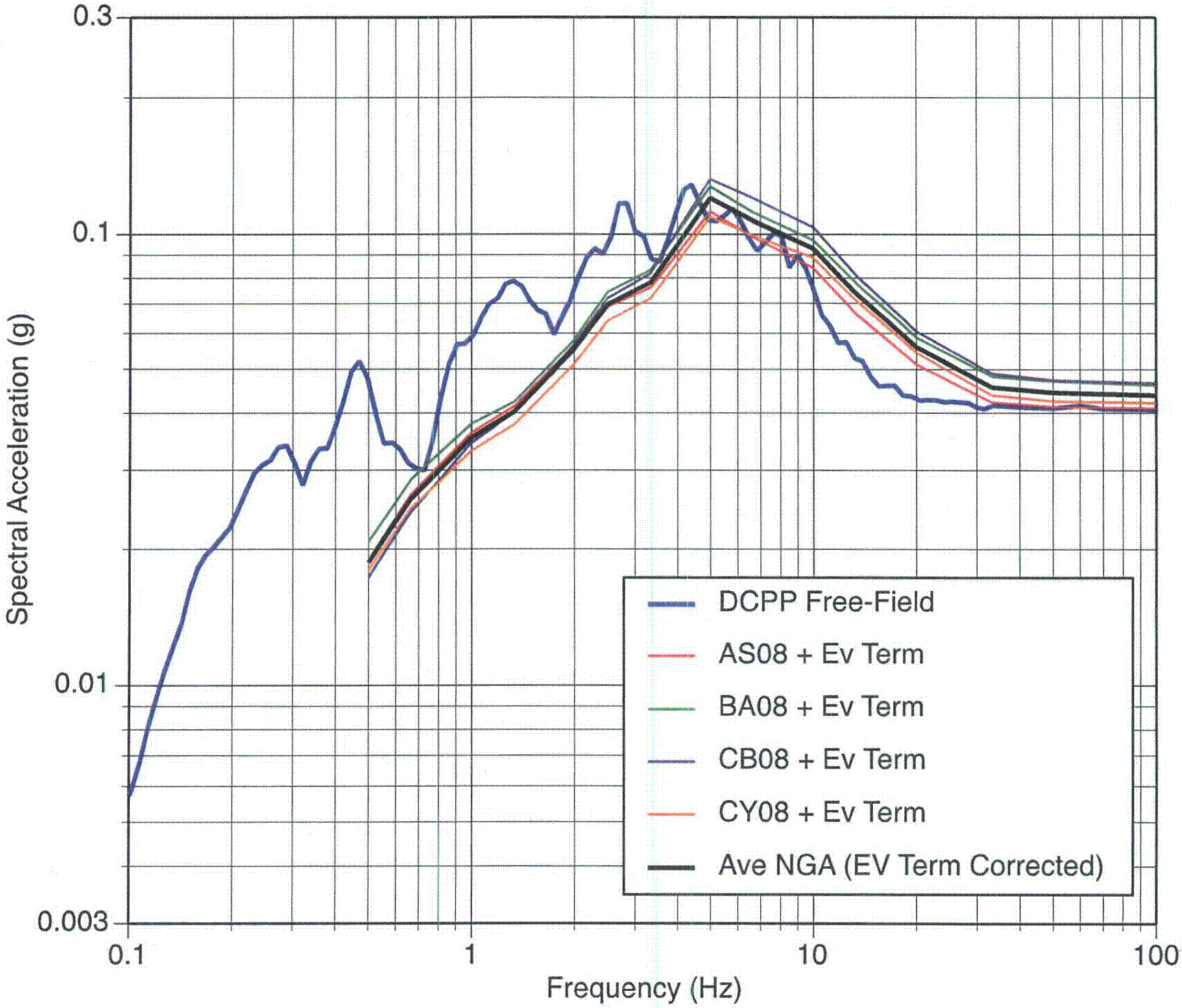

Figure 6-12. Comparison of the event-term adjusted medians from the NGA models with the observed ground motions from the 2003 San Simeon earthquake.

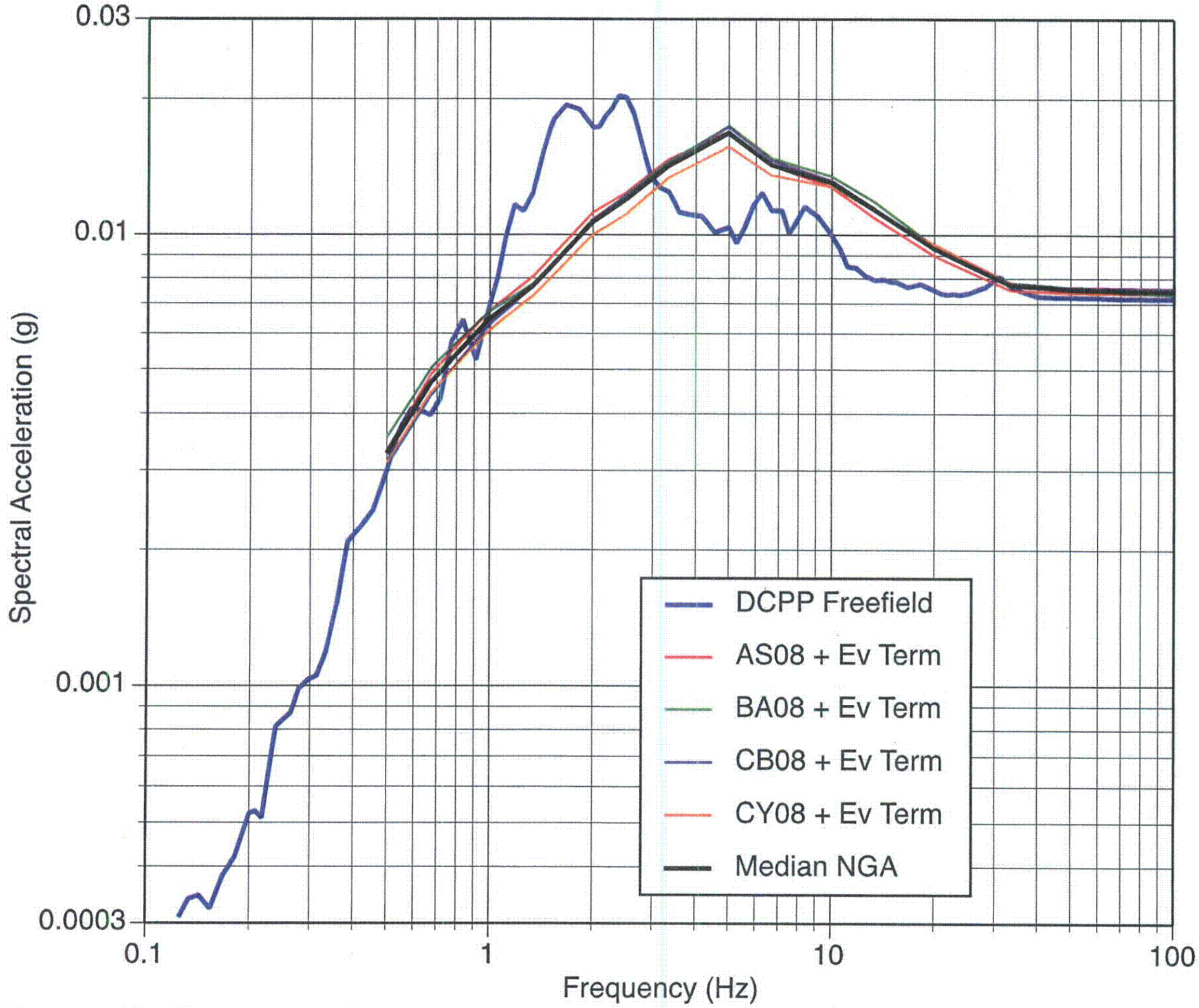

Figure 6-13. Comparison of the event-term adjusted medians from the NGA models with the observed ground motions from the 2004 Parkfield earthquake.

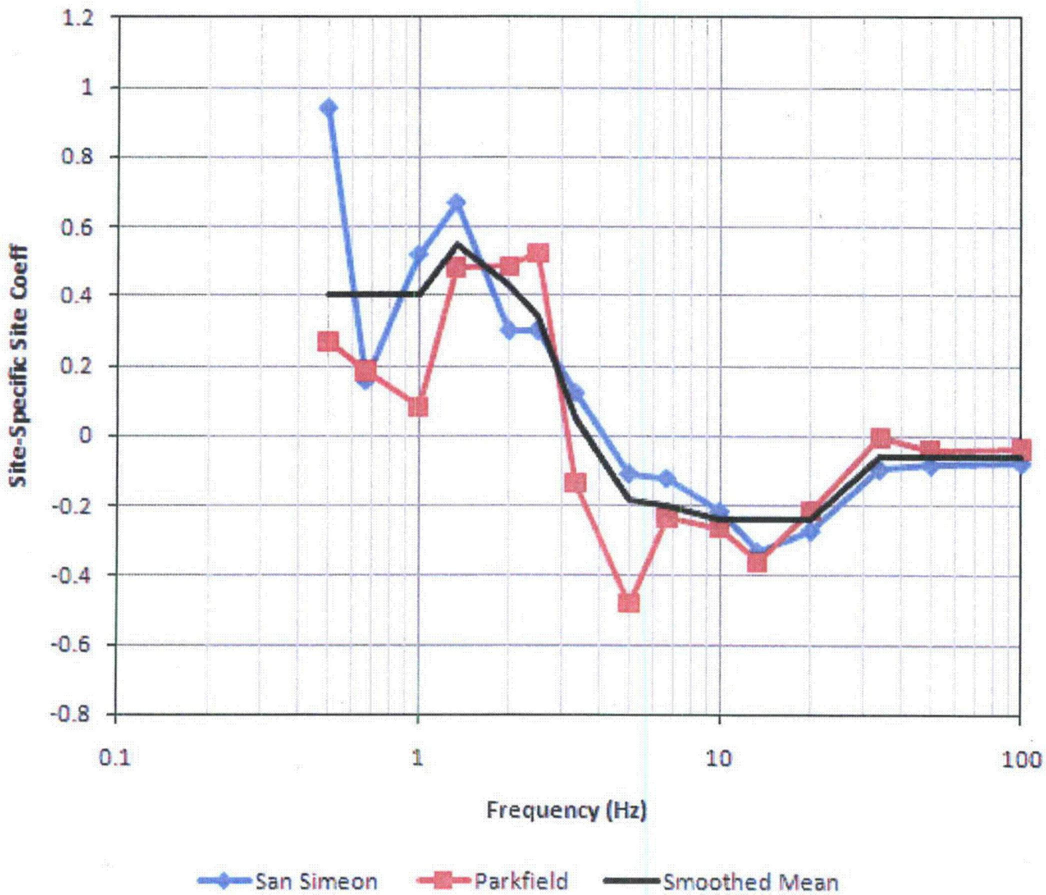

Figure 6-14. Site-specific site amplification terms for DCPP. This shows that the rock site response at DCPP leads to amplified low frequencies (< 0.3 Hz) and reduced high frequencies (5-30 Hz) as compared to average rock sites with V_{S30}=1200 and kappa = 0.04 sec.

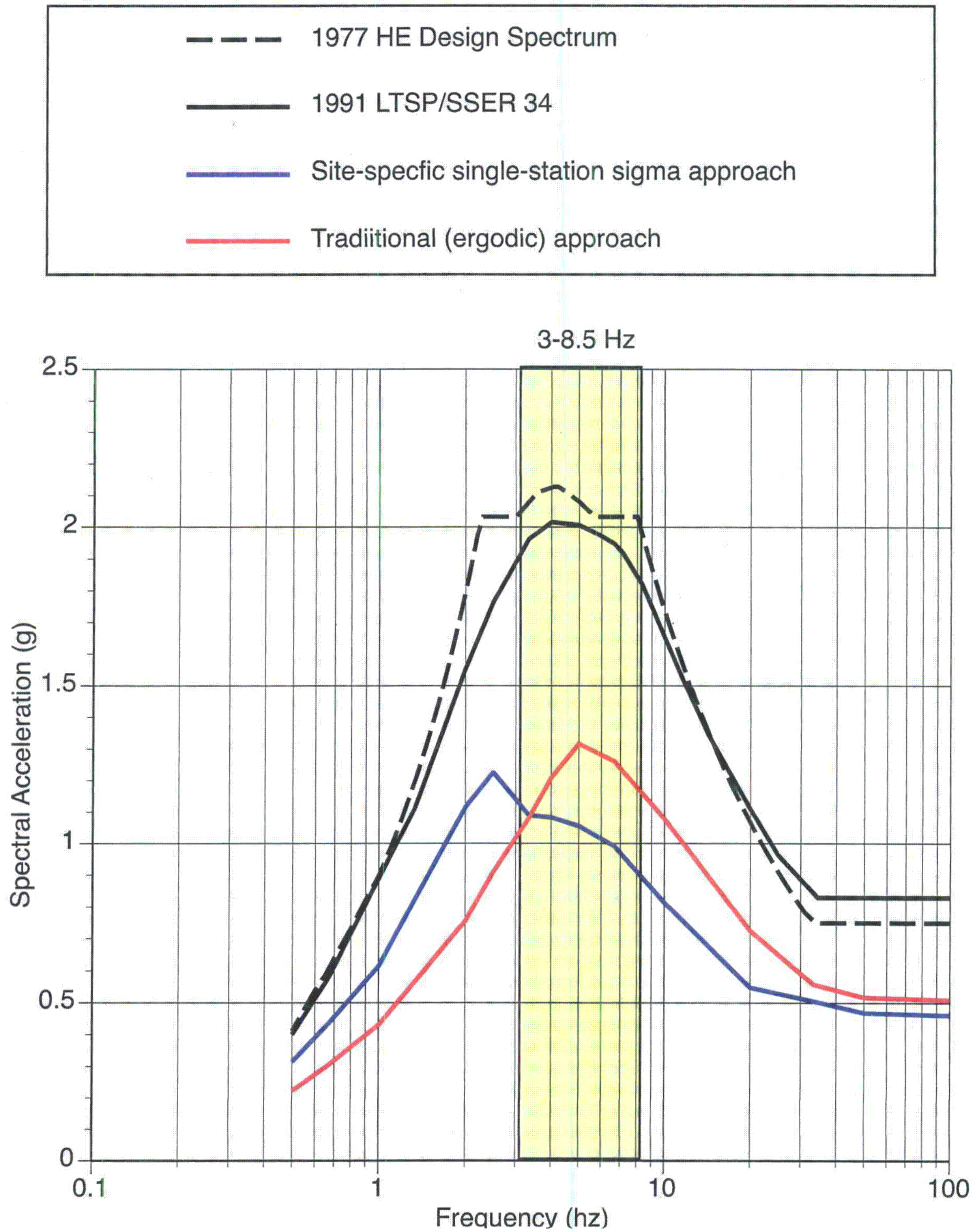

Figure 6-15. Effect of the NGA ground motion models and the site-specific single-station approach for estimating hard-rock motions for nearby strike-slip as compared to the HE design spectrum and the LTSP/SSER spectrum. This example is for a magnitude 7.1 strike-slip earthquake at a distance of 5 km.

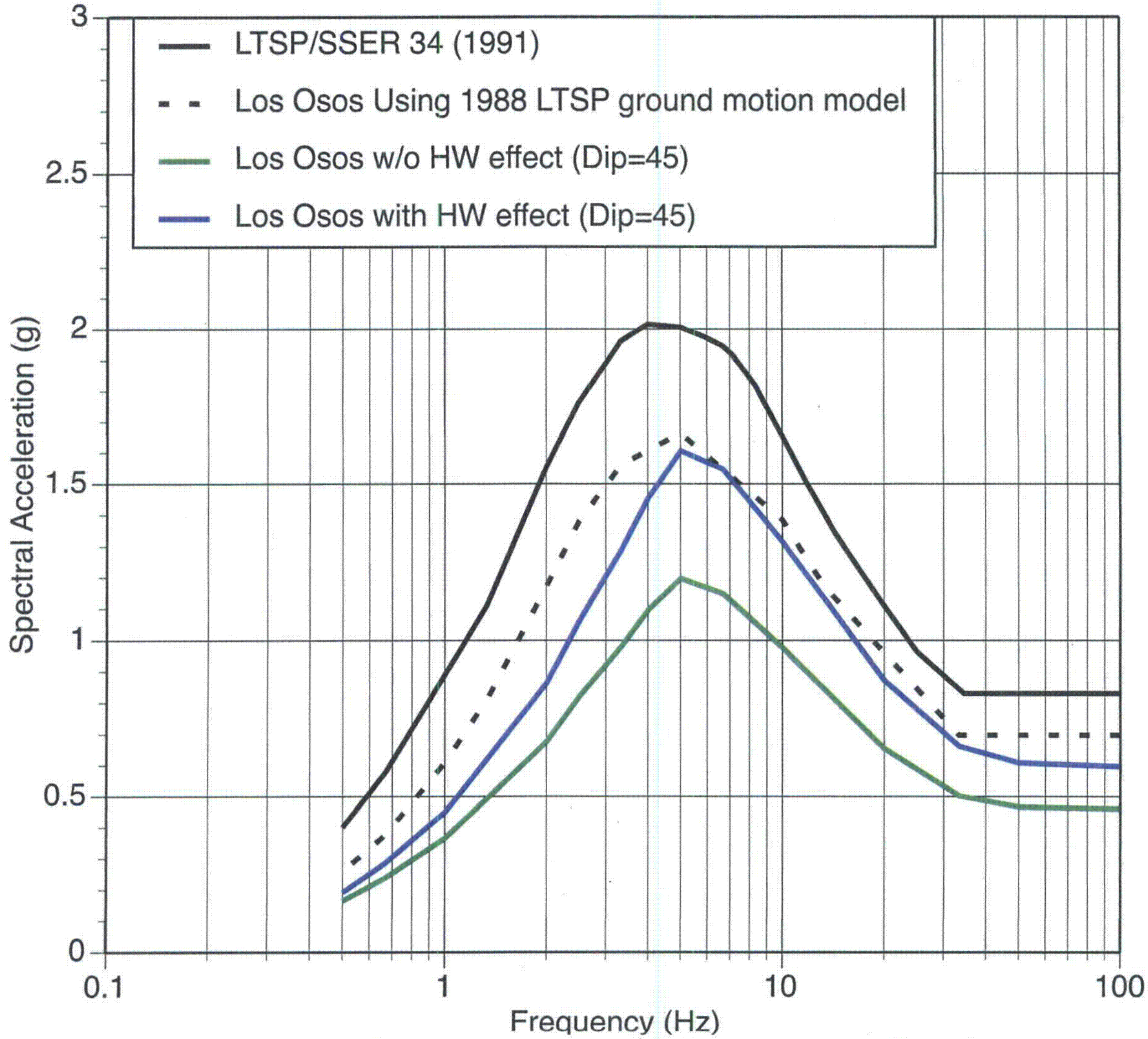

Figure 6-16. Effect of the NGA ground motion models for the Los Osos fault source for the traditional ergodic approach. The hanging wall effect included in the NGA models leads to larger high-frequency ground motions for sites on the hanging wall.

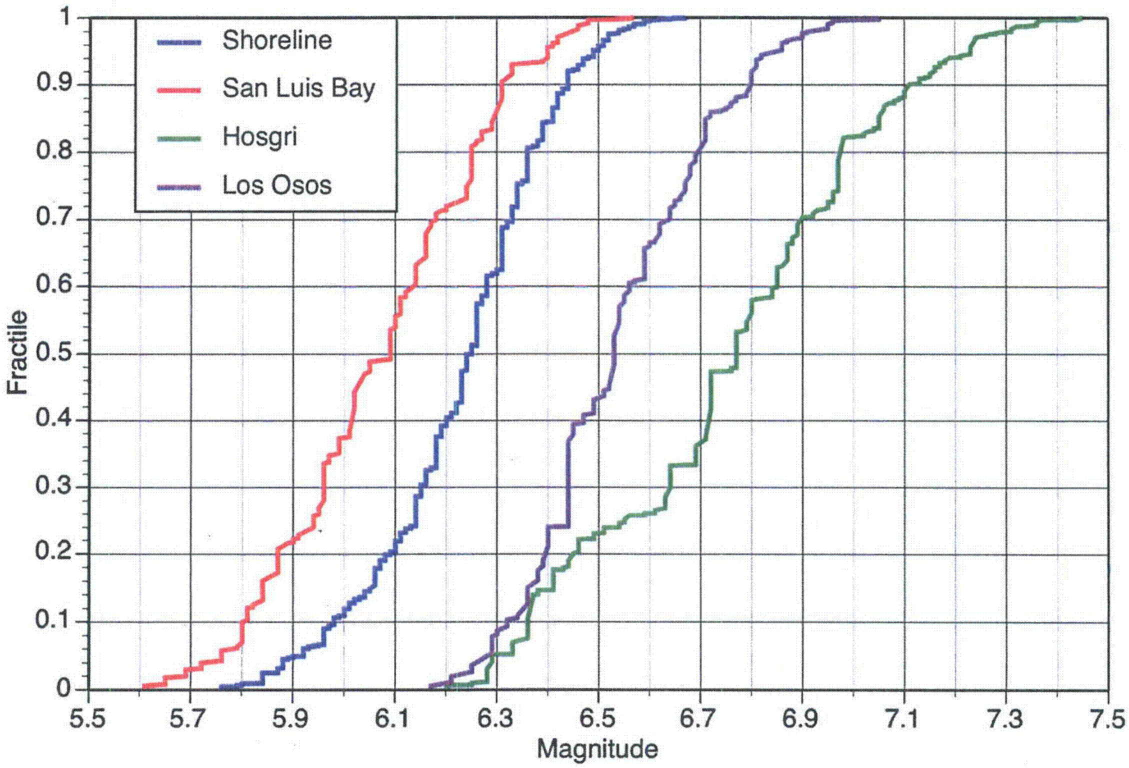

Figure 6-17. Magnitude fractiles from the logic trees for four fault sources

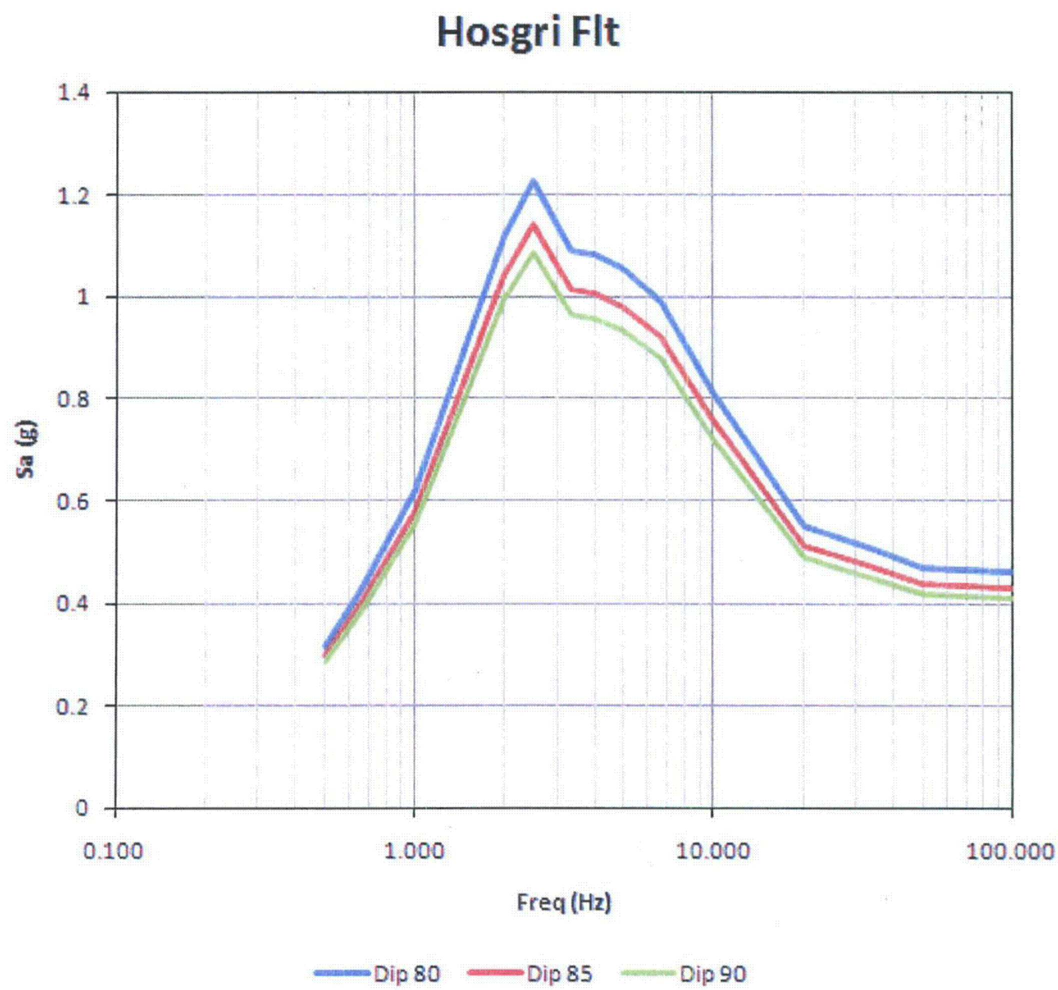

Figure 6-18a. Sensitivity of the deterministic ground motions to the dip of the Hosgri fault source.

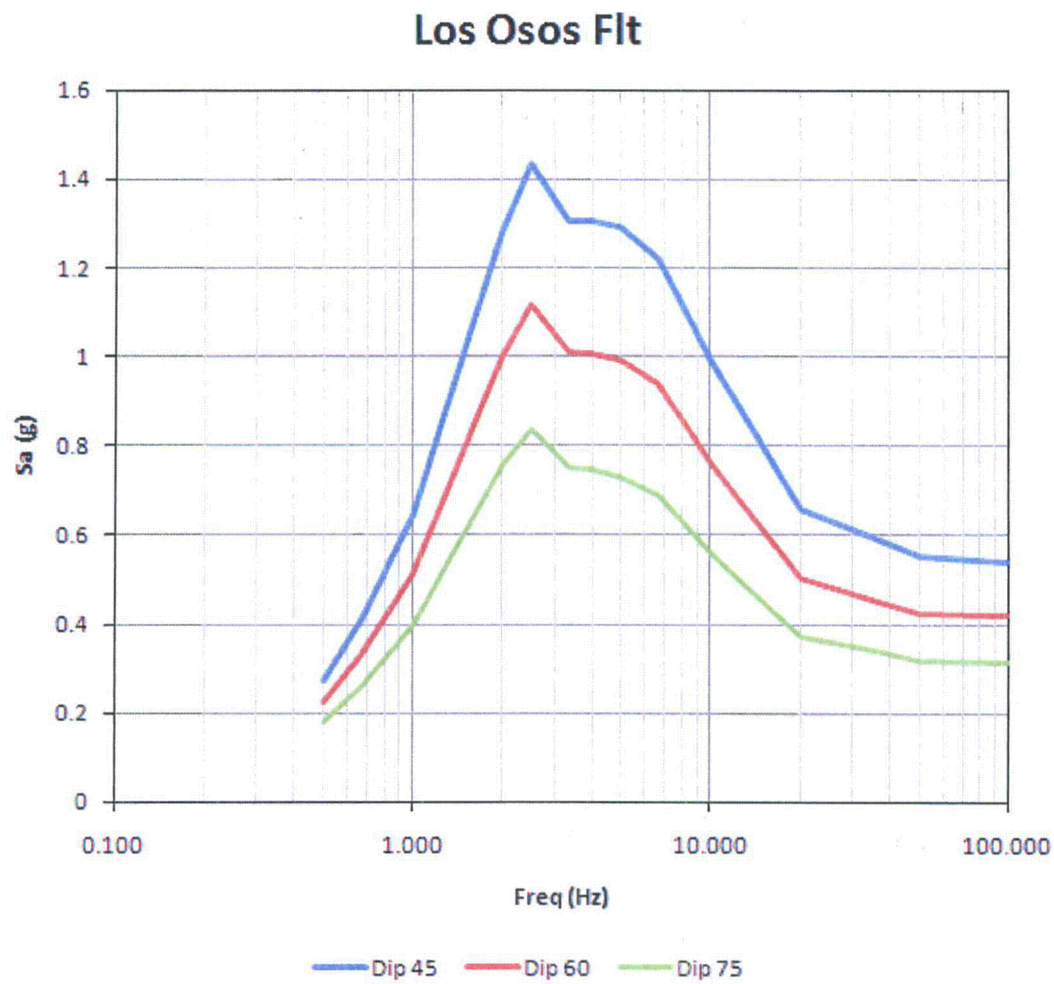

Figure 6-18b. Sensitivity of the deterministic ground motions to the dip of the Los Osos fault source.

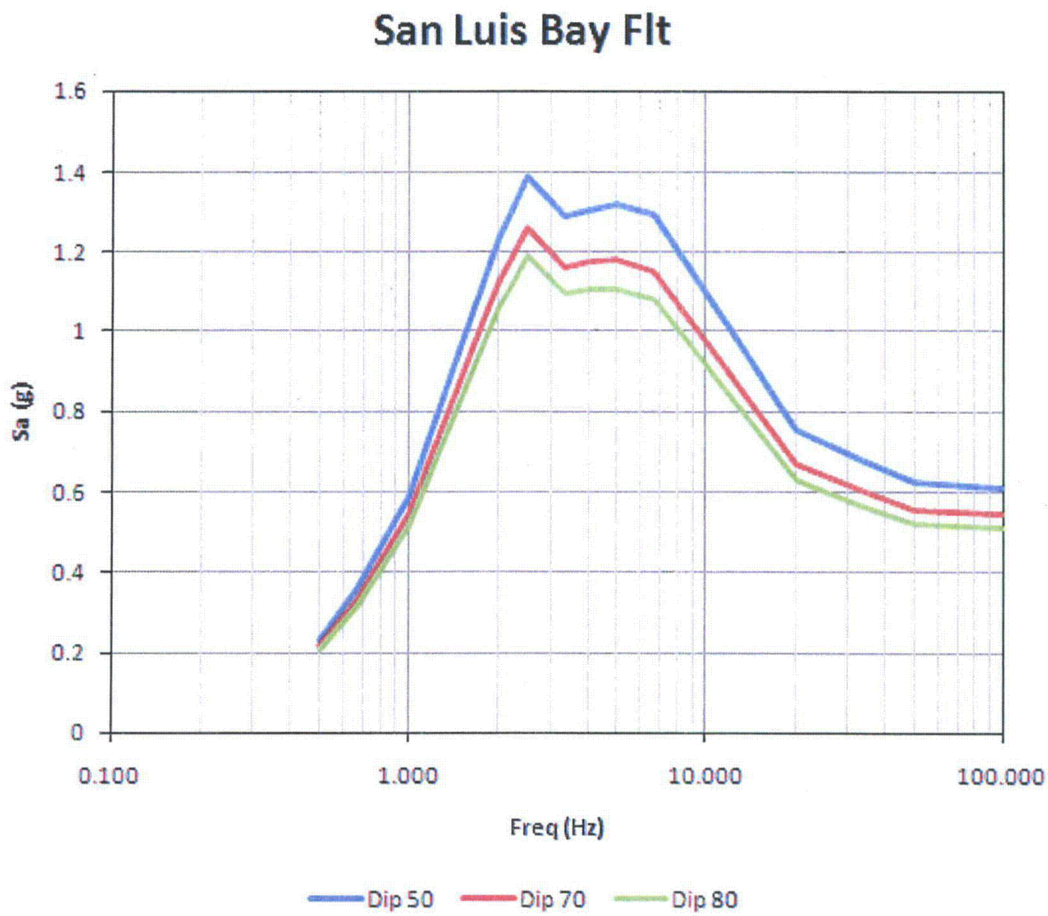

Figure 6-18c. Sensitivity of the deterministic ground motions to the dip of the San Luis Bay fault source.

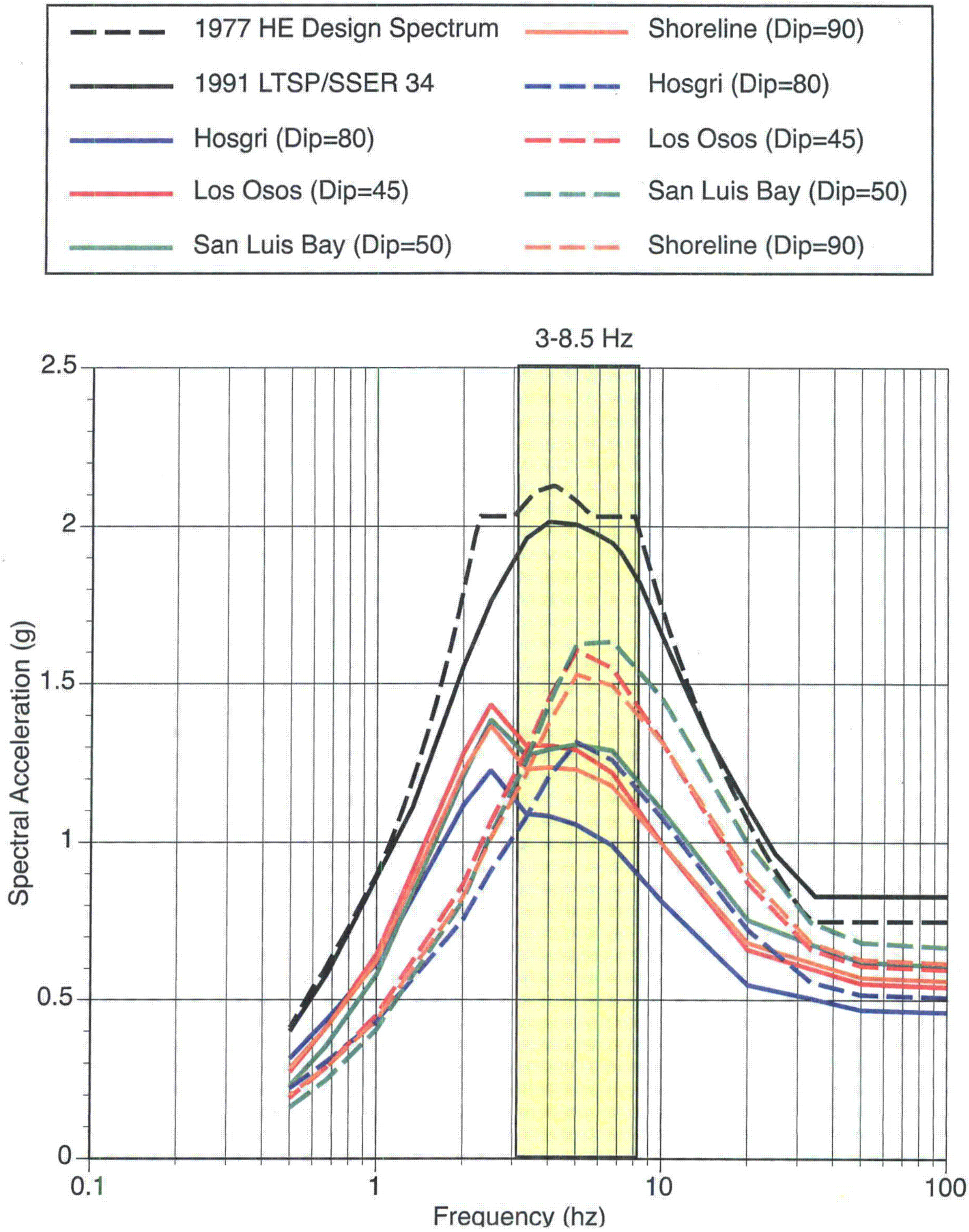

Figure 6-19. 84th percentile ground motion from the four nearby fault sources using the site-specific single-station sigma approach (solid lines) and the traditional ergodic approach (dashed lines). The 2.5 Hz peak in the site-specific spectrum reflects the DCPP site amplification.

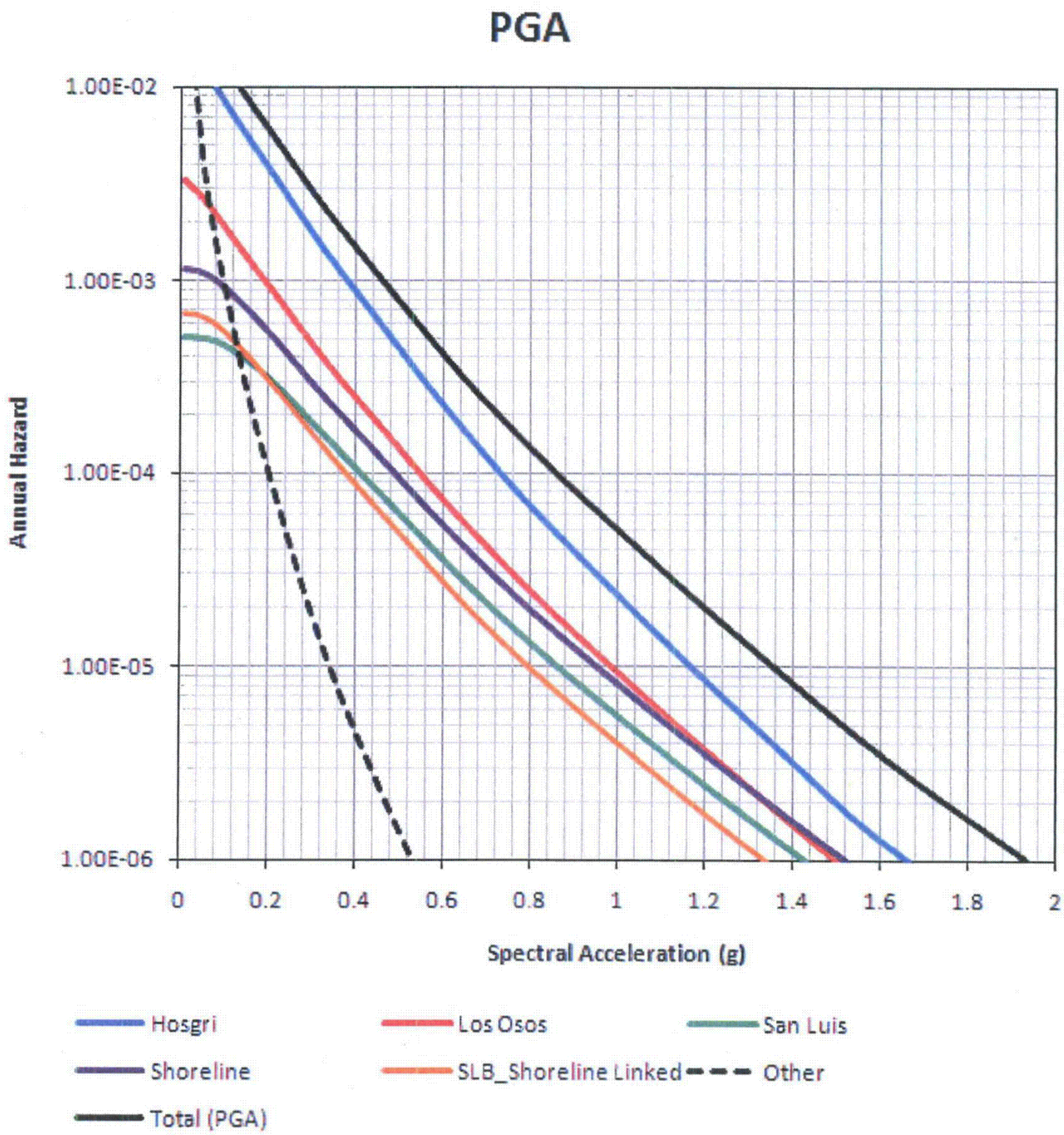

Figure 6-20a. Hazard by fault sources for PGA; the Other source includes regional sources listed on Table 6-9.

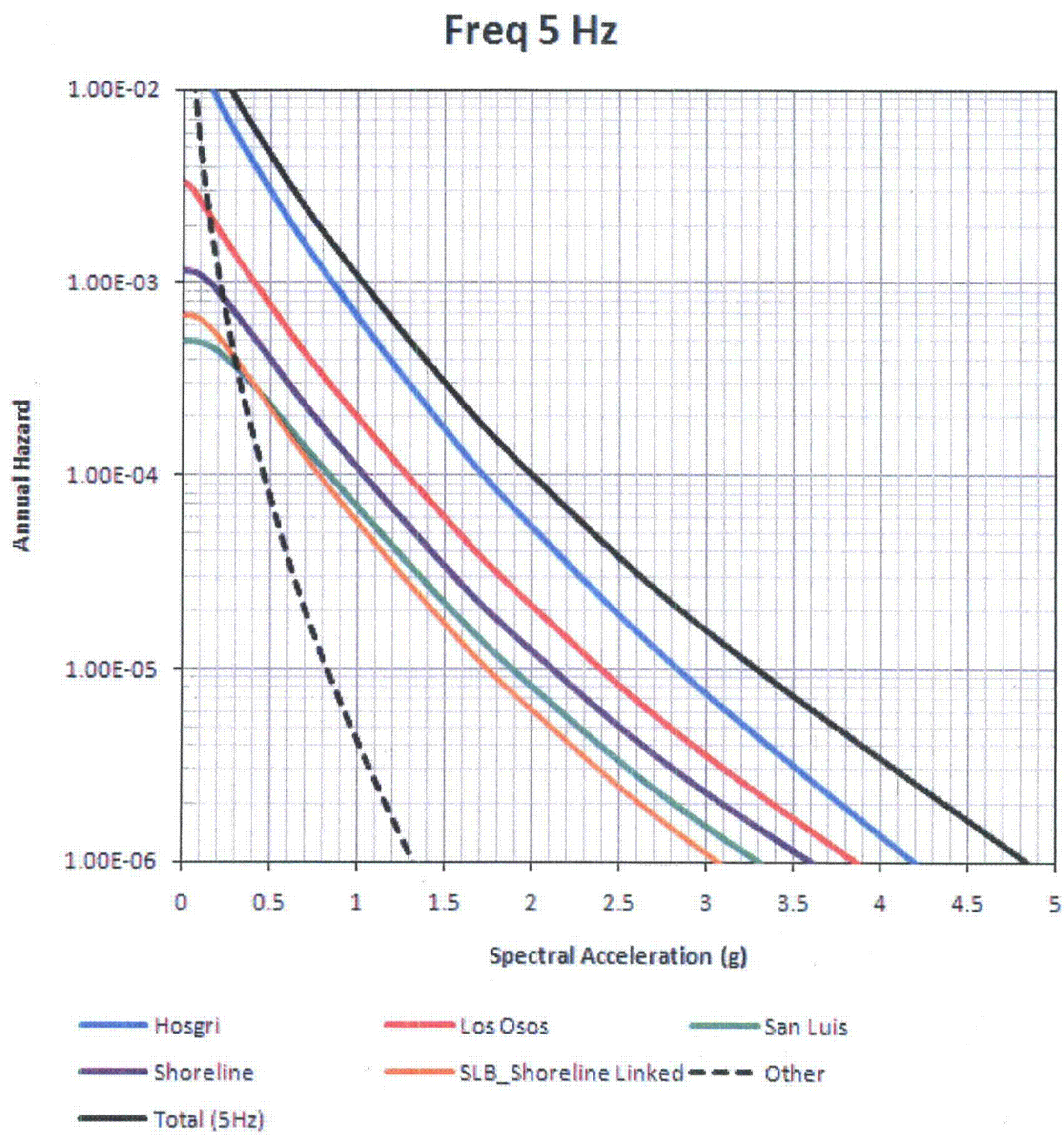

Figure 6-20b. Hazard by source for 5 Hz spectral acceleration.

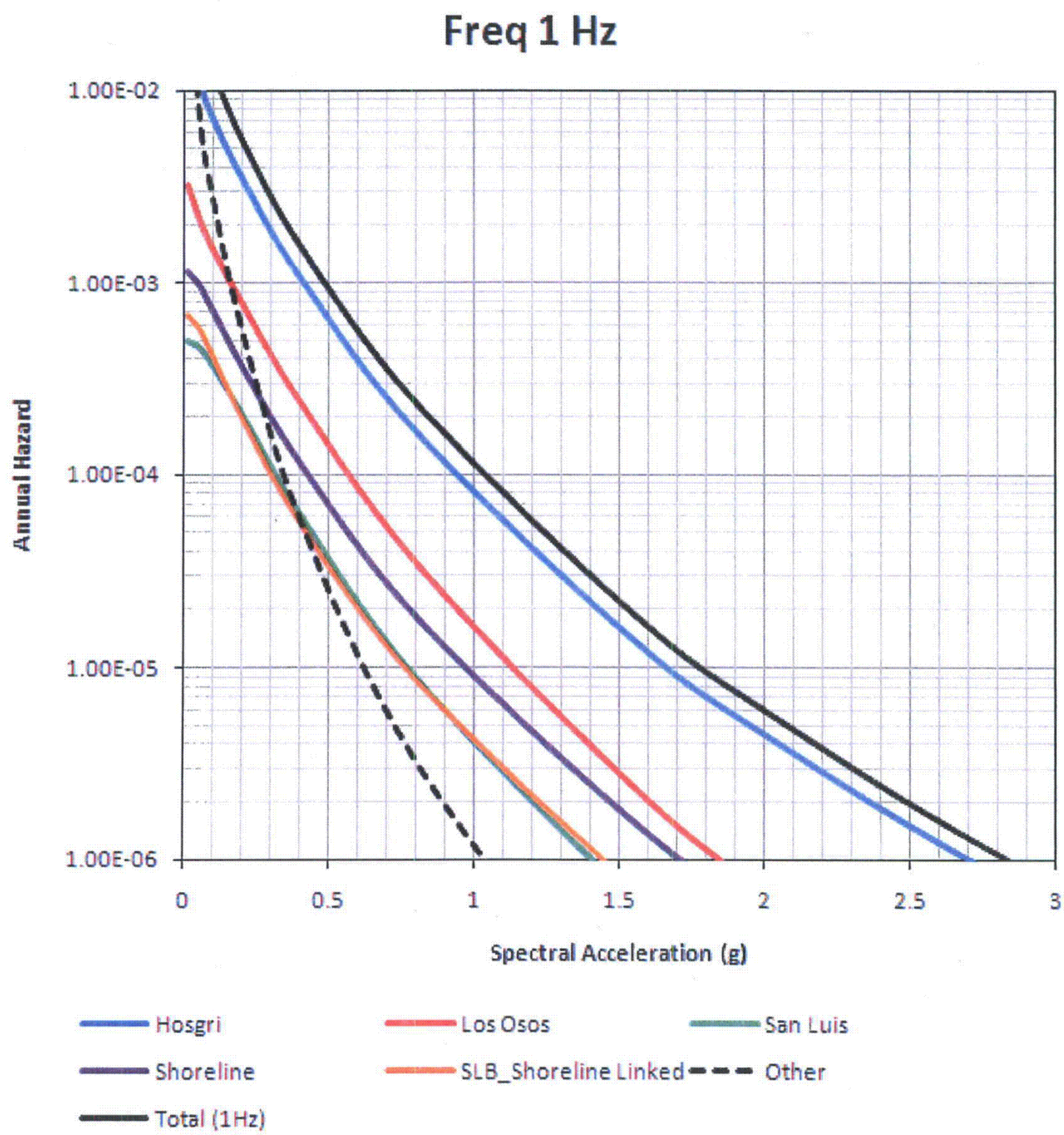

Figure 6-20c. Hazard by source for 1 Hz spectral acceleration.

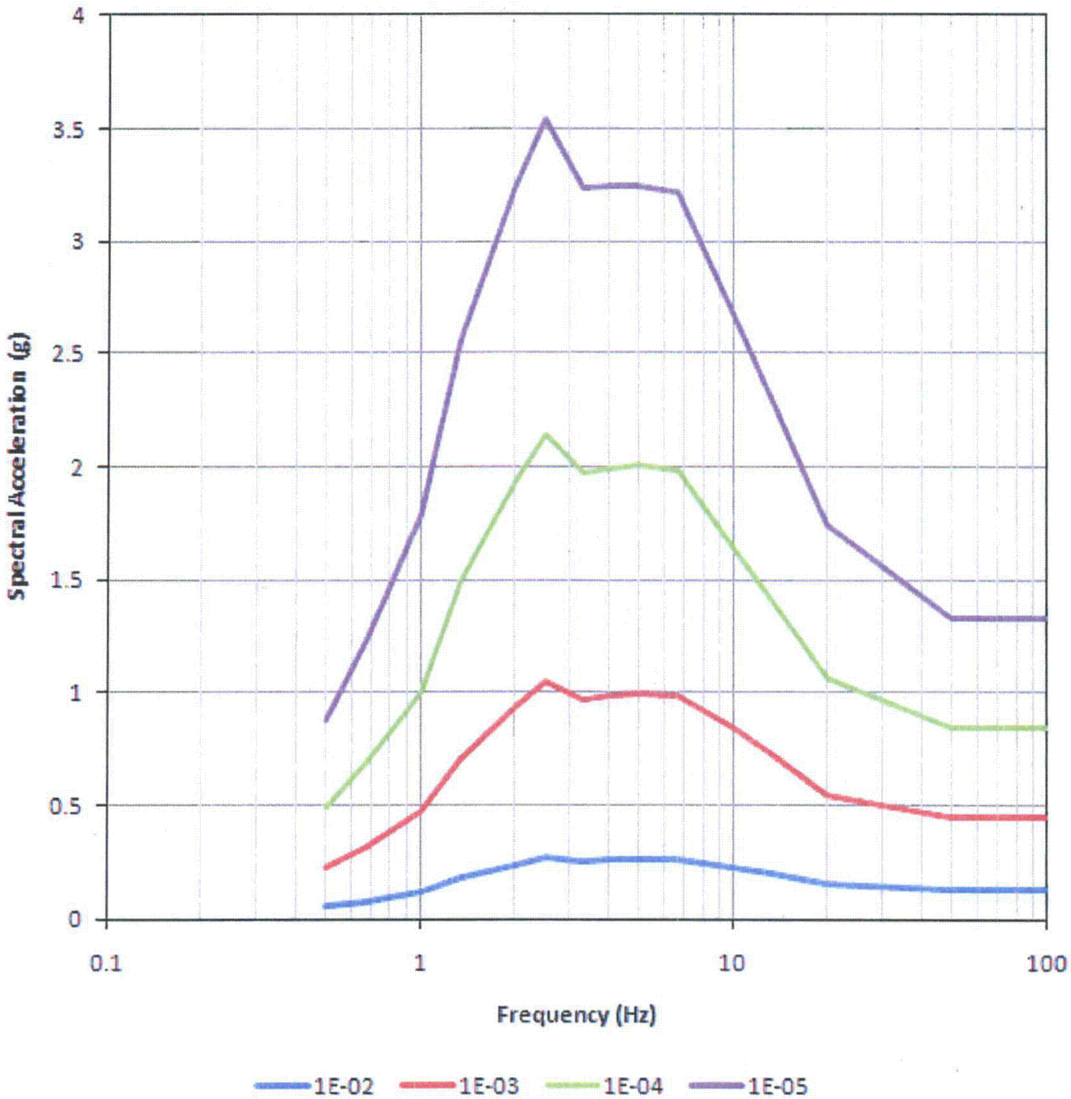

Figure 6-21. Uniform hazard spectra for four hazard levels. The peak at 2.5 Hz reflects the site-specific amplification at DCPP.

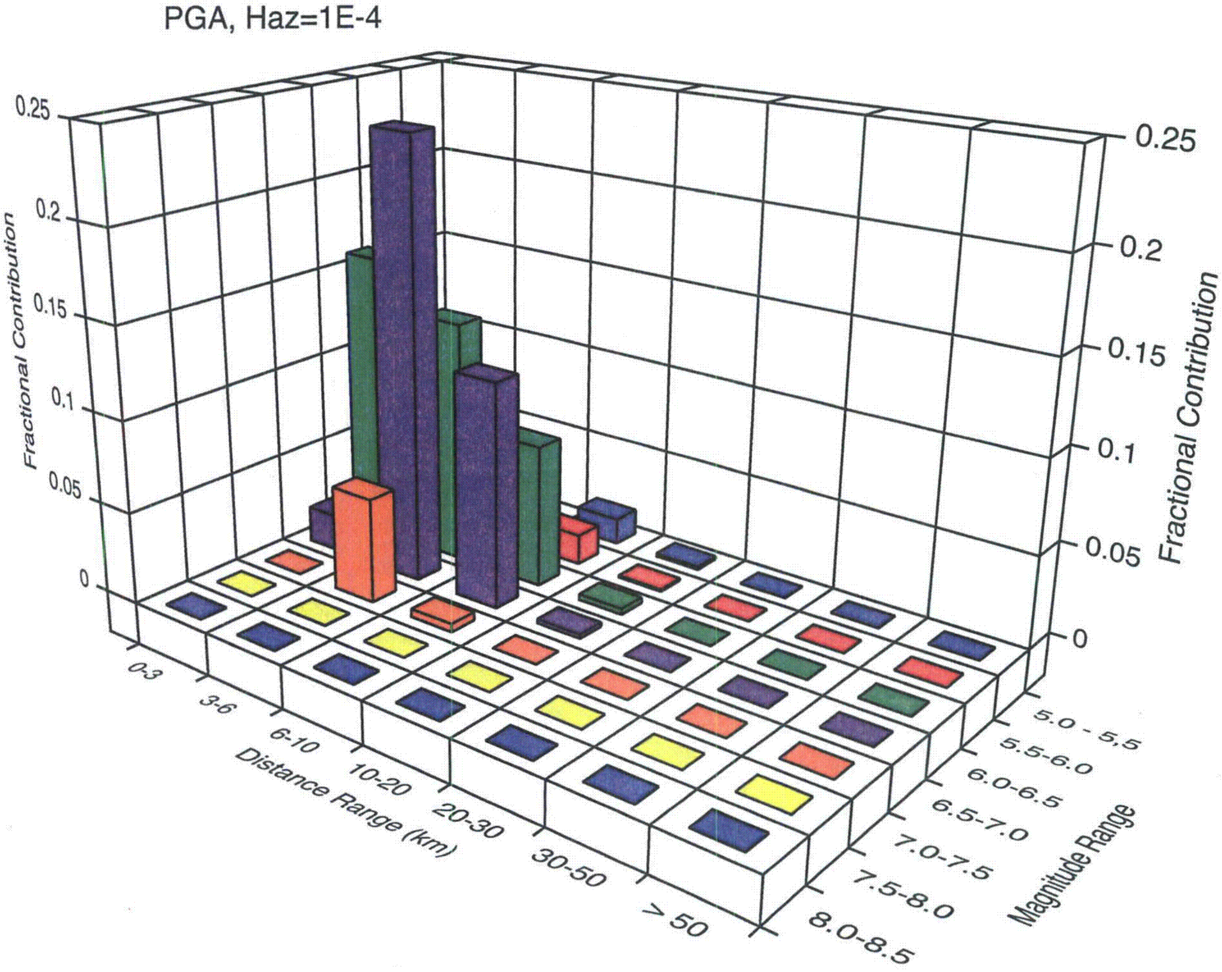

Figure 6-22a. Deaggregation for PGA for a hazard level of 1E-4.

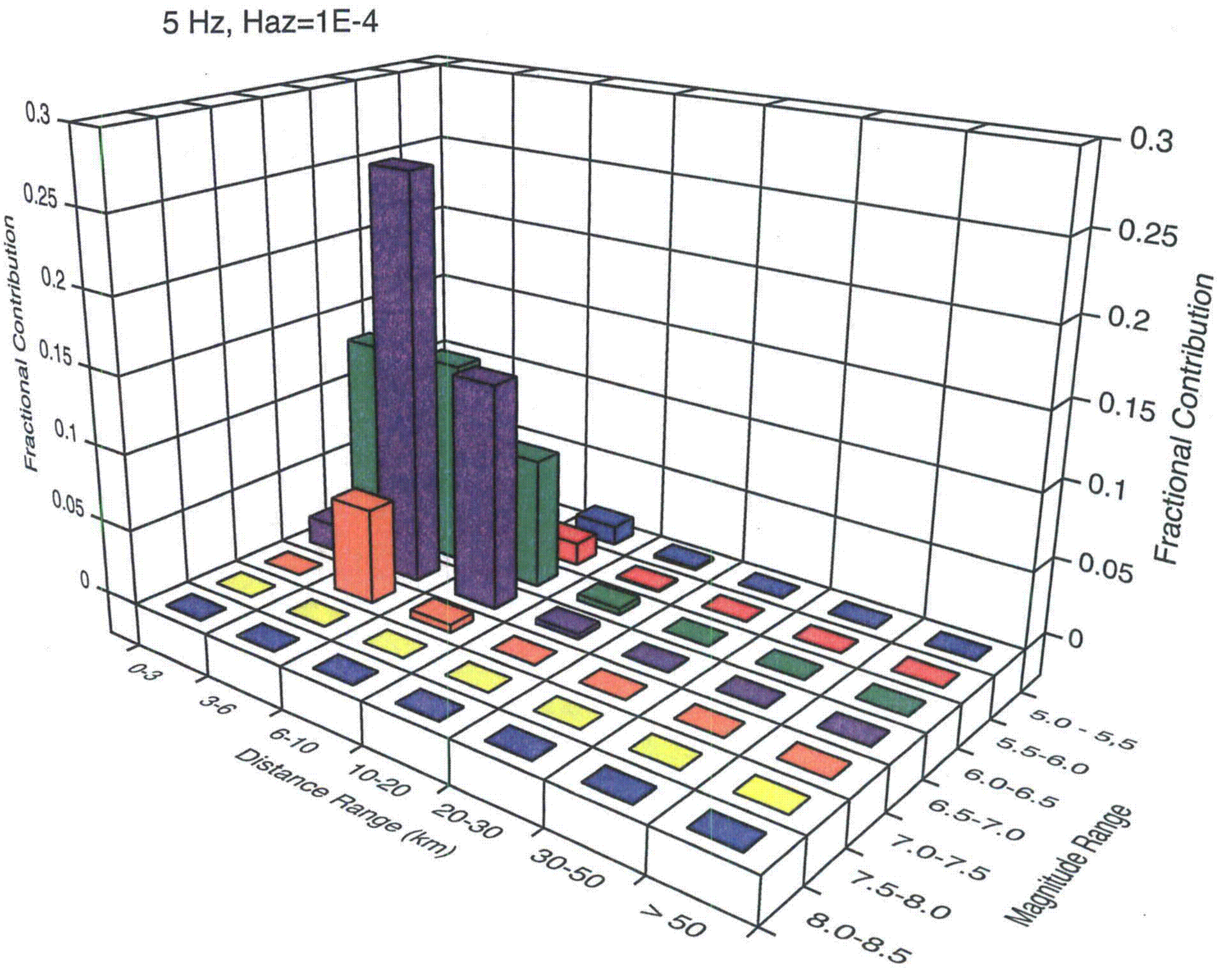

Figure 6-22b. Deaggregation for 5 Hz for a hazard level of 1E-4.

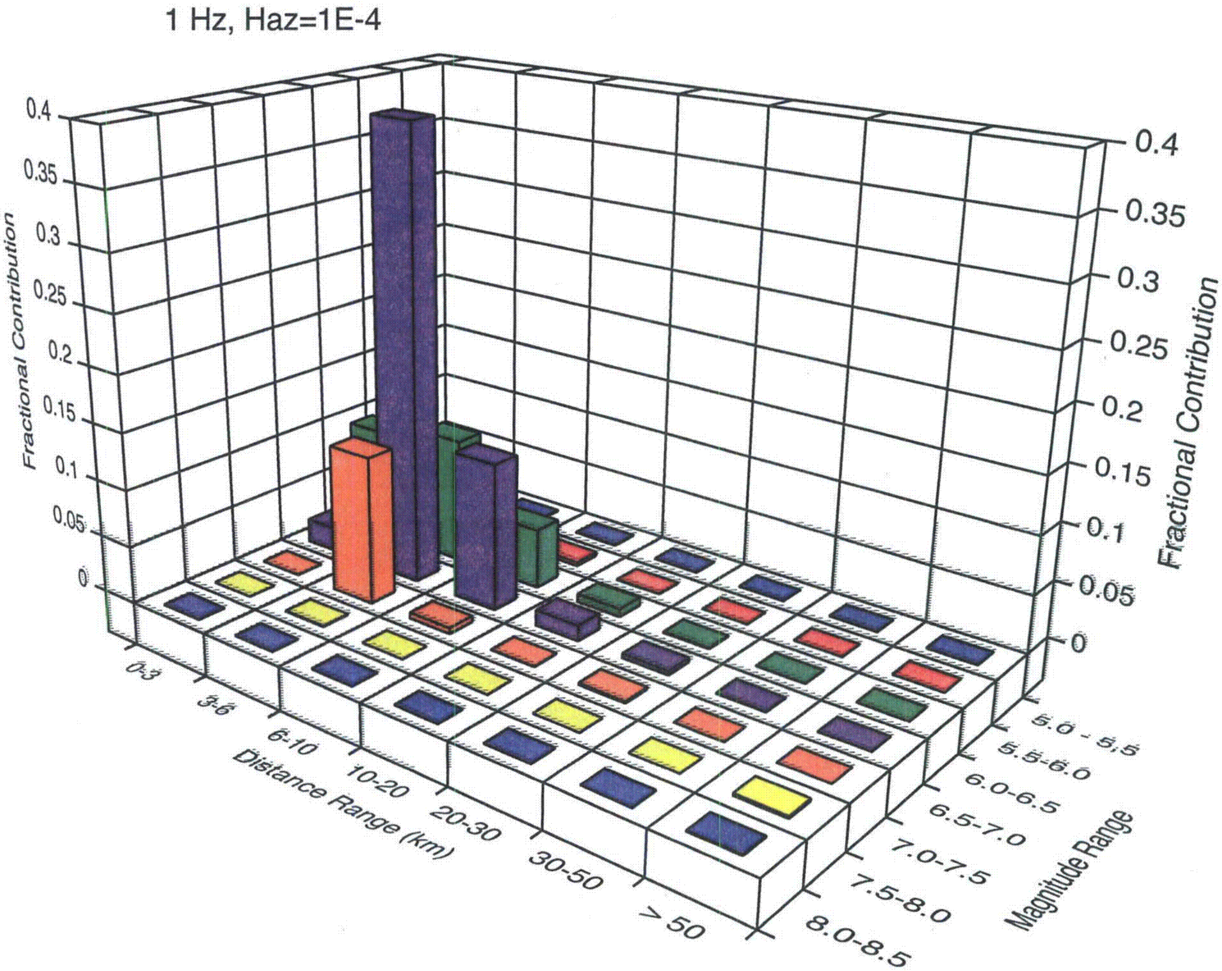

Figure 6-22c. Deaggregation for 1 Hz for a hazard level of 1E-4.

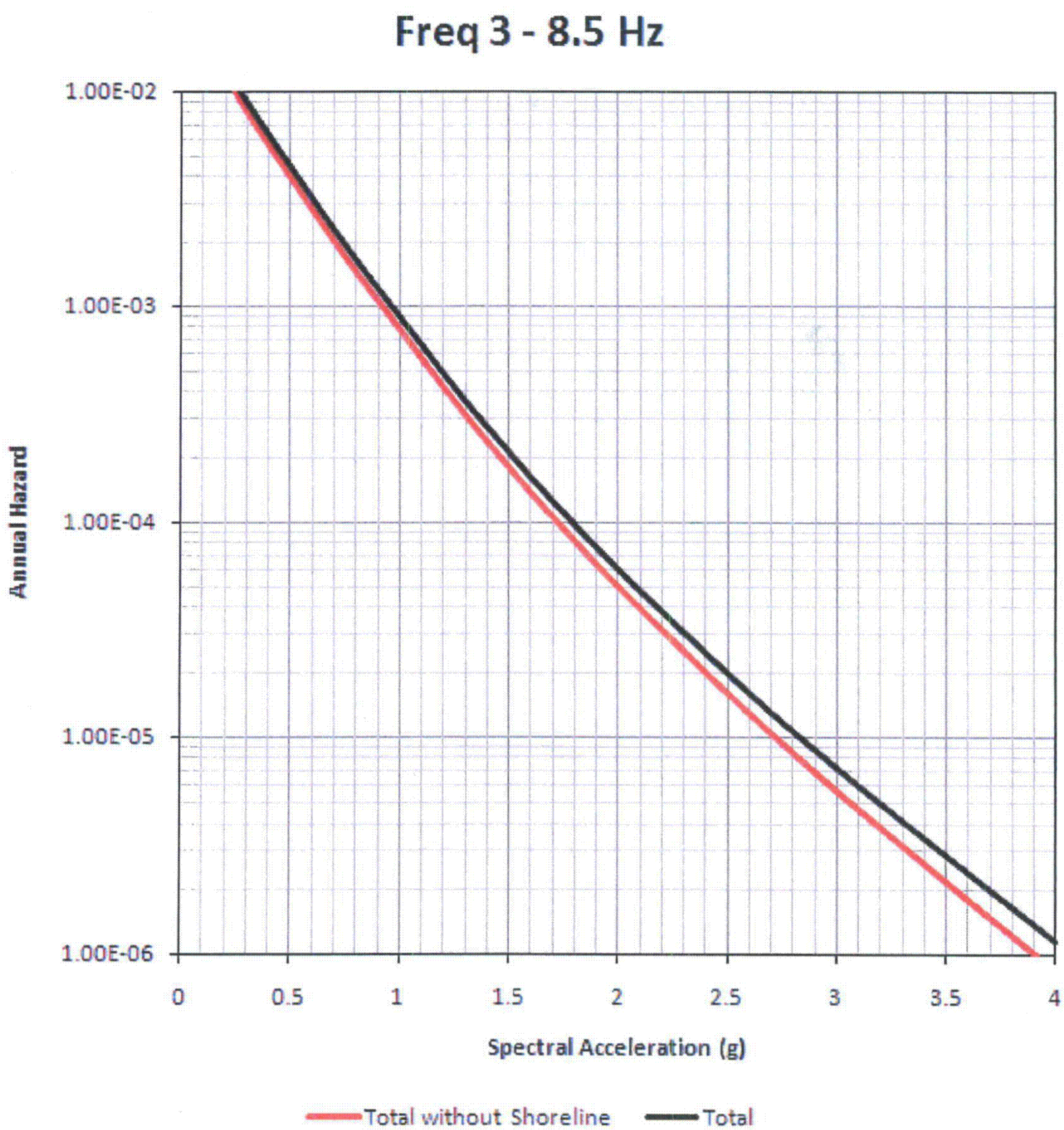

Figure 6-23. Hazard for spectral acceleration average over 3–8.5 Hz showing the contribution from the Shoreline fault source to the total hazard.

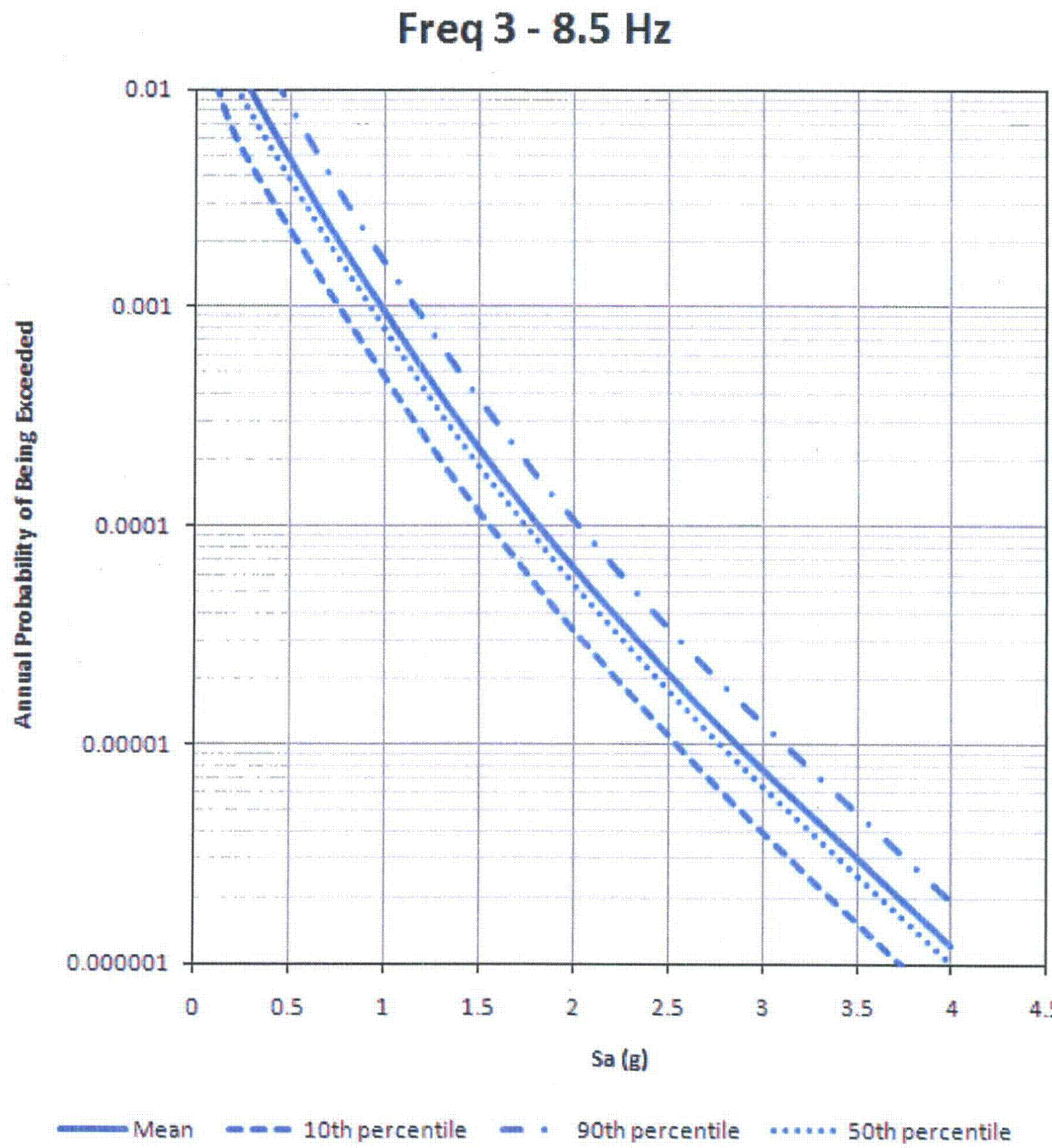

Figure 6-24. Fractiles of the hazard for 3-8.5 Hz.

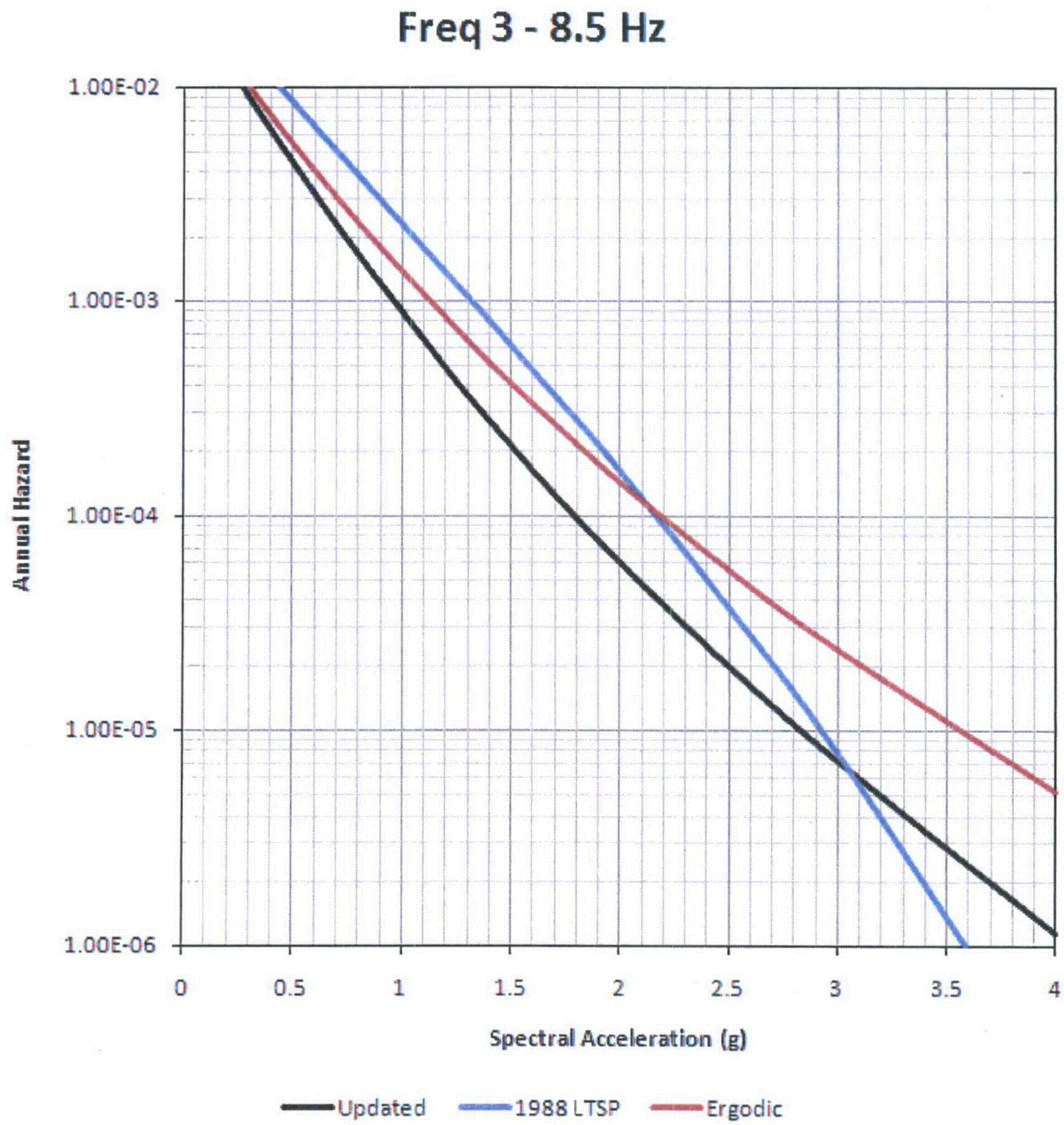

Figure 6-25. Comparison of the mean hazard for 3-8.5 Hz with the mean hazard from the 1988 LTSP (PG&E, 1988) and with the mean hazard using the traditional ergodic assumption.

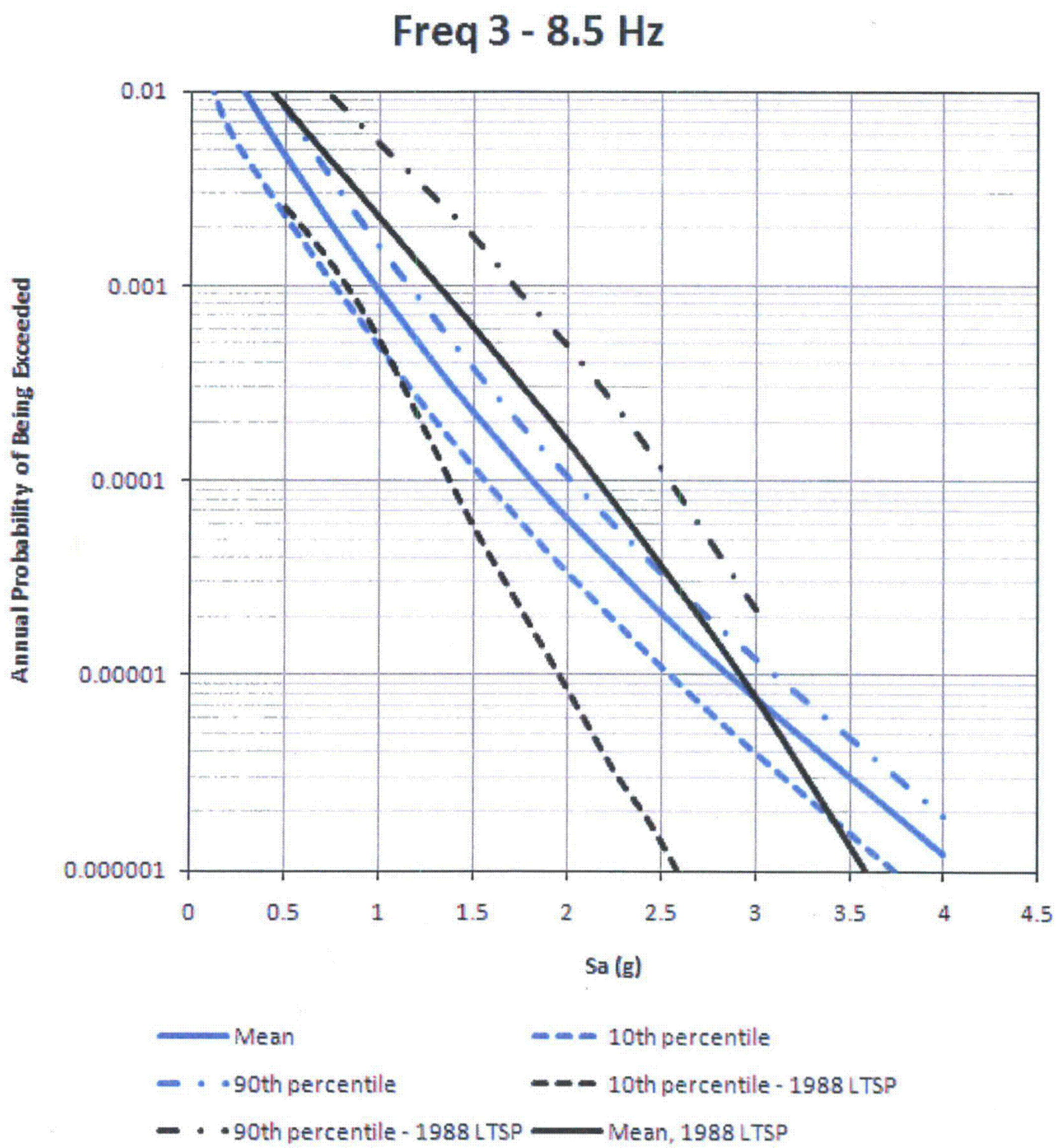

Figure 6-26. Comparison of the 3-8.5 Hz hazard fractiles from the 1988 LTSP (PG&E, 1988) (black) with the updated results (blue).

7.0 POTENTIAL FOR SECONDARY FAULT DEFORMATION

The Central segment of the Shoreline fault zone is 600 m from the power block and 300 m from the cooling water intake. Given this proximity of the fault zone to the DCPP site, a deterministic approach is needed to evaluate the potential for secondary fault deformation. The Progress Report (PG&E, 2010a) used a probabilistic approach based on the geology known at the time. The results of that calculation demonstrated the low probability of any secondary rupture of the auxiliary salt water (ASW) pipes based on the existing geologic mapping at the plant site. Additional mapping of the site geology done for the Shoreline fault zone investigations in 2009 and 2010 shows that the critical components of the ASW pipes lie outside the zone of potential deformation (a zone of weaker rock referred to in the Progress Report as T_{ofc}), and therefore the probabilistic analysis is not needed.

Detailed studies were performed to characterize the location and width of faulting along the offshore Shoreline fault zone and to assess the potential for secondary fault rupture or related surface deformation that might project onshore east of the fault zone through the DCPP site. These studies included detailed analysis of bathymetric data, seismic-reflection and LiDAR data, gravity and magnetic potential-field data, and onshore and near-shore geologic mapping; as well as review of the site investigations carried out for the DCPP FSAR (PG&E, 2010b, Section 2.5.1.2.5). The results of these investigations accurately document not only the location of the Shoreline fault zone 300 m west of the Intake structure, but also the absence of either primary or secondary faulting through the DCPP site area.

Four independent lines of evidence support these conclusions:

1. **Location of the Shoreline fault zone.** Interpretation of recently acquired bathymetric data clearly show a geomorphically and structurally well-defined fault trace 300 m west of the intake structure (Plate 1 and Figures 4-10 and 7-1). At this location, the fault trace is linear and does not exhibit significant geometric complexity (i.e., there are no fault bends or steps) within the 250 m wide fault zone that could lead to a broad zone of secondary deformation. In addition, the bathymetric data show the absence of lineaments or zones of bedrock shearing that could splay from the primary fault trace and project toward the site.
2. **Detailed mapping of onshore marine terraces.** The DCPP site is located on a sequence of emergent marine terraces ranging in age from 120,000 to 214,000 years old (PG&E, 1988; Hanson et al., 1994). Detailed mapping of the wave-cut platforms and shoreline angles associated with these marine terraces for the original LTSP (PG&E, 1988) documents the absence of faulting, folding, or tilting that could have displaced these terraces across the DCPP site area, confirming the lack of late Quaternary secondary fault deformation at the site.
3. **Detailed geologic mapping.** The geologic conditions of the DCPP site are well exposed along the sea cliff directly southwest of the site (Figure7-1). During the current investigations for the Shoreline fault zone, detailed mapping of the geologic stratigraphy and structure was performed along the sea cliff and on the modern wave-cut platform during low tide from near Lion Rock on the north, to south of the Intake Cove on the south. Potential bedrock faults were identified and characterized. None of the bedrock faults show evidence of late Quaternary tectonic activity (e.g., fissures filled with soil,

open fractures, fragile shear fabric); they appear to have formed during the Tertiary related to development of the Pismo syncline. Thus these faults can be associated with a well-known period of preexisting Miocene and Pliocene tectonic deformation.

4. **Detailed site investigations for the FSAR** (PG&E, 2010b). Investigations for the FSAR included detailed mapping of the site and extensive trenching to evaluate the potential for surface fault rupture through the site. The initial investigations for the power plant, the investigations for the ISFSI, and the current mapping document the absence of Quaternary primary or secondary fault deformation through the site area. The power block excavation was logged prior to construction; and nearly 5,000 linear feet of trenches to depths of 10–40 feet were excavated, evaluated, and logged for the power plant for the FSAR. The trenches and other exposures showed that faults within bedrock appear to be generally laterally discontinuous older structures, and that these faults do not offset either the 120,000 and 214,000 marine wave-cut platforms (i.e., the bedrock-soil interface) or the overlying marine terrace deposits. The marine terrace deposits, in turn, are overlain by both fluvial and colluvial deposits that also are not deformed. Observations from the trench investigation, therefore, provide direct evidence documenting the absence of primary and secondary fault deformation for the areas trenched and mapped in detail, including the coastal cliffs bordering the DCPP site.

The investigations described above extend over the entire 750 m wide control zone east of the Shoreline fault zone, including the entire DCPP site. These investigations document Tertiary-age geologic structures and the absence of late Quaternary surface faulting (primary or secondary) or other forms of late Quaternary tectonic deformation (e.g., tilting, folding, subsidence) through the DCPP site that may be associated with a conservative characteristic earthquake of magnitude 6.4 (Section 6.4.1) on the nearby Shoreline fault zone.

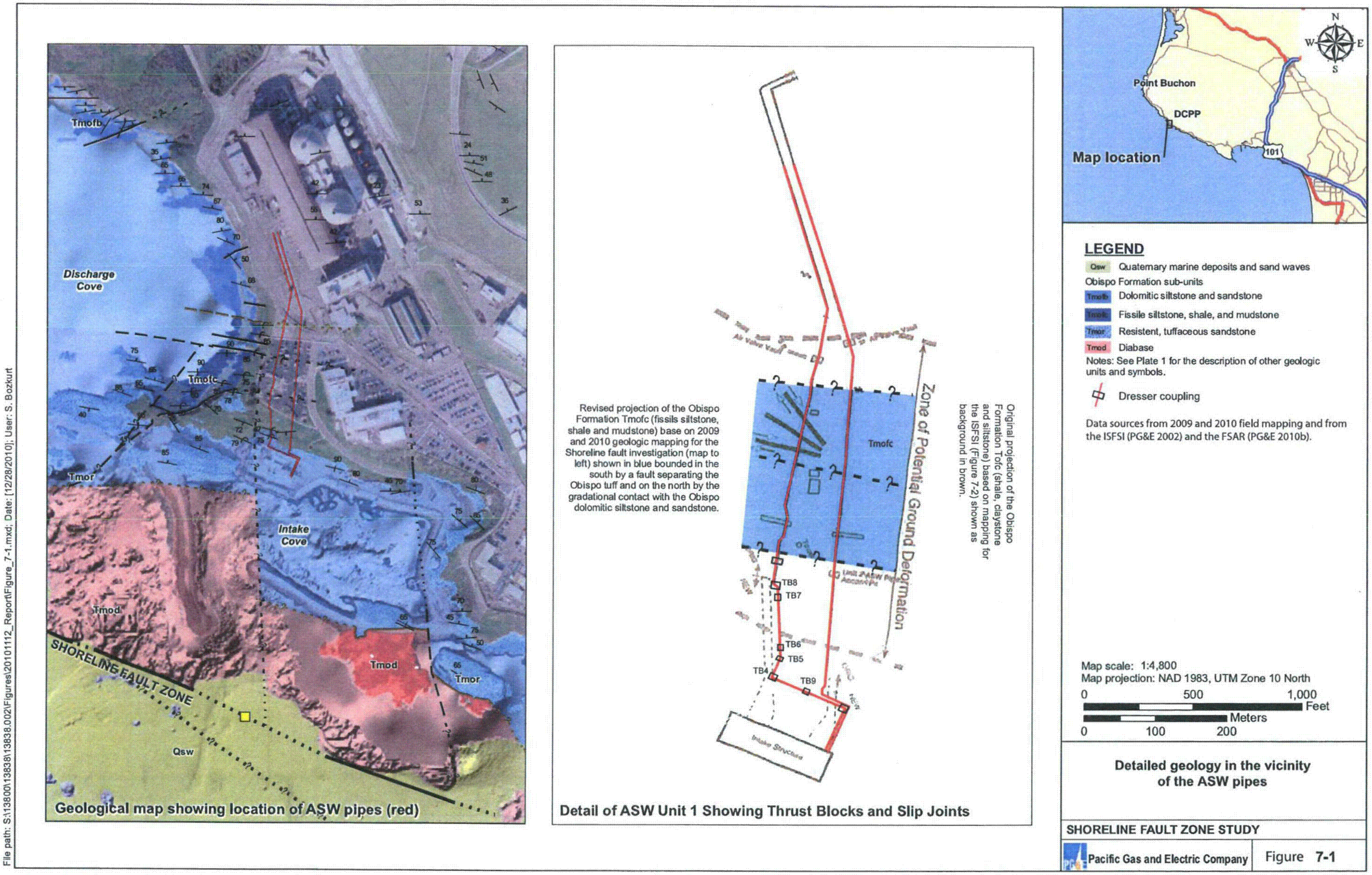

Tmofb
Discharge Cove
Tmofc
Tmor
Intake Cove
Tmod
SHORELINE FAULT ZONE
Qsw
Geological map showing location of ASW pipes (red)
Revised projection of the Obispo Formation Tmofc (fissils siltstone, shale and mudstone) base on 2009 and 2010 geologic mapping for the Shoreline fault investigation (map to left) shown in blue bounded in the south by a fault separating the Obispo tuff and on the north by the gradational contact with the Obispo dolomitic siltstone and sandstone.
Original projection of the Obispo Formation Tofc (shale, claystone and siltstone) based on mapping for the ISFSI (Figure 7-2) shown as background in brown.
Zone of Potential Ground Deformation
Tmofc
TB8
TB7
TB6
TB5
TB4
TB9
Detail of ASW Unit 1 Showing Thrust Blocks and Slip Joints
Point Buchon
DCPP
Map location
101
LEGEND
Qsw Quaternary marine deposits and sand waves
Obispo Formation sub-units
Tmofb Dolomitic siltstone and sandstone
Tmofc Fissile siltstone, shale, and mudstone
Tmor Resistent, tuffaceous sandstone
Tmod Diabase
Notes: See Plate 1 for the description of other geologic units and symbols.
Dresser coupling
Data sources from 2009 and 2010 field mapping and from the ISFSI (PG&E 2002) and the FSAR (PG&E 2010b).
Map scale: 1:4,800
Map projection: NAD 1983, UTM Zone 10 North
0 500 1,000 Feet
0 100 200 Meters
Detailed geology in the vicinity of the ASW pipes
SHORELINE FAULT ZONE STUDY
Pacific Gas and Electric Company
Figure 7-1
File path: S:\13800\13838\13838.002\Figures\20101112_Report\Figure_7-1.mxd; Date: [12/28/2010]; User: S. Bozkurt

8.0 SUMMARY AND CONCLUSIONS

In November 2008, Pacific Gas and Electric (PG&E) informed the U.S. Nuclear Regulatory Commission (NRC) that preliminary results from the Diablo Canyon Power Plant (DCPP) Long Term Seismic Program (LTSP) Update showed that there was an alignment of microseismicity indicating the presence of a previously unidentified fault located about 1 km offshore of DCPP. This previously unidentified fault was named the Shoreline fault zone.

The existence of an offshore fault zone between Point Buchon and Point San Luis had been discussed by NRC staff in 1989 in relation to the linear nature of the coastline in this area and the presence of bathymetric lineaments and escarpments parallel to the coast near Point Buchon. Prominent subsea escarpments that could be traced from Point Buchon to Point San Luis had been identified and interpreted as a series of closely spaced shoreline features that formed during previous low sea-level conditions. Although the general trend of the escarpment cuts obliquely across bathymetric contours, the individual slope breaks were subparallel to the bathymetric contours, sinuous and irregular, and thus were interpreted as submerged paleostrandlines and not as tectonically controlled features. NRC staff concluded that while the evidence presented by PG&E supported the absence of a coast-parallel fault, the presence of such a fault could not be completely ruled out (NRC, 1991, pp. 2-29 and 2-30).

As part of the notification to the NRC in 2008, PG&E conducted an initial sensitivity study to evaluate the potential impact of the Shoreline fault zone on the seismic safety of DCPP using a seismic margin approach (PG&E, 2008). A magnitude 6.5 strike-slip earthquake at a distance of 1 km from DCPP was considered, using conservative assumptions about the total length of the fault zone. The results of this sensitivity study demonstrated that the 84th percentile ground motion from the Shoreline fault zone was lower than the 1991 LTSP 84th percentile ground motion for which the plant had been evaluated and shown to have adequate margin (NRC, 1991). Therefore, PG&E concluded that the plant had adequate seismic margin to withstand the ground motions from the Shoreline fault zone. In early 2009, the NRC conducted an independent study of the potential impacts of the Shoreline fault zone on DCPP and also concluded that there was adequate seismic margin (NRC, 2009).

Although the initial seismic sensitivity studies showed that the plant has adequate margin to withstand ground motion from the potential Shoreline fault zone, both the NRC and PG&E recognized the need to better constrain the four main parameters of the Shoreline fault zone for a seismic hazard assessment: geometry (fault length, fault dip, downdip width), segmentation, distance offshore from DCPP, and slip rate. To address this need, PG&E conducted an extensive program in 2009 and 2010 to acquire and interpret new geological, geophysical, seismic, and bathymetric data as part of the PG&E LTSP Update. The following section summarizes the results of these investigations.

8.1 Shoreline Fault Zone Characterization

The 2009 and 2010 LTSP Update investigations have improved the understanding of the Shoreline fault zone, providing information on its location, geometry, segmentation, slip rate, and relationship to other structures, including the Hosgri and Southwestern Boundary faults.

8.1.1 Shoreline Seismicity Lineament

The Shoreline seismicity lineament was first identified by Hardebeck in 2008 (Hardebeck, 2010) and was subsequently verified through independent analysis by PG&E. The seismicity lineament is defined by microearthquakes ($1 \leq M < 3$) that have occurred during the period of instrumental recording (1970 to the present) along with one larger earthquake (M 3.5 on 10 August 2000). The seismicity lineament is divided into three distinct en échelon sublineaments referred to as the Northern, Central, and Southern seismicity sublineaments. The three Shoreline fault zone segments (discussed below) correspond spatially in both length and location to the three seismicity sublineaments, supporting the segmented nature of the fault zone. Two M ~5 events, on 20 October 1913 and 1 December 1916, are located in Avila Bay and could have been associated with the Southwestern Boundary zone or the South segment of the Shoreline fault zone.

8.1.2 Fault Length and Segmentation

The Shoreline fault zone is conservatively assumed to be up to 23 km long and has an overall strike of N60° W to N70° W. The Shoreline fault zone is divided into three segments based on differences in the geologic and geomorphic expression of surface and near-surface faulting, intersections with other mapped structures, features observed in the high-resolution magnetic field data, and variations in the continuity, trend, and depth of seismicity along the lineament. These segments of the Shoreline fault zone were named the North, Central, and South segments. The Shoreline fault zone appears to locally represent the reactivation of a preexisting Tertiary fault that is associated with distinct bathymetric lineaments and a pronounced series of magnetic anomalies that parallel the coast. This prior episode of faulting dates to either a mid-Miocene (~14 million years ago [Ma]) to early Pliocene (~4 Ma) period of transtensional deformation, or to a middle to late Pliocene (~3 Ma) episode of transpressional deformation.

South Segment

The South segment of the Shoreline fault zone extends from south of Point San Luis to the vicinity of Pecho Creek and Rattlesnake Creek and is approximately 7 km long. It follows a reactivated older fault that has a weak to moderate bathymetric expression, but does truncate bedding and is coincident with a strong linear magnetic anomaly.

Central Segment

The Central segment of the Shoreline fault zone extends from offshore of Pecho Creek, near the intersection with the Rattlesnake fault (the southern strand of the San Luis Bay fault zone), to Lion Rock, north of DCPP, and is approximately 8 km long. The Central segment is further subdivided into three en echelon subsegments (C-1, C-2, and C-3) based on discontinuities or steps in the bathymetric lineament. The Central segment is well expressed in the near-shore seafloor bathymetry as the result of differential erosion along the fault trace, and is associated with a series of distinct magnetic anomalies. These magnetic anomalies are spatially coincident with mapped Franciscan mélange that contain strongly magnetized metavolcanic rocks (greenstone) and serpentinite. The Central sublineament of the Shoreline seismicity lineament aligns with the preexisting Tertiary fault, within the resolution of the earthquake locations, indicating that the older fault has been reactivated in the current tectonic regime.

North Segment

The North segment of the Shoreline fault zone extends from Lion Rock, north of DCPP, to the Hosgri fault zone and is up to 8 km long, based on the extent of the Northern seismicity sublineament. While the preferred interpretation is that the North segment coincides with the location of the Northern seismicity sublineament, the bedrock surface is covered by sand sheets and marine deposits, and no faulting is visible at the seafloor. Analysis of the 2008 high-resolution seismic-reflection data indicates that the fault has produced only minor displacement in the buried Tertiary strata.

8.1.3 Fault Dip

The seismicity along the entire Shoreline lineament defines a nearly vertical zone. The magnetic anomalies along the Central segment of the Shoreline fault zone are consistent with a steeply dipping or vertical source that extends from the near-surface to a depth between approximately 0.5 and 4–5 km.

8.1.4 Downdip Width

The depth of seismicity along the Shoreline seismicity lineament is used to define the downdip width of the Shoreline fault zone. The seismicity along the Central and Southern sublineaments of the Shoreline seismicity lineament is between 2 and 10 km. Seismicity generally becomes more diffuse spatially and extends to greater depths (up to 15 km) along the Northern sublineament as it approaches the Hosgri fault zone.

8.1.5 Style of Faulting

The style of faulting is considered to be primarily right-lateral strike-slip based on the linear expression of the surface fault trace and earthquake focal mechanisms that indicate vertical right-lateral strike-slip motion.

8.1.6 Relationship to Other Structures

The Shoreline fault zone lies between the Southwestern Boundary fault zone on the south and east and the Hosgri fault zone on the west. Three alternatives are considered for the kinematic relationship of the Shoreline fault zone to these nearby structures.

In the first alternative, the Shoreline fault zone is part of a primarily strike-slip fault system that borders the southwestern margin of the uplifting San Luis Range. In this model, the Shoreline fault zone is kinematically linked to the San Luis Bay fault zone, and potentially other faults of the Southwestern Boundary fault zone (i.e., Wilmar Avenue, Los Berros, Oceano, and Nipomo faults) via left-restraining step-overs. Uplift of the San Luis range is accommodated primarily by reverse slip on the Los Osos fault zone and possibly transpressional oblique slip on the Southwestern Boundary fault zone.

In the second alternative, the Shoreline fault zone is an independent strike-slip fault within the San Luis–Pismo structural block. In this model, the Southwestern Boundary fault zone is a system of primarily reverse faults, and the Shoreline fault zone is a minor tear fault accommodating differential slip in the hanging wall of the fault zone. Uplift of the San Luis Range is accommodated by reverse slip on both the Los Osos and Southwestern Boundary fault zones.

In the third alternative, the Shoreline fault zone is an integral part of the Southwestern Boundary fault zone system of reverse-slip and oblique-slip faults. In this model, the Shoreline fault zone is kinematically linked to and may be, in part, the offshore continuation of the San Luis Bay fault zone. Uplift of the San Luis Range is accommodated by oblique slip on the Shoreline fault zone as part of the overall Southwestern Boundary fault zone.

All three alternatives are considered in the logic tree characterization of source parameters for the Shoreline fault zone. Alternatives one and two are given equal preference, assuming that the fundamental observation from seismicity that the fault zone is a near-vertical strike-slip fault. Alternative three is given a low preference, since the seismicity data and additional observations from offshore marine wave-cut platforms show little or no vertical separation across the Shoreline fault zone in the past 75,000 years.

Numerical models indicate that fault branching, where rupture begins on the Hosgri fault and then branches onto the Shoreline fault zone, would be inhibited under the current stress regime.

8.1.7 Slip Rate

The Shoreline fault zone lies entirely offshore and thus it is difficult to develop direct evidence of recent fault displacement or slip rate. The MBES bathymetric data were extensively examined to identify piercing points (i.e., potentially datable geomorphic features such as paleostrandlines or channels on both sides of the fault zone) that could be used to constrain cumulative slip and, from that, estimate slip rate. No late Quaternary piercing points have been identified to directly constrain horizontal slip across the Shoreline fault zone. In the absence of more direct information, constraints on slip rate are provided by several qualitative and indirect quantitative estimates of slip rate. These include (1) comparison of the geomorphic and structural features to the Hosgri–San Simeon fault system; (2) estimates of vertical separation based on the evaluation of submerged late-Pleistocene wave-cut platforms and paleostrandlines; (3) estimates of cumulative right-lateral strike slip based on offset of magnetic anomalies; (4) estimates of right slip on the Rattlesnake fault; and (5) seismicity rates. Based on these five estimates, the maximum horizontal slip rate on the Shoreline fault zone potentially ranges from 0.05 to possibly 1 mm/yr, with a preferred value of 0.2 to 0.3 mm/yr.

8.1.8 Location of the Shoreline Fault Zone Offshore of DCPP

The mapping based on high-resolution MBES bathymetric data clearly shows a sharp, well-defined lineament that lies offshore and west of the DCPP. This lineament is interpreted as the surface expression of the Central segment of the Shoreline fault zone. Immediately offshore of DCPP, the Central segment is located 300 m southwest of the intake structure and 600 m southwest of the power block.

8.2 Earthquake Hazard Implications for DCPP

Inclusion of the Shoreline fault zone in the seismic hazard analysis for the DCPP follows the methodology used in the original LTSP (PG&E, 1988) and uses both deterministic and probabilistic seismic hazard analyses (DSHA and PSHA, respectively). The source characterization used to model ground motions at the power block is represented in terms of a logic tree that captures the range of values that characterize each fault source. In addition to using new ground motion prediction equations (GMPEs) and the new Shoreline fault zone source, logic trees for the Hosgri, Los Osos, and San Luis Bay fault sources are based on the current understanding of those faults and the regional tectonic setting.

8.2.1 Ground Motion Results

For the deterministic analysis, the new estimates of the 84th percentile ground motion fall below the 1991 LTSP 84th percentile deterministic spectrum, indicating that the deterministic seismic margins for the new estimates of the ground motion are at least as large as those found in the LTSP.

Probabilistic hazard calculations show that the primary contribution to the total hazard at DCPP is from the Hosgri fault zone, and that both the Los Osos and Shoreline fault zones represent similar, but secondary, contributions to the hazard. The inclusion of new GMPEs and using updated source characterization, that includes the Shoreline fault zone, to the DCPP hazard model has resulted in changes to both the level and slope of the hazard curve. The hazard for 3–8.5 Hz spectral acceleration is lower than the LTSP hazard for spectral acceleration less than 3.0 g and is greater than the LTSP for spectral accelerations greater than 3.0 g. This change in the hazard curve is primarily due to the change in the ground motion models. The NGA models result in lower median ground motions for sites close to large earthquakes, but with an increased standard deviation. The flattening of the new hazard compared to the LTSP hazard curves is due to the larger standard deviation. Because the updated hazard curve is not enveloped by the 1988 LTSP hazard curve, the seismic core damage frequency (CDF) has been reevaluated. The seismic CDF estimated during the 1988 LTSP is 3.8E-5. Using the revised source characterization and ground motion models decreases the seismic CDF to 2.1 E-5. The reduction is mainly due to the use the NGA ground motion models with the single-station sigma approach incorporating the site-specific amplification.

8.2.2 Secondary Fault Deformation Results

The analysis presented in this report addresses the potential for secondary fault deformation associated with rupture of the Shoreline fault zone using a deterministic approach and concludes that secondary deformation does not affect the safety of the DCPP. The deterministic assessment of the geology at the DCPP site and vicinity documented the absence of late Quaternary primary or secondary surface faulting or other forms of late Quaternary tectonic deformation (e.g., tilting, folding, and subsidence) within the DCPP site that may be associated with a conservative maximum M 6.5 earthquake on the nearby Shoreline fault zone. These investigations encompassed the entire 750 m wide control zone east of the Shoreline fault zone, including the entire DCPP site, and included detailed mapping of onshore marine terraces, detailed geologic mapping of the sea cliffs directly west of the DCPP site, and review of the initial site investigations that were conducted for the FSAR.

8.3 Continued Studies

The original completion date of 2011 for the LTSP Update, as stated in the Action Plan and Revised Action Plan (Appendix A-1 and A-3), has been extended to allow completion of additional studies to further refine the models presented in this report. These studies include three-dimensional (3-D) marine and two-dimensional (2-D) onshore seismic reflection profiling, additional potential field mapping, GPS monitoring, and the feasibility of installing an ocean bottom seismograph network. These activities will further refine the characterization of those seismic sources and ground motions most important to the DCPP: the Hosgri, Shoreline, Los Osos, and San Luis Bay fault zones and other faults within the Southwestern Boundary zone.

9.0 REFERENCES

Abrahamson, N.A. (2000). Effects of rupture directivity on probabilistic seismic hazard analysis, *Proc. 6th Int. Conf. on Seismic Zonation*, Palm Springs, California.

Abrahamson, N.A., and W. Silva (2008). Summary of the Abrahamson and Silva NGA ground-motion relations, *Earthq. Spectra* **24**, no. 1, 67-98.

Anderson, J. G. and J. N. Brune (1999). Probabilistic seismic hazard assessment without the ergodic assumption, Seism. Res. Let., 70, 19-28.

Al Atik, L., N.A. Abrahamson, J.J. Bommer, F. Scherbaum, F. Cotton & N. Kuehn (2010). The variability of ground-motion prediction models and its components. *Seismological Research Letters* **81**(5), 783-793.

Anderson, J. G. (2010). Engineering Seismology: Directions in probabilistic seismic hazard analysis. In Kazuhiko Kasai, H. Sakata, A. Takahashi, K. Tokimatsu, S. Yamada, T. Morgan (Ed.), Joint Conference Proceedings 7th International Conference on Urban Earthquake Engineering (7CUEE) & 5th International Conference on Earthquake Engineering (5ICEE) (pp. 1-10 of 2091). Tokyo: Center for Urban Earthquake Engineering, Tokyo Institute of Technology.

Atkinson, G. M. (2006). Single-station sigma, Bull. Seism. *Bull. Seismol. Soc. Am.* **96**, 446-455.

BCHydro (2010). Probabilistic Seismic Hazard Analysis, Volume 3: Ground Motion Report, Draft Nov 3, 2010.

Bolt, B.A., and R.D. Miller (1975). Catalogue of earthquakes in Northern California and adjoining areas, 1 January 1910–31 December, 1972, Seismographic Stations, University of California at Berkeley, Berkeley, California, 567 pp.

Boore, D.M., and G.M. Atkinson (2008). Ground-motion predication equations for the average horizontal component of PGA, PGV, and 5%-damped PSA at spectral periods between 0.01 s and 10.0 s, *Earthq. Spectra* **24**, no. 1, 99-138.

Campbell, K.W., and Y. Bozorgnia (2008). NGA ground motion model for the geometric mean horizontal component of PGA, PGV, PGD and 5% damped linear elastic response spectra for periods ranging from 0.01 s to 10.0 s, *Earthq. Spectra* **24**, no. 1, 139-172.

Chapman, R.H., L.A. Beyer, and L.G. Youngs (1989). Bouguer gravity and magnetic anomaly map of the south-central California Continental margin (Map 4c), in California Continental Margin Geologic Map Series: South-Central California continental margin—Area 4 of 7, Greene, H.G., and M.P. Kennedy (Editors), California Division of Mines and Geology, scale 1:250,000.

Chen Y-H., and C-C. P. Tsai (2002). A new method for estimation of the attenuation relationship with variance components, Bull. Seism. Soc. Am., 92, 1984-1991.

Chiou, B.S-J., and R.R. Youngs (2008). An NGA model for the average horizontal component of peak ground motion and response spectra, *Earthq. Spectra* **24**, no. 1, 173-216.

Chiou, B., R. Youngs, N. Abrahamson, and K. Addo (2010). Ground-Motion Attenuation Model for Small-To-Moderate Shallow Crustal Earthquakes in California and Its Implications on Regionalization of Ground-Motion Prediction Models, Earthquake Spectra, 26:4, pp. 907-926.

Cornell, C.A. (1968). Engineering seismic risk analysis, *Bull. Seismol. Soc. Am.* **58**, 1583-1606.

EPRI (2006). Truncation of the lognormal distribution for ground motion models. EPRI Report Number: 1014101

Geomatrix (1993). Seismic ground motion study for Dumbarton Bridge, report to Caltrans, July, 1993, Contract No. 59N772.

Hall, C.A., Jr. (1973). Geologic map of the Morrow Bay South and Port San Luis quadrangles, San Luis Obispo County, California: *U.S. Geol. Surv. Misc. Field Studies Map MF-511*, scale 1:24,000.

Hall, C.A., W.G. Ernst, S.W. Prior, and J.W. Wiese (1979). Geologic map of the San Luis Obispo-San Simeon region, California, *U.S. Geol. Surv. Misc. Investig. Series Map I-1097*, scale 1:48,000.

Hall, T., T.D. Hunt, and P.R. Vaughan (1994). Holocene behavior of the San Simeon fault zone, south-central coastal California, in Seismotectonics of the central California Coast Ranges, Alterman, I.B., R.B. McMullen, L.S. Cluff, and D.B. Slemmons (Editors), Geological Society of America Special Paper 292, 167-189.

Hanks, T.C., and W.H. Bakun (2008). **M**-Log*A* observations for recent large earthquakes: *Bull. Seismol. Soc. Am.* **98**, 490-494.

Hanson, K.L., J.R. Wesling, W.R. Lettis, K.I. Kelson, and L. Mezger (1994). Correlation, ages, and uplift rates of Quaternary marine terraces: South-central coastal California, in Seismotectonics of the Central California Coast Ranges, Alterman, I.B., R.B. McMullen, L.S. Cluff, and D.B. Slemmons (Editors), *Geol. Soc.Am. Special Paper 292*, 45-71.

Hanson, K.L., W.R. Lettis, M.K. McLaren, W.U. Savage, and N.T. Hall (2004). Style and rate of Quaternary deformation of the Hosgri fault zone, offshore south-central California, in Evolution of Sedimentary Basins/Offshore Oil and Gas

Investigations—Santa Maria Province, Keller, M.A. (Editor), *U.S. Geol. Surv. Bull. 1995-BB*, 33 pp.

Hardebeck, J.L. (2010). Seismotectonics and fault structure of the California central coast: *Bull. Seismol. Soc. Am.* **100**, 1031-1050, doi: 10.1785/0120090307.

Hardebeck, J.L., and P.M. Shearer (2002). A new method for determining first-motion focal mechanisms, *Bull. Seismol. Soc. Am.* **92**, 2264–2276.

Hecker, S., N. Abrahamson, D. Schwartz, and K. Wooddell (2010). Variation in slip at a point: Implications for earthquake size distributions and rupture hazard on faults, in preparation.

Idriss, I.M. (2008). An NGA empirical model for estimating the horizontal spectral values generated by shallow crustal earthquakes, *Earthq. Spectra* **24**, no. 1, 217-242.

Killeen, K. (1989). Timing and deformation of the Pismo Syncline, San Luis Obispo, California, M.S. thesis, University of Nevada at Reno, 90 pp.

Klein, F.W. (2002). Users guide to HYPOINVERSE-2000: A Fortran program to solve for earthquake locations and magnitudes, *U.S. Geol. Surv. Open-File Rept. 02-171*, version 1.0.

Langenheim, V.E., R.C. Jachens, R.W. Graymer, and C.M. Wentworth (2008). Implications for fault and basin geometry in the central California Coast Ranges from preliminary gravity and magnetic data, *EOS* (Abs. AGU), Fall Meeting 2008, abstract #GP43B-0811.

Langenheim, V.E., R.C. Jachens, and K. Moussaoui (2009). Aeromagnetic survey map of the central California Coast Ranges, *USGS Open File Rept. 2009-1044*, http://pubs.usgs.gov/of/2009/1044/.

Lee, W.H.K., and S.W. Stewart (1981). *Principles and Applications of Microearthquake Networks*, Academic Press, 293 pp.

Leonard, M. (2010). Earthquake fault scaling: Self-consistent relating of rupture length, width, average displacement, and moment release, *Bull. Seismol. Soc. Am.* **100**, 1971-1988, doi: 10.1785/0120090189.

Lettis, W.R. and N.T. Hall (1994). Los Osos fault zone, San Luis Obispo County, California, in Seismotectonics of the Central California Coast Ranges, Alterman, I.B., R.B. McMullen, L.S. Cluff, and D.B. Slemmons (Editors), *Geol. Soc. Am. Special Paper 292*, 73-102.

Lettis, W.R., K.L. Hanson, J.R. Unruh, M. McLaren, and W.U. Savage (2004). Quaternary tectonic setting of south-central coastal California, *U.S. Geol. Surv. Bull. 1995-AA*, 24 pp., http://pubs.usgs.gov/bul/1995/aa [web only].

Lettis, W.R., K.I. Kelson, J.R. Wesling, M. Angell, K.L. Hanson, and N.T. Hall (1994). Quaternary deformation of the San Luis Range, San Luis Obispo County, California, in Seismotectonics of the Central California Coast Ranges, Alterman, I.B., R.B. McMullen, L.S. Cluff, and D.B. Slemmons (Editors), *Geol. Soc. Am. Special Paper 292*, 111-132.

Lin, P-S., B. Chiou, M. Walling, N. Abrahamson, C-T Lee, and C-T Cheng (2010). Repeatable Source, Site, and Path Effects on the Standard Deviation for Empirical Ground-Motion Prediction Models, submitted to Bull Seism. Soc. Am.

Lindh, A., C. Motooka, S. Ball, and R. Dollar (1981). Current seismicity of the central California coastal region from Point Buchon to Point Piedras Blancas: A preliminary report, *U.S. Geol. Surv. Open-File Rept. 81–44*, 16 pp.

Manighetti, I., M. Campillo, S. Bouley, and F. Cotton (2007). Earthquake scaling, fault segmentation, and structural maturity, *Earth Planet. Sci. Lett.* **253**, no. 3-4, 429-438.

McCulloch, D.S. (1987). Regional geology and hydrocarbon potential of offshore central California, in *Geology and Resource Potential of the Continental Margin of Western North America and Adjacent Ocean Basins, Beaufort Sea to Baja California*, Scholl, D.W., A. Grantz, and J. Vedder (Editors), American Association of Petroleum Geologists, Circum-Pacific Council for Energy and Mineral Resources, Earth Sciences Series **6**, 353-401.

McLaren, M.K. and W.U. Savage (2001). Seismicity of south-central coastal California: October 1987 through January 1997, *Bull. Seismol. Soc. Am.* **91**, 1629-1658.

McLaren, M.K., J.L. Hardebeck, N. van der Elst, J.R. Unruh, G.W. Bawden, and J.L. Blair (2008). Complex faulting associated with the 22 December 2003 M_w 6.5 San Simeon, California, earthquake, aftershocks and postseismic surface deformation, *Bull. Seismol. Soc. Am.* **98**, 1659-1680.

National Oceanic and Atmospheric Administration (NOAA), 2009. Digital Coast, http://maps.csc.noaa.gov/dataviewer/viewer.html?davlayer=lidar, accessed 26 March 2009.

New Sense Geophysics (2010). Point Buchon: Helicopter aeromagnetic geophysical survey for Pacific Gas and Electric Company, December 2nd – December 5th, 2009. PG&E No. 2500257867, NSG No. HM191015, Toronto, Canada, 40 pp.

Nitchman, S.P. (1988). Tectonic Geomorphology and Neotectonics of the San Luis Obispo County, California, M.S. thesis, University of Nevada at Reno, 120 pp.

Northern California Earthquake Data Center (NCEDC) (2010). Northern California Earthquake Catalog Search, http://www.ncedc.org/ncedc/catalog-search.html, accessed September 2010.

Nuclear Regulatory Commission (NRC) (1991). Supplement No. 34 to NUREG-0675, Safety evaluation report Related to the operation of Diablo Canyon Nuclear Power Plant, Units 1 & 2, July 1991.

Nuclear Regulatory Commission (NRC) (2009). Research Information Letter 09-001: Preliminary Deterministic Analysis of Seismic Hazard at Diablo Canyon Nuclear Power Plant from Newly Identified "Shoreline Fault," ADAMS ML090330523, April 8, 2009.

Pacific Earthquake Research (PEER) (2010a). Description of the NGA-west2 Project, http://peer.berkeley.edu/ngawest2/index.html

Pacific Earthquake Research (PEER) (2010b). Description of the NGA-east Project, http://peer.berkeley.edu/ngaeast/index.html

Pacific Gas and Electric Company (PG&E) (1988). Final report of the Diablo Canyon long-term seismic program, U.S. Nuclear Regulatory Commission Docket No. 50-275 and No. 50-323.

Pacific Gas and Electric Company (PG&E) (1989a). Response to question Q43e, in Response to questions 43, 43a, 43b, 43c, 43d, 43e, 43f, 43g and 43h, U.S. Nuclear Regulatory Commission Docket No. 50-275 and No. 50-323, January 1989.

Pacific Gas and Electric Company (PG&E) (1989b). Long term seismic program: Plate Q43i-2-1, Geologic map of coastal California from Morrow Bay to the Santa Maria Valley, south-central California, U.S. Nuclear Regulatory Commission Docket No. 50-275 and No. 50-323.

Pacific Gas and Electric Company (PG&E) (1989c). Long term seismic program: Plate Q43i-2-4, Model B longitudinal profile of marine terrace shoreline angles from Morrow Bay to the Santa Maria Valley, south-central California, U.S. Nuclear Regulatory Commission, Docket No. 50-275 and No. 50-323.

Pacific Gas and Electric Company (PG&E) (1990), Long term seismic program: Response to Question GSG 16. U.S. Nuclear Regulatory Commission Docket No. 50-275 and No. 50-323, March 1990.

Pacific Gas and Electric Company (PG&E) (1991a). Addendum to the 1988 Final Report of the Diablo Canyon Long Term Seismic Program, U.S. Nuclear Regulatory Commission Docket No. 50-275 and No. 50-323, February 1991.

Pacific Gas and Electric Company (PG&E) (1991b). Benefits and insights of the Long Term Seismic program, Letter from J.D. Shiffer to the U.S. Nuclear Regulatory Commission, Enclosure 1, PG&E Letter DCL-91-091, April 17, 1991.

Pacific Gas and Electric Company (PG&E) (2002). Diablo Canyon Independent Spent Fuel Storage Installation Final Safety Analysis Report.

Pacific Gas and Electric Company (PG&E) (2004). Final safety analysis report of the Diablo Canyon independent spent fuel storage installation, Figure 2-6.6, U.S. Nuclear Regulatory Commission Docket No. 72-26.

Pacific Gas and Electric Company (PG&E) (2008). E-mail to Alan Wang and Vincent Gaddy (NRC) from Bill Guldemond (PG&E), Subject: Preliminary data for seismic discussion, with attachment, DCPP_Nov 20-2008_v2 (3).ppt.

Pacific Gas and Electric Company (PG&E) (2010a). Progress Report on the Analysis of the Shoreline fault zone, central coast California, Enclosure 1, PG&E Letter DCL-10-003, January 2010. See Appendix A of this report.

Pacific Gas and Electric Company (PG&E) (2010b). DCPP Final Safety Analysis Report (FSAR) (Rev. 19, May 2010, Section 2.5.1.2.5).

Petersen, M., T. Cao, T. Dawson, A. Frankel, C. Wills, and D. Schwartz (2004). Evaluation fault rupture hazard for strike-slip earthquakes, *Proc. Geo-Trans*, 787-796.

Reasenberg, P.A., and L.M. Jones (1994). Earthquake aftershocks: Update, *Science* **265**, 1251–1252, DOI: 10.1126.

Reasenberg, P.A., and D. Oppenheimer (1985). FPFIT, FPPLOT, and FPPAGE: Fortran computer programs for calculating and displaying earthquake fault-plane solutions, *U.S. Geol. Surv. Open-File Rept. 85–739.*

Sliter, R.W., P.J. Triezenberg, P.E. Hart, J.T. Watt, S.Y. Johnson, and D.S. Scheirer (2009; revised 2010). High-resolution seismic reflection and marine magnetic data along the Hosgri Fault Zone, Central California, *USGS Open File Rept. 2009-1100*, version 1.1, http://pubs.usgs.gov/of/2009/1100.

Somerville, P. (2009). Analysis of inhibition of faulting at fault branches, URS report to PG&E, April 2009. See Appendix J.

Somerville, P.G., N.F. Smith, R.W. Graves, and N. Abrahamson (1997). Modification of empirical strong ground motion attenuation relations to include the amplitude and duration effects of rupture directivity, *Seismol. Res. Lett.* **68**, 199-222.

Spudich, P., and N. Chiou (2008). Directivity in NGA ground motions: Analysis using isochrone theory, *Earthq. Spectra* **24**, no. 1, 299-318.

Thurber, C.H. (2009). Central California Offshore Earthquake Assessment, August 18, 2009. See Appendix C.

Toppozada, T.R. (1987). Earthquake history of Parkfield and surroundings, *EOS Trans. Am. Geophys. Union* **68,** no. 44, 1345.

Waldhauser, F. (2009). Central California Offshore earthquake location assessment. See Appendix C.

Waldhauser, F., and W.L. Ellsworth (2000). A double-difference earthquake location algorithm: Method and application to the northern Hayward Fault, California, *Bull. Seismol. Soc. Am.* **90**, 1353-1368.

Watson-Lamprey, J. (2007). The search for directivity (abs.), *Seismol. Soc. Am. Ann. Mtg.*, 11-13 April 2007.

Watt, J.T., S.Y. Johnson, J.L. Hardebeck, D.S. Scheirer, M.A. Fisher, R.W. Sliter, and P.E. Hart (2009). Geophysical characterization of the Hosgri fault zone, Central California (abs.), *Seismol. Res. Lett,* **80**, 323-324.

Weichert, D.H. (1980). Estimation of the earthquake recurrence parameters for unequal observation periods for difference magnitudes, *Bull. Seismol. Soc. Am.* **70**, 1337-1346.

Wells, D.L., and K.J. Coppersmith (1994). Empirical relationships among magnitude, rupture length, rupture width, rupture area, and surface displacement, *Bull. Seismol. Soc. Am.* **84**, 974-1002.

Youngs, R.R. (2009). Epistemic uncertainty in the NGA models, Appendix D in Ground Motion Models for the Pacific Northwest, Report to B.C. Hydro, December 2010.

Youngs, R.R., and K.J. Coppersmith (1985). Implications of fault slip rates and earthquake recurrence models to probabilistic seismic hazard estimates, *Bull. Seismol. Soc. Am.* **75**, 939-964.

Zhang, H., and C.H. Thurber (2003). Double-difference tomography: The method and its application to the Hayward fault, California, *Bull. Seismol. Soc. Am.* **93**, 1875-1889.

Appendix A

A1: Action Plan for the Study of the Shoreline Fault

A2: Progress Report on the Analysis of the Shoreline Faults Zone, Central coastal California

A-3: Revised Action Plan for the Study of the shoreline Fault

Appendix A-1

ACTION PLAN FOR THE STUDY OF THE SHORELINE FAULT

PG&E Geosciences Department

Submitted to the Diablo Canyon Power Plant
December 15, 2008

ACTION PLAN FOR THE STUDY OF THE SHORELINE FAULT

I. INTRODUCTION

Recent processing of seismic recordings from small earthquakes (1987-2007, magnitudes <1 to 3.5) using improved earthquake location computer programs shows an alignment of epicenters along the coast offshore, approximately one km from DCPP that is suggestive of a vertical strike-slip fault at depth (~3-11 km). The seismicity alignment has a length of 15 km. If it is extended to the intersection with the Hosgri fault, the length is 24 km. In addition to the seismicity data, raw (unprocessed) aero-magnetic and marine-magnetic data that were recently collected by the USGS show a magnetic anomaly with a trend that is consistent with the seismicity alignment. Although the geophysical survey results are preliminary, taken together, the available seismicity and geophysical data suggest that there is an active fault located offshore DCPP which we call the Shoreline fault.

Based on this preliminary data, PG&E estimated magnitudes of 6.25 and 6.5 for the Shoreline fault based on rupture lengths of 15 and 24 km, respectively, and an average rupture depth of 12 km. The potential ground motion at DCPP from these two events was evaluated and was found to be lower than the current design ground motions based on a larger earthquake on the more distant Hosgri fault.

The Action Plan below is designed to collect data and conduct analyses to better constrain the characteristics of the Shoreline fault and the potential ground motions at DCPP and ground deformation west of the power block. The Plan has three objectives. The first objective is to characterize the Shoreline fault in terms of its location, geometry, activity rate, rupture characteristics, and relation to the Hosgri fault zone. The second objective is to evaluate the ancient (Tertiary) shear zone west of the power block structure for evidence of secondary deformation that may have been associated with the Shoreline fault. The third objective is to estimate potential ground motions from the Shoreline fault, including both independent rupture of the Shoreline fault and possible synchronous rupture with the Hosgri fault.

This Action Plan describes the geology, seismology, geophysics, and ground motions studies to be performed over the next 2 years to achieve the above objectives. Results from these new studies will be integrated with results from the PG&E/USGS CRADA which is developing new regional tectonic models. An updated evaluation of the seismic hazard at DCPP will be conducted by PG&E Geosciences as part of the Long Term Seismic Program (LTSP) hazard update, which is scheduled to be completed in 2011. PG&E Geosciences and their consultants will perform the majority of the work; as part of the CRADA, the USGS will perform the balance of their marine magnetic survey and evaluate additional seismicity data in the region.

II. GEOLOGIC STUDIES (G)

Purpose: Locate, if possible, the surface expression of the Shoreline fault through geologic mapping and geophysical surveys (as described in Section IV). If located, then assess the last displacements for timing and amount of displacement. In addition, evaluate whether or not the shear zone has experienced secondary ground deformation related to the Shoreline fault. The shear zone is considered in this context as the shears in the shale unit of the Obispo Formation that crops out west of the power block.

Task G-1 Geologic mapping between Montana del Oro and Point San Luis

This Task will update existing knowledge of the geology along the coast between Montana del Oro and Point San Luis to provide the geologic framework for interpretation of the geologic setting of the Shoreline fault.

Subtask G-1A - Review and compile the 1988-1991 LTSP and other data concerning the geology of the coast, including diver geology videos and notes.

Subtask G-1B – Map geologic contacts and faults along the coast; inspect the coast in detail for exposures of the Olson and Rattle Snake faults where recent erosion may have exposed them. Use the offshore geophysics information (Task GP-2) as a guide to where the Shoreline fault may come onshore and be exposed in the sea cliffs. This Subtask includes detailed geologic mapping to improve existing geological maps at the DCPP site, including mapping the wave-cut platforms in Diablo Cove and elsewhere.

Subtask G-1C - Use divers and/or remotely operated vehicles (ROV) to extend mapping offshore at sites identified by the LiDAR and offshore geophysics (Task GP-2) and onshore mapping. This Subtask is focused on extending mapped geologic contacts and/or strata offshore to document fault offsets, if any.

Subtask G-1D - Profile selected streams that discharge from the Irish Hills to identify breaks in slope and channel offsets related to faulting. The LiDAR data and shallow bathymetry (Task GP-2) and other pertinent data from the offshore geophysics will be used in this analysis.

Task G-2 - Evaluation of secondary deformation in the shear-zone

This Task will improve the location of the shear zone as mapped for the ISFSI FSAR and will evaluate the amount of secondary ground deformation that may have been associated with earthquakes on the Shoreline fault.

Subtask G-2A - This Subtask will evaluate the potential for secondary deformation using the methodology of Peterson et al (2004) to calculate the probabilistic fault rupture hazard for strike-slip faults and will compare these results with geologic analogs.

Subtask G-2B - This Subtask will conduct detailed field investigations to improve the location of the shear zone and evaluate the amount of secondary deformation that may have been associated with the Shoreline fault. This Subtask has several elements:

a. Clean the cliffs at Diablo Cove to expose the 120,000-year-old wave-cut contact at top of rock over bedrock shears and faults in order to look for evidence of past secondary deformation.

b. Conduct local shallow seismic reflection surveys (and/or Ground Penetrating Radar) to improve the location of the shear zone and the depth of the wave-cut platforms in the area.

c. Based on the shallow seismic reflection data (from element b), drill borings to better define the depths of the wave-cut platforms, find the depths of colluvium and marine deposits over the wave-cut platform to help locate trench sites, and delineate the extent of the shear zone south of the plant where it is covered by colluvium.

d. Excavate trenches to measure the orientation of the shears and to confirm the location of the shear zone and evidence for recent deformation (or lack thereof) observed in the cleaned cliff exposures.

III. SEISMICITY STUDIES (S)

Purpose: Analyze and document the earthquakes that make up the seismicity alignment. Studies will include quantifying uncertainties of the hypocentral locations and focal mechanisms, and studying the depth distribution and activity rate.

Task S-1: Expand the time period covered by the data set used by the USGS in their analysis of the regional seismicity and determine the locations and focal mechanisms. This Task will add earthquakes that occurred from 1980 to 1987 and from Mar 2007 to Dec 2008 to the original data set and will estimate their location and focal mechanisms using the TomoDD and HASH computer programs. This work will be performed by the USGS as part of the CRADA.

Task S-2: Provide independent reviews of USGS data analyses described in Task S-1.

Task S-3: Analyze and document the expanded data set for the Shoreline fault. After completion of Tasks S-1 and S-2, this Task will address the following parameters:

a. Hypocentral and focal mechanism uncertainties

b. Differences between 1D, 3D, hypoDD and tomoDD locations

c. Temporal and spatial development of the lineament

d. Magnitude recurrence model for the Shoreline fault based on historical seismicity

Task S-4: Evaluate the feasibility of offshore seismic stations

This Task will evaluate the feasibility of installing ocean bottom seismometers (OBS) offshore from DCPP, west of the Hosgri fault zone to improve the accuracy of past and future earthquake locations and focal mechanisms in the offshore DCPP region. Earthquakes that occur offshore, outside the PG&E and USGS seismographic on-land networks, have inherent location errors, particularly depth errors. OBSs would improve the azimuthal coverage, resulting in more accurate locations.

IV. GEOPHYSICAL STUDIES (GP)

Purpose: Conduct additional offshore geophysical studies to improve characterization of the Shoreline fault and its relation to the Hosgri fault. High priority tasks will build on the marine work done by the USGS in 2008. These tasks include GP-1 (high resolution marine magnetics), GP- 2 (nearshore geophysics), and GP-3 (scoping study for a 3-D seismic survey). Supplemental tasks (GP-4 through GP-6) will be considered as collaborative opportunities present themselves or the need arises.

Task GP-1: High Resolution Marine Magnetics.

Subtask GP-1A: High Resolution Marine Magnetics Data Collection: This Subtask will complete the USGS marine field work that was delayed due to equipment malfunction in 2008.

Subtask GP-1B: Marine Magnetics Data Integration and Interpretation: This Subtask will provide support for the interpretation of the high resolution marine magnetic data and integration of these data with the regional aeromagnetic survey data.

Task GP-2: Offshore Geology/Geophysics

This Task will provide uniform, high-resolution bathymetric and topographic coverage from Montana del Oro to south of Point San Luis to define the extent and character of the Shoreline fault to support Task G-1. Shallow water depths necessitate the use of various geophysical techniques to complete this Task.

Subtask GP-2A: Multi beam Bathymetry

This Task will conduct multibeam bathymetric mapping between the 30 and 5 meter contour using a shallow draft boat. This mapping will provide shallow water coverage from Point Buchon to San Luis Bay.

Subtask GP-2B: Airborne LiDAR bathymetry and coastal topography

This Task will map the coastline and surf zone using LiDAR to provide both shallow (< 5 m) bathymetry and coastal topography at a 2 meter horizontal resolution with 25 cm vertical accuracy.

Task GP-3: 3-D Seismic Survey Scoping Study

This Task will develop a scope and cost estimate for conducting a 3-D Seismic Survey within approximately 5 km of DCPP. The scope of the survey will include both onshore and offshore seismic reflection and refraction from the offshore Hosgri to the onshore Los Osos fault zone. Part of this scope will include preliminary 2-D seismic surveys to optimize the later full scale 3-D seismic survey. This Task will also include support for PG&E consultants to familiarize themselves with the LTSP and USGS CRADA datasets to develop data collection strategies that will complement and leverage previously collected information.

Supplemental Geophysical Tasks (as needed)

Task GP-4: Multi beam Bathymetry – from Hosgri shoreward to the 30 m depth contour

NOAA and the State of California are currently conducting multibeam bathymetric mapping of California state waters. This mapping may be extended to the Central California coast in 2009. If extended, PG&E would propose to supplement the NOAA/California multibeam mapping program through additional coverage beyond the 3 mile limit to map the Hosgri fault zone and shoreward to the 30 m depth contour.

Task GP-5: 2D High Resolution seismic survey (multi channel, Chirp)

This Task would conduct additional high resolution seismic reflection studies to augment already collected USGS marine data and to improve the resolution of marine structures in critical locations as needed.

Task GP-6: Vibrocoring for sediment age dating.

Based on marine mapping, Geosciences may identify candidate sites for age dating to constrain the rate of motion on both the Hosgri and Shoreline faults.

V. SOURCE CHARACTERIZATION OF THE SHORELINE FAULT

Purpose: Integrate of all the data from the G, S, and GP tasks and develop a set of alternative models for the characterization of the Shoreline fault in terms of its location, geometry, activity rate, rupture characteristics, and relation to the Hosgri fault zone

Task SC-1: Compile existing data on geology into a GIS data base

Create a GIS data-base for the coast and plant site that will include existing topographic maps, orthophotos, LiDAR, as well as LTSP and more recent geologic maps.

Task SC-2: Characterize the Shoreline fault

Using the GIS database, integrate the various data layers and interpret the results. Build alternative models of the location, geometry, activity rate, rupture characteristics of the Shoreline fault, and its relation to the Hosgri fault zone. Develop a logic tree structure and assign weights for the Shoreline fault characterization.

VI. GROUND MOTION STUDIES (GM)

Purpose: Evaluate the ground motions at DCPP for the case with synchronous rupture of the Hosgri and Shoreline faults using numerical simulation methods. Ground motions from independent ruptures of the Shoreline fault are adequately characterized by the existing models. These tasks will include defining the rupture characteristics for the case in which there is synchronous rupture on the Hosgri and Shoreline faults and computing the resulting ground motions at the DCPP site.

Task GM-1: This Task will use dynamic rupture models to evaluate the rupture characteristic for the generic problem of a vertical strike-slip fault with a splay fault.

Subtask GM-1A: Validate dynamic rupture models for a vertical strike-slip fault with a vertical splay fault.

The SCEC working group on dynamic rupture model code validation will add an additional validation case for a vertical strike-slip earthquake with a vertical splay fault. The working group will identify which dynamic rupture computer programs are applicable for this case.

Subtask GM-1B: Simulate a suite of ruptures on a vertical strike-slip fault with a vertical splay with a strike that is 30 degrees from the strike of the main fault.

Based on the results of Subtask GM-1A, two different computer programs will be selected and used to simulate the rupture characteristics (slip distribution, rise time, rupture velocity, and hypocenter location) for the main fault and the splay fault. This Task will also provide information on the relative rates of independent verses synchronous rupture of the main trace and the splay fault.

Subtask GM-1C: Develop kinematic source inputs.

The dynamic rupture sources from Subtask GM-1B will be converted to kinematic source models so that they can be used to simulate broadband ground motions (Task GM-2).

Task GM-2. Compute site-specific ground motions at the DCPP site using the generic kinematic sources developed in Subtask GM-1C.

The SCEC broadband simulation platform will be used to simulate the ground motions at the DCPP site from a suite of representative rupture scenarios that were developed in Subtask GM-1C.

Task GM-3. Parameterize the site-specific ground motions into a fault-specific attenuation relation for the synchronous rupture case.

The ground motion response spectra from the kinematic simulations (Task GM-2) will be parameterized into a set of attenuation equations and will be incorporated into the seismic hazard computer program.

VII. REPORT

The above results will be summarized in a report to be completed by 4th quarter 2010.

The report will address the issues investigated in this study:

- Characterization of the Shoreline fault in terms of its location, geometry, activity rate, rupture characteristics, and relation to the Hosgri fault zone.
- Evaluation of the ancient (Tertiary) shear zone west of the power block structure for evidence of secondary deformation that may have been associated with the Shoreline fault and estimate potential amount of ground deformation in the shear zone.
- Estimation of potential ground motions from the Shoreline fault, including both the independent rupture of the Shoreline fault and its synchronous rupture with the Hosgri fault.
- Summary of the feasibility studies of the Ocean-Bottom Seismometers and a 3-D seismic survey.

Appendix A-2

PROGRESS REPORT ON THE ANALYSIS OF THE SHORELINE FAULT ZONE, CENTRAL COASTAL CALIFORNIA

Report to the U.S. Nuclear Regulatory Commission

December 2009

Submitted by

PG&E Geosciences and the Diablo Canyon Power Plant

PROGRESS REPORT ON THE ANALYSIS OF THE SHORELINE FAULT ZONE, CENTRAL COASTAL CALIFORNIA

Report to the U.S. Nuclear Regulatory Commission
December 2009

1.0 INTRODUCTION

In November 2008, PG&E informed the NRC that preliminary results from the Diablo Canyon Power Plant (DCPP) Long Term Seismic Program (LTSP) seismic hazard update indicated that there was an alignment of microseismicity that may indicate a previously unidentified fault located about 1 km offshore of DCPP (Figure 1). This seismicity alignment was called the Shoreline fault zone.

PG&E conducted an initial sensitivity study to evaluate the potential impact of the Shoreline fault zone on the seismic safety of DCPP (PG&E, 2008) using a seismic margin approach. Using conservative assumptions about the total length of the fault zone, a magnitude 6.5 strike-slip earthquake at a distance of 1 km was considered. The results of this sensitivity study demonstrated that the 84th percentile ground motion from the Shoreline fault zone was lower than the 1991 LTSP ground motion for which the plant had been evaluated and shown to have adequate margin (NRC, 1991). Therefore, PG&E concluded that the plant had adequate seismic margin to withstand the ground motions from the Shoreline fault zone. In early 2009, the NRC conducted an independent study of the potential impacts of the Shoreline fault zone on DCPP (NRC, 2009) and they also concluded that there is adequate seismic margin.

Although these initial sensitivity studies show that the plant had adequate margin to withstand ground motion from the potential Shoreline fault zone, three main parameters of the Shoreline fault zone are not well constrained: geometry (length, width, dip) and segmentation, location offshore of DCPP and slip-rate. To reduce the uncertainties in these source parameters, PG&E prepared a 2-year Action Plan to collect additional data to better characterize the Shoreline fault zone. Once completed, the improved characterization will be used to update the ground motion hazard at DCPP and to also assess the potential for secondary deformation along the Auxiliary Salt Water (ASW) intake pipe corridor.

This report describes the data collection and initial results from new geologic interpretations for the first year of this study. This report distinguishes between the seismicity lineament as defined by Hardebeck (2009) and the Shoreline fault zone as currently defined by bathymetry and the interpretations presented in this report. The report is organized into the following sections:

2.0 Data Collection - describes the new geologic and geophysical data, including multibeam echo sounding (MBES) swath mapping and high resolution seismic reflection profiling, that were used to identify the surface expression of the Shoreline fault zone.

3.0 Seismicity Lineament - evaluates the Shoreline seismicity lineament including estimates of earthquake location uncertainty.

4.0 Initial Results - integrates the new geologic and geophysical data with the seismicity to improve the characterization of the Shoreline fault zone in terms of its geometry and segmentation, location offshore from DCPP, and activity rate.

5.0 Impacts at DCPP - presents an updated evaluation of the ground motion and initial evaluation of secondary fault deformation at DCPP related to surface faulting on the Shoreline fault zone.

6.0 Summary and Planned 2010 Studies - summarizes PG&E's conclusions to date and the research program that has been identified for 2010 to address unresolved issues and questions.

7.0 References

The study area addressed in this report is the offshore region between the Hosgri fault zone on the west, the Irish Hills on the east, Estero Bay on the north and San Luis Obispo Bay on the south (Figure 1). Tectonically the study area lies within the Pacific-North American transpressional plate margin between the San Simeon/Hosgri system of near-coastal faults to the west and the San Andreas fault system to the east in a region called the Los Osos-Santa Maria (LOSM) domain, as first described in the PG&E Long Term Seismic Program Final Report (PG&E, 1988) (Figure 1 inset). The domain consists of northwest-striking reverse and oblique slip faults that border intervening uplifted blocks and subsiding basins (PG&E, 1988, Lettis et al., 2004). The Shoreline fault zone is located within the San Luis Pismo block of the LOSM domain.

2.0 DATA COLLECTION

Modern high resolution potential field (magnetics and gravity) and bathymetric data have significantly improved the ability to resolve geologic structures in the vicinity of DCPP since the original LTSP (PG&E, 1988). During 2008 and 2009, new marine magnetic, high resolution seismic profiling, and multibeam echo sounding (MBES) data were collected offshore DCPP. New aeromagnetic data were collected onshore in 2008 and

2009, and new gravity measurements were collected in 2009 to update earlier models for the area (Figure 2).

2.1 Magnetics

Figure 2a shows the coverage of a fixed wing aeromagnetic survey that was flown in 2008 under the PG&E/USGS CRADA program. A total of 20,508 line-kilometers of data were collected at an altitude of 305 m (~1000 feet) with an 800 m line spacing using differential GPS navigation. A contour map of this aeromagnetic data was published as USGS Open File Report 2009-1044 (Langenheim et al., 2009).

Marine magnetic data were collected at 400 m line spacing during 2008 and 2009 as part of a joint marine magnetics and high resolution seismic reflection study as part of the PG&E/USGS CRADA and the California State Waters Mapping Program. The data collected in 2008 were published as USGS Open File Report 2009-1100 (Sliter et al., 2009). Figure 2b shows the track lines for both marine studies.

The USGS "merged" the marine magnetic data, collected at sea level, with the aeromagnetic data, collected at an altitude of 305 m above terrain, by applying a simple datum shift (Watt et al., 2009; see Figure 2c). The data "merge" quite well despite the difference in measurement height. This is confirmed by the similar magnetic character between the aeromagnetic data and the marine magnetic data that have been filtered to effectively place those data at the same height as that of the aeromagnetic data (upward continuation).

In order to capture the shorter wavelength features of the magnetic field in the vicinity of the Shoreline fault zone and fill the gap between the fixed wing and marine surveys, PG&E conducted a helicopter-based magnetic survey along the coast line in December 2009. An additional 933 line-kilometers of total field aeromagnetic data were collected between Pt. Buchon and Pt. San Luis along flight lines spaced 150 m apart and at a nominal altitude of ~100m above terrain (see Figure 2b for survey area). Processing of these data is in progress.

2.2 Gravity

The USGS compiled, edited and reprocessed nearly 30,000 gravity measurements to produce an isostatic residual gravity map for the region, spanning Monterey on the north to the Santa Barbara channel on the south (Langenheim et al., 2008). Data includes the PG&E LTSP offshore data base as well as data collected at ~ 1 mile spacing by NIMA (formerly the Defense Mapping Agency) for the area south of 36°15'N near Vandenberg Air Force Base. Terrain corrections were applied using 30 m DEMs to create a roughly 2 km grid over the central California coastal area The USGS also collected about 180 new gravity measurements in the Pt. Buchon /Pt. San Luis area and in the Santa Maria basin during 2009. Several older measurement sites were reoccupied to aid in editing the old data and highlighted the inaccuracy of the older data. Figure 2d shows the isostatic gravity anomalies in the vicinity of the DCPP at a grid spacing of 400 meters (Watt et al, 2009).

2.3 High Resolution Seismic Reflection Profiling

Single-channel seismic-reflection data were acquired in 2008 and 2009 by the U.S. Geological Survey between Piedras Blancas and Pismo Beach, along shore-perpendicular transects spaced 800 m apart extending from close to shore to beyond the 3-mile limit of California State waters (Figure 2b). Data were collected as part of the PG&E/USGS CRADA and the California State Waters Mapping Program. The 2008 data were published as USGS Open File Report 2009-1100 (Sliter et al., 2009). Data collected in 2009 are still being processed. In general, the USGS survey vessel was not able to approach as close to shore as the CSU Monterey Bay vessel (see below) due to the presence of shallow rocks and kelp. Specific attempts were made in 2009 to image portions of the Shoreline fault zone based on locations mapped by MBES; however, these attempts were not successful.

2.4 Multibeam Echo Sounding

Multibeam echo sounding (MBES) data for the Estero Bay to San Luis Bay nearshore region were acquired by the Seafloor Mapping Lab at California State University Monterey Bay during 2008 and 2009. Figure 2e shows the areas mapped in 2006 (Point Buchon- grey colored track lines) and 2009 (Point Buchon to San Luis Bay – red colored track lines). The acquired MBES bathymetry data are shown on Figure 2f. The spatial resolution in water depths less than 50 m is 1 m, and is 2 m for water depths greater than 50 m. Multibeam databases can be accessed at the CSU Sea Floor Mapping Lab Data Library http://seafloor.csumb.edu/SFMLwebDATA_c.htm. Data bases for 2006 Pt. Buchon survey are currently on line, and the databases for the 2009 Pt. Buchon to Avila Beach survey will be available at the end of 2009.

3.0 SEISMICITY LINEAMENT

3.1 Hardebeck Studies

In November 2008, Dr. Jeanne Hardebeck (USGS) presented relocations of earthquakes that have occurred from 1987 to 2007 in the south-central coastal region of California at a PG&E/USGS Cooperative Research and Development Agreement (CRADA) workshop. Dr. Hardebeck's study, supported by the CRADA as part of the regional LTSP Update program, used the Double Difference (DD) program, *hypoDD* (Waldhauser and Ellsworth, 2000) and found a microseismicity lineament about one km offshore of DCPP.

In 2009, Hardebeck relocated the earthquakes through 2008 using a new relocation technique called *tomoDD* (Zhang and Thurber, 2003). *TomoDD* is a more robust program than *hypoDD* because it incorporates absolute and relative arrival time data from the phase picks and waveform cross correlations, respectively, and it uses DD tomography to determine a 3D velocity model jointly with absolute and relative event locations (Zhang and Thurber, 2003). Hardebeck's *tomoDD* results also show the Shoreline seismicity lineament (Figure 1). The seismicity lineament consists of approximately 50 microearthquakes of magnitude 0.8 to 3.5 located between 2 and 15 km depth.

We evaluated why the seismicity lineament was not previously visible using typical catalog locations based on a 1D velocity model. We found that a diffuse pattern of earthquakes between the shoreline and the Hosgri fault zone centered about 1½ km west of DCPP was visible, but they did not show a strong alignment (Figure 3, frame CAT08). The diffuse pattern was due primarily to imprecise locations of earthquakes occurring offshore and outside the seismic networks using a 1D velocity model.

During the 1988 through 2008 time period, the seismographic station coverage did not change. The yearly plots in Figure 3 show that during this time period the Shoreline microseismicity lineament began in the northern end and, in about 1992, the seismicity began to fill in the central and southern parts. Analysis of earlier seismicity data with less station coverage identified possibly 3 additional microearthquakes associated with the seismicity lineament (J. Hardebeck, personal communication, 2009).

3.2 Peer Review of Seismicity Lineament

Regardless of the location method used, hypocentral accuracy depends on several factors such as the quality of the *P*- and *S*- arrival time picks, an adequate velocity model and good station geometry (<180° azimuthal gap). The accuracy of the offshore Shoreline fault zone earthquake locations is likely affected by all of these factors.

Hardebeck's *tomoDD* location results for earthquakes within the study area were reviewed by Dr. Clifford Thurber, co-author of *tomoDD* (Zhang and Thurber, 2003). He first reproduced the *tomoDD* results of Hardebeck using her same assumptions, and then relocated the earthquakes using *tomoDD* with his preferred parameters and velocity model. Thurber also estimated the hypocentral location uncertainty for comparison with Hardebeck's uncertainty estimates (Hardebeck, 2009). Thurber concluded that the seismicity lineament identified by Hardebeck is a robust feature (Thurber, 2009).

Figure 4 shows both the Hardebeck and Thurber locations with the 2009 Shoreline fault zone interpretation (this study). The earthquakes that are associated with the seismicity lineament are defined here as those events whose 0.5 km uncertainty circles (buffers) intersect the mapped traces of the Shoreline fault zone (as described in Section 4.2) or the cross section line A-A' to the northwest. Thurber's locations are generally farther offshore than Hardebeck's and the difference in location generally increases with distance offshore (i.e., there is less offset between Thurber and Hardebeck along the seismicity lineament and more offset along the Hosgri fault zone). Thurber's locations are also approximately 1 km shallower than Hardebeck's locations (Figure 5).

3.3 Location Uncertainty

Hardebeck and Thurber each estimated location uncertainties for earthquakes within the Shoreline seismicity lineament. Their methods are described below. In this report, we estimate location uncertainty by comparing the individual Hardebeck and Thurber uncertainty estimate to our estimate based on a comparison of the two *tomoDD* results.

Hardebeck (2009) estimated the absolute earthquake location uncertainty by relocating shots with known locations. For 13 shots (Murphy and Walter, 1984; Sharpless and Walter, 1988) located inside her 3D velocity model, the RMS shift from the true location was 0.9 km horizontal and 1.3 km vertical. She concluded that the absolute uncertainty of the earthquake locations, which should be better located than the shots, was ≤ 0.9 km horizontal and ≤ 1.3 km vertical. She acknowledges that the offshore shot location errors are larger. The location errors in shots tend to be about twice the location errors for earthquakes because the ray path for shots samples the shallow surface structure twice.

Thurber assessed the relative and absolute location uncertainties. Using a jackknife approach, he estimated relative location uncertainties of 140 m in the direction parallel to the lineation, 190 m perpendicular to the lineation, and 280 m in depth. For the absolute location uncertainty he obtained a rough estimate by considering the variations in absolute locations resulting from the use of different starting velocity models and different control parameter settings. He considers 500 meters to be a reasonable estimate of the absolute location uncertainty (horizontal and vertical) for the Shoreline earthquakes within the Shoreline seismicity lineament.

Hardebeck (2009) also estimated uncertainties for the San Luis Obispo region based on the stability of the locations determined using various location methods. The median absolute shift between her *hypoDD* and 3D locations is 470 m horizontal and 450 m vertical. The median absolute location shift between her *hypoDD* and *tomoDD* locations is 390 m horizontal and 510 m vertical.

In a similar approach, we compared location results specifically between Hardebeck and Thurber's *tomoDD* earthquake locations. The average shift values between the two *tomoDD* runs are 0.50 ± 0.34 km (RMS 0.60 km) horizontal shift and 1.39 ± 0.82 km (RMS 1.61 km) vertical shift. Our results are consistent with the Hardebeck and Thurber error estimates. In this progress report, we use the Hardebeck locations with uncertainties of 0.50 km horizontal and 1.4 km vertical to study the relation of the seismicity lineament to the Shoreline fault zone.

4.0 INITIAL RESULTS

4.1 Geologic Setting

Identifying a potential candidate structure as the cause of the seismicity lineament requires an understanding of the geologic setting in terms of the geomorphology, stratigraphy, and structure of the offshore region west and southwest of the Irish Hills. The geologic setting of this offshore region is partly known from previous studies (e.g. PG&E, 1988) but has been greatly improved by interpretation of the recently acquired MBES bathymetric, seismic reflection, and potential field data.

Geomorphology

The Shoreline seismicity lineament traverses the inner continental shelf west and south of the Irish Hills. The inner shelf in this area consists of a gentle, westward-sloping (less than 1 degree) bedrock platform between the coastline and a prominent break-in-slope coincident with the Hosgri fault zone. The bedrock platform is underlain by Cretaceous (~ 100 million years ago (mya)) and Tertiary rocks (~ 2 to 65 mya) that have undergone multiple phases of deformation (Hall 1978), and thus are extensively folded, fractured and faulted. In addition, the bedrock platform was eroded during multiple cycles of Pleistocene (~ 10,000 years to 2 mya) and Holocene (10,000 years ago to present) sea level rise and fall, producing both submerged paleo-seacliffs (former coastlines) and sea stacks, as well as enhanced lineaments along the previously folded and faulted strata. Locally, extensive thin mobile sand sheets veneer and obscure the bedrock surface.

Identification of a potential candidate structure associated with the Shoreline seismicity lineament, therefore, must consider several factors of the geologic, geomorphic, and structural setting:

(1) The multiple phases of Tertiary deformation have produced an inherited structural grain. Most (or all) of these structures are no longer active; however, current active faulting may locally re-activate a pre-existing structure.

(2) Many of the most prominent sea floor lineaments are the result of marine erosion, including multiple paleo-seacliffs and enhanced erosion along inherited, pre-existing geologic structures and bedding.

(3) Marine erosion likely obliterates or obscures subtle geomorphic features associated with low rates of fault activity.

(4) Drifting, mobile sand sheets of modern age cover not only large parts of the bedrock surface, but also locally infill many bathymetric lineaments and seafloor channels, obscuring subtle geomorphic evidence of active faulting.

(5) A potentially active fault must exhibit clear evidence of cross cutting, and thus post-dating, the inherited Tertiary stratigraphic and structural grain, and ideally would have geomorphic evidence of cross-cutting relationships to the Pleistocene erosion surfaces.

Stratigraphy and Structure

Rock strata on the offshore bedrock platform are identified through correlation to onshore stratigraphic units following the nomenclature of Hall (1973). The bedrock consists primarily of unnamed Cretaceous greywacke (sandstone) and Franciscan Mélange, and Tertiary Obispo, Monterey, and Pismo formations. These units are recognized and mapped based on changes in seafloor texture and structure seen on the MBES bathymetry and locally confirmed by cores and diver samples.

Understanding the distribution of stratigraphic units provides critical information for interpreting both the inherited Tertiary structural features on the inner shelf, as well as potential Quaternary structural features that either locally reactivate pre-existing structures, or "cross cut", and thus post-date, these earlier structural features.

During the Tertiary (~ 2 to 65 mya), northeast-southwest-directed compression produced the northwest-trending anticlines and synclines in the Irish Hills and the offshore inner shelf. Onshore deformation ended sometime in the late Tertiary (Pliocene (2 to 5 mya) and transitioned into uplift of the San Luis/Pismo structural block during the early Quaternary (Pleistocene) (Hanson et al., 1994; Lettis et al., 2004). We infer that offshore deformation also ended by the late Tertiary and was replaced by uplift of the offshore bedrock platform as an extension of the San Luis/Pismo structural block. MBES bathymetry and high resolution seismic reflection data clearly show folded and faulted Tertiary strata (Figure 6). The deformation also warps and folds pre-existing fault contacts or angular unconformities that separate the Tertiary section from the underlying Cretaceous basement section. This pre-existing stratigraphic and structural grain, therefore, provides the basis for identifying and characterizing potential faults that crosscut older structures.

Further to the west, the marine bedrock platform and geologic structures are truncated by the Hosgri fault zone (Figure 6). The Hosgri fault zone is an active transpressional right slip fault that forms one of the major strike slip faults separating the Pacific and North American tectonic plates. It is approximately 110 kilometers long, has a slip rate of 1 to 3 mm/yr, and lies approximately 4 kilometers offshore of the DCPP (Hanson et al., 2004; PG&E, 1988, 1990).

4.2 Potential Candidate Structure for the Shoreline Fault Zone

Based on our analysis of the MBES bathymetry and seismic reflection data and interpretation of offshore geology, we identify a candidate geologic structure that we call the Shoreline fault zone. The fault zone cuts across all Cretaceous and Miocene structures and, thus, is younger than the Miocene (5 to 24 mya). It consists of three distinct segments separated by right en echelon steps of several hundred meters width (Figure 6). The characteristics of these three segments are summarized in Table 1 and described below.

<u>Segmentation and Length</u>

The Shoreline fault zone consists of three segments: (1) a 6 to 9 km Northern Segment defined by a distinct N40W-trending escarpment that locally truncates Miocene bedding and structures; (2) a 8 km Central Segment expressed as a sharp bathymetric lineament and scarp that locally juxtaposes unlike bedrock lithologies, truncates bedding and structures (folds and faults), and has associated gas-related pock marks and mud extrusions; and (3) a 6 km Southern Segment expressed as a poor to moderate bathymetric lineament with local truncation of bedding. The geomorphology of all the segments shows that differential erosion is the primary cause of the bathymetric lineaments on the seafloor. Fault line scarps accentuated by wave erosion are common where faults juxtapose resistant and weak rock. The weaker materials in the fault zone are eroded into troughs.

The northern part of the seismicity lineament and the Central and Southern fault segments forms a right-stepping en echelon pattern with an overall strike of North 60° to 70° West. Within the Central Segment, the bathymetric lineament also shows a right-stepping en echelon pattern at both the kilometer scale and 10 to 100 meter scale. The en echelon right stepping fault pattern strongly suggests right-lateral strike-slip surface displacements consistent with the focal mechanisms of the recent microseismicity (Figure 7).

The Shoreline seismicity lineament coincides with the surface trace of the Central and Southern segments of the Shoreline fault zone, and thus these two segments of the fault zone appear to have been reactivated in the current tectonic setting. The alignment of seismicity with the fault zone occurs from directly west of the DCPP southward along the coastline to directly southwest of Point San Luis, where both the seismicity lineament and the Shoreline fault zone die out (Figure 4).

To the north, however, the seismicity lineament is more diffuse and diverges along a more westerly trend than the Northern segment of the Shoreline fault zone. No fault has been identified that can be associated with the northern part of the seismicity lineament. To the contrary, six shallow high resolution seismic reflection lines that cross the northern part of the seismicity lineament provide direct stratigraphic evidence showing the absence of faulting within the upper hundred meters of the bedrock platform and the Quaternary sediments that overly the platform (e.g., Figures 8 and 9a and 9b). It may be that this part of the seismicity lineament is associated with a fault that does not reach the surface. Some of the seismicity may be associated with the western trace of the Hosgri fault zone at depth.

The total length of the seismicity lineament is 22 to 23 kilometers (Table 1). The northern part that is not associated with a known fault extends from the Hosgri fault zone southward to near the discharge cove of DCPP for a distance of 8 to 9 kilometers.

The microseismicity defines nearly vertical fault planes (Figure 5) and the composite focal mechanisms indicate vertical strike-slip earthquakes. In the Central and Southern parts of the seismicity lineament, the seismicity reaches a depth of about 10 km. Along the northern part of the seismicity lineament, there is a change in the depth distribution with depths up to 15 km. The seismicity lineament appears to be most active near the Hosgri fault zone and decreases in activity to the southeast.

4.3 Location of the Shoreline Fault Zone with Respect to DCPP

Our analysis of the MBES data in the DCPP area (Figure 10a) locates the Central Segment of the Shoreline fault zone southwest of the Intake Cove breakwater, 600 meters from the Power Block and 300 meters from the intake structure (Figure 10b). The high quality of the MBES data clearly shows the Shoreline fault zone in this area as a sharp lineament whose northern end projects beneath the sand sheet west of the Discharge Cove.

4.4 Activity Rate of the Shoreline Fault Zone

Evidence of Activity

The offshore seismicity lineament correlates well with the Central and Southern segments of the Shoreline fault zone. As described previously, most of the microseismic events along the Central and Southern segments locate along the fault zone within the ½ kilometer uncertainty bound (Figure 4). Because of this direct association with microseismicity, we conclude that the Central and Southern segments of the Shoreline fault zone are active and that the evidence of activity is sufficient to warrant inclusion of the fault zone in sensitivity analyses to assess implications of ground motion and secondary deformation at the DCPP.

In contrast, the Northern part of the seismicity lineament is not associated with a mapped fault. Seismic reflection records confirm that the underlying wave cut platform and the overlying Quaternary sediments are not deformed (Figures 8 and 9a and 9b). The lack of coincidence of the seismicity with a mapped fault indicates that the northern part of the lineament should be considered separate from the Central and Southern segments of the Shoreline fault zone.

Our preliminary analysis of the MBES bathymetry and seismic reflection data along the Central and Southern segments of the Shoreline fault zone has not identified conclusive geologic, geomorphic, or geophysical evidence of late Quaternary (Holocene) fault activity; however, the prominent seafloor scarps, local gas pock marks, subtle geomorphic features that crosscut talus and colluvium are consistent with a late Quaternary active fault. Further analysis is required during 2010 to test these observations.

Slip Rate on the Shoreline Fault Zone

Slip rate on the Shoreline fault zone is poorly constrained at this point of our preliminary analysis. Several approaches are being used to constrain slip rate or activity rate on the Shoreline fault zone. Progress on each of these approaches is as follows:

(1) *Direct quantitative estimate of slip rate.* The Northern Segment of the Shoreline fault zone crosses numerous submerged marine terrace surfaces and paleo-coastlines. These marine terraces represent former still stands of sea level, and thus form an excellent strain gauge to assess the amount and age of late Quaternary deformation if they can be mapped and dated with confidence. A preliminary map of these terraces has been prepared, and work is in progress to correlate and assign ages to the terraces. At this point, our preliminary observation is that the Northern Segment of the Shoreline fault zone has not produced significant deformation (greater than one meter) of the 80,000 and 125,000 year old terrace sequences suggesting that the fault is not active or has a slip rate that is less than 0.01 mm/yr.

(2) *Qualitative estimate of slip rate.* Many active faults with known slip rates cross the inner continental shelf of California. Comparing the geomorphic, geologic, and geophysical signature of these faults to the Shoreline fault zone provides a qualitative estimate of slip rate. We compare the Shoreline fault zone to the Hosgri fault zone that has a known slip rate of 1 to 3 mm/yr. The Hosgri fault

zone forms a prominent geomorphic break-in-slope, clearly deforms late Pleistocene and Holocene marine deposits, and is associated with a prominent gravity and magnetic anomaly (Figures 6 and 11). In contrast, the Shoreline fault zone does not form a prominent break-in-slope and does not appear to significantly offset offshore submerged marine terraces. It is also not associated with a major geophysical anomaly indicating that it has had relatively minor cumulative bedrock offset. We interpret the contrast between theses faults to show that the slip rate on the Shoreline fault zone is one to two orders of magnitude lower than the Hosgri fault zone. Hence, our preliminary qualitative estimate of slip rate on the Shoreline fault zone using this approach is 0.01 to 0.3 mm/yr.

Table 1 Characteristics of the Shoreline Fault Zone and the Northern Microseismicity Lineament

Segment	Location Strike	Length Width Dip	Geomorphic (bathymetric) Expression	Lithology	Structure	Microseismicity	Seismic Reflection
				SHORELINE FAULT ZONE			
North Segment	Offshore of Point Buchon to Lyon Rock N40°W	6 km; may extend north additional 3km Not known* 90° (?)	Moderate geomorphic expression with fault line scarps in resistant rock in contact with sand sheets. Strong morphology where not covered by sand sheet. Wave-cut platform not displaced across fault.	Locally Sharp lithologic contacts (Obispo/Monterey)	Strong; south end changes strike and trends onshore as 'horsetail' strands south of Lion Rock and may connect with bedrock faults mapped onshore	A few microseismic events	No deformation of wavecut terraces within 1 meter resolution
Central Segment	Lyon Rock to Rattlesnake Creek N65°W	8 km 2 to 10 km* 90°	Strong geomorphic expression, with fault line scarps in resistant rock units. Locally sharp morphology with en echelon offsets C-1 moderately prominent C-2 prominent; particularly where not covered by sand sheet C-3 moderately prominent	C-1 contact within Obispo rocks but covered by sand sheet C-2 sharp lithologic contact (Obispo/Franciscan?) C-3 sharp contact in Franciscan	Strong with 100 to 500 m stepover between segments C-1 Strong; truncated bedding, no onshore connection (?) C-2 Very strong; may connect to Olson fault C-3 Locally strong; truncated bedding; may connect to Rattlesnake fault	Best expression 3 to 8 km deep No differentiation of geologic segments C1, C-2, C-3 Right lateral focal mechanisms	No reflection data due to proximity to shore Acoustically opaque basement
South Segment	Rattlesnake Creek to end of seismicity lineament south of Point San Luis N50°W	5 to 5 ½ km 2 to 10 km* 90°	Weak to moderate; local fault line scarps in resistant rocks in contact with sand sheets	Sharp lithologic contact in Franciscan	Locally strong; truncated bedding	Weakest expression With cluster and largest earthquake at marking the southern end Right lateral focal mechanisms	Wavecut platform and overlying Quaternary sediments not deformed
				MICROSEISMICITY LINEAMENT			
Northern Micro-seismicity trend	Hosgri fault to Lyon Rock N45°W	9 km 2 to 15 km* 90°	No surface expression	No lithologic contact	No structural offsets No association with North Segment of Shoreline fault 'Blind'?	Locally diffuse toward north 3 to 15 km deep Right lateral focal mechanisms	Wavecut platform and overlying Quaternary sediments not deformed

Footnote: * Width of fault zone is estimated from the depth of the microseismic events

5.0 IMPACTS AT DCPP

5.1 Ground Motion

The previous analysis of the impacts of the ground motion at DCPP assumed a M6.5 strike-slip earthquake at a distance of 1 km. The results from the 2009 studies indicate that the length of the combined central and southern segments corresponds to a magnitude 6.25 earthquake. The distance from DCPP to the power block is 0.6 km, not 1 km as previously assumed.

For the same magnitude, the change from 1 km to 0.5 km distance leads to about a 4% increase in the 84th percentile ground motions. Reducing the magnitude from 6.5 to 6.25 leads to a 5-10% reduction in the 84th percentile ground motions. As shown in Figure 12, the spectrum from the Shoreline fault zone remains lower than the LTSP spectrum. In the frequency range of 3-8.5 Hz used for the fragility curves, the Shoreline fault spectra are 10-30 percent lower than the LTSP. Therefore, using the new results, the deterministic ground motion will remain smaller than the LTSP spectrum and there is adequate seismic margin.

5.2 Potential for Secondary Fault Deformation

The central segment of the Shoreline fault zone is 600 meters from the Power Block and 300 meters from the cooling water intake. Given this short distance, the potential for secondary fault deformation is evaluated. The geology in the plant region is shown in Figure 10b. There is a unit labeled Tfoc, consisting of shale, claystone and siltstone that is a weaker rock material. If secondary fault ruptures occur, they would most likely occur in the weaker Tofc unit.

The Auxiliary Salt Water (ASW) pipes are the only safety related Structures, Systems and Components (SSC) that could be affected by small fault deformations in the Tfoc unit. A study of the deformation capacity of the ASW pipes found that there are eight 1-ft long Dresser coupling sections that are susceptible to small ground deformations.

An initial probabilistic analysis of the secondary fault deformation occurring at any of the eight Dresser coupling sections was conducted following the method of Petersen et al (2004). Two rupture segmentation models are considered; rupture of the Central segment by itself (M6.0) and rupture of the combined Central and Southern segments (6.25). As described in Section 4.4, the slip-rate is uncertain but is judged to be between 0.01 and 0.3 mm/yr. The hazard for secondary fault deformation occurring at any of the eight Dresser couplings is shown in Table 2 for the two rupture models. The range of values for each case represents the range of slip rates. The probability of 1 cm or larger occurring is very small: between 4.2E-9 to 2.4E-7. The NRC allows for events with less than 1E-8 to be excluded from the risk assessment for Yucca Mountain (10-CFR.63-342).

This screening level falls within the lower range of the probabilities of secondary fault deformation.

Secondary fault deformation was not previously considered in the license of DCPP. The potential impacts are evaluated in terms of the potential change in the seismic Core Damage Frequency (CDF). The seismic CDF at DCPP is 3.7 E-5 (LTSP, 1988). Therefore, with the probability of secondary fault rupture in the range of 4.2E-9 to 2.4E-7, the increase in seismic CDF due to secondary fault deformation will be much less than 1%. We conclude that secondary fault deformation impacting the ASW pipes leads to a negligible change in the seismic CDF and does not affect the seismic safety of DCPP.

Table 2. Annual probability of secondary fault rupture at any of the eight Dresser couplings of the ASW in the Tofc unit.

Secondary Deformation	Central (M6.0)	Central & Southern (M6.25)
>1.0 cm	4.2E-9 - 1.3E-7	8.0E-9 - 2.4E-7
>2.0 cm	1.7E-11 -5.1E-10	2.3E-9 - 6.9E-8

6.0 SUMMARY AND PLANNED 2010 STUDIES

6.1 Summary

Initial analyses of the seismicity, multibeam (MBES) bathymetry, and high resolution seismic profiles collected to date allow for several preliminary observations and conclusions as summarized below. These preliminary conclusions will be further evaluated during Year 2 (2010) of our planned Investigation Program.

Seismicity Lineament

1. The seismicity lineament as defined by Hardebeck (2009) is a robust feature and consists of approximately 50 events from 1988 to 2008. All of the events are small (most are in the M 1 to 2 range) with the largest being a M3.5 in 2000. Horizontal location uncertainty is approximately ± 0.5 km, vertical uncertainty is ±1.4 km.

2. Seismicity generally becomes more diffuse spatially and extends to greater depths (2 to 15 kilometers) along the northern part of the lineament as it approaches the Hosgri fault zone. The depth range of the seismicity along the central and southern parts of the lineament extends from 2 to 10 kilometers. The seismicity

along the entire lineament defines a nearly vertical zone. Focal mechanisms indicate primarily right lateral strike slip movement.

Shoreline Fault Zone

1. The Shoreline fault zone has been identified based on MBES and high resolution seismic profiling data The Shoreline fault zone displaces Tertiary and older geologic structures, and thus is younger. The fault zone consists of three distinct segments, the Northern, Central and Southern segments. These segments are well expressed in the sea floor bathymetry as the result of differential marine erosion along the fault trace.

2. The total length of the active portions of the Shoreline fault zone is 13 to 14 km: 8 km for the Central segment and 5- to 5 1/2 km for the Southern Segment. The Northern segment is 6 to 9 km long and is not considered active.

3. The seismicity lineament is coincident with and indicates reactivation of the Central and Southern segments of the Shoreline fault zone. The seismicity lineament diverges northward away from the Northern Shoreline fault zone segment. Therefore, we consider the Northern Shoreline fault zone segment to be a separate structure in the current tectonic setting.

4. Seismic reflection lines across the northern part of the seismicity lineament provide direct stratigraphic evidence that demonstrates the lineament is not associated with surface faulting. The northern part of the seismicity lineament may be occurring on a buried fault in the crust between the Shoreline and the Hosgri fault zones or it may be occurring on faults at depth within the Hosgri fault zone.

Location with Respect to DCPP

1. The Central segment of the Shoreline fault zone is 300 meters southwest of the Intake structure and 600 meters southwest of the Power Block.

Activity Rate

1. Currently, the activity or slip rate on the Shoreline fault is poorly constrained. Developing constraints on the slip rate will be a focus of our 2010 investigations. Qualitative comparison of the Shoreline fault zone to the more prominent Hosgri fault zone suggests a slip rate one to two orders of magnitude less than the Hosgri fault zone, or approximately 0.01 to 0.3 mm/yr. At this time, we believe that this qualitative assessment bounds the range of uncertainty in slip rate on the Shoreline fault zone.

Implications to DCPP

1. The vibratory ground motion impacts were evaluated using a margin approach. The 84^{th} percentile ground motions from the Central and Southern segments of the Shoreline fault zone are bounded by the LTSP. Therefore, there is adequate seismic margin due to vibratory ground motion.

   The secondary fault deformation impacts were evaluated using a Probabilistic Risk Assessment (PRA) approach. The probability of 1 cm or larger deformation at any of the eight Dresser coupling ranges from 4E-9 to 2E-7 depending on the slip-rate (0.01 to 0.3 mm/yr) and rupture segmentation (Central segment versus combined Central and Southern segments). The potential change in the seismic CDF is much less than 1%. Therefore, we conclude that the secondary deformation leads to a negligible change in the seismic CDF.

6.2 Planned 2010 studies

PG&E's research program for 2010 will focus on integrating and interpreting the geologic and geophysical data sets collected in 2008 and 2009 in a regional context. A high priority task is to better characterize the slip rate, long-term style of deformation, and slip along the Shoreline fault zone. This will involve completion of our interpretations of the marine multibeam survey and, working with the USGS, completion of the processing and interpretation of the high resolution marine reflection, magnetics, and gravity data. Specific geologic studies to asses the possible relationship of the Shoreline fault zone to the Southwestern Boundary Zone and to improve our estimates of the slip rate for the Shoreline fault will also be conducted.

All of the geologic and geophysical information collected to date will be integrated to develop an initial three dimensional tectonic model of the region in 2010. This compilation will be used as input to a 3-D finite element model to evaluate various kinematic interpretations of crustal deformation in the central California coastal region. The characterization of the Shoreline fault zone will be incorporated into the seismic hazard update being conducted as part of the LTSP. This complete seismic hazard update is scheduled to be completed in 2013.

7.0 REFERENCES

California State University Monterey Bay Sea Floor Mapping Lab (2009). Website at http://seafloor.csumb.edu/SFMLwebDATA_c.htm (visited 3/26/2009).

Hall, C.A., Jr. (1973). Geologic map of the Morrow Bay South and Port San Luis Quadrangles, San Luis Obispo County, California: U.S. Geological Survey Miscellaneous Field Studies Map MF-511, scale 1:24,000.

Hall, C.A., Jr. (1978). Origin and development of the Lompoc-Santa Maria pull-apart basin and its relation to the San Simeon-Hosgri strike-slip fault, Western California: in Silver, E.A. and Normark, W.R., eds, San Gregorio-Hosgri fault zone, California; California Division of Mines and Geology Special Report 137, p. 25-32.

Hanson, K. L., Wesling, J.R., Lettis, W.R., Kelson, K.I. , and Mezger, L.(1994).. Correlation, ages, and uplift Rates of Quaternary marine terraces, South-central California., *in* I.B. Alterman, R.B. McMullen, L.S. Cluff, and D.B. Slemmons *(eds.),* Seismotectonics of the Central California Coast Range: Geological Society of America Special Paper 292. p. 45-72. 1994.

Hanson, K.L., Lettis, W.R., McLaren, M.K., Savage, W.U., and Hall, N.T. (2004). Style and rate of Quaternary deformation of the Hosgri fault zone, offshore south-central California: submitted to Keller, M., ed., Santa Maria Province Project, U.S. Geological Survey Bulletin No. 1995-BB, p 37.

Hardebeck, J.L. (2009). Seismotectonics and fault structure of the California central coast, in review to Bull. Seismol. Soc. Amer., August 14, 2009.

Langenheim, V.E., Jachens, R.C., Graymer, R.W. and Wentworth, C.M. (2008). Implications for fault and basin geometry in the central California Coast Ranges from preliminary gravity and magnetic data, EOS (Abs. AGU), Fall Meeting 2008, abstract #GP43B-0811.

Langenheim, V.E., Jachens, R.C, and Moussaoui, K. (2009). Aeromagnetic survey map of the central California Coast Ranges , USGS Open File Report 2009-1044 http://pubs.usgs.gov/of/2009/1044/.

Lettis, W.R., Hanson, K.L., Unruh, J.R., McLaren, M., and Savage, W.U (2004). Quaternary tectonic setting of south-central coastal California: U.S. Geological Survey Bulletin 1995-AA, 24 p., http://pubs.usgs.gov/bul/1995/aa [web only].

Murphy, J.M. and Walter, A.W. (1984). Data report for a seismic-refraction investigation; Morro Bay to the Sierra Nevada, California, U.S. Geol. Surv. Open File Rep., 84-0642, 39 pp.

Nuclear Regulatory Commission (NRC) (1991).Supplement No. 34 to NUREG-0675, Safety evaluation report Related to the operation of Diablo Canyon Nuclear Power Plant, Units 1 & 2, July 1991.

Nuclear Regulatory Commission (NRC) (2009) NRC (2009). Research Information Letter 09-001: Preliminary Deterministic Analysis of Seismic Hazard at Diablo Canyon Nuclear Power Plant from Newly Identified "Shoreline Fault", ADAMS ML090330523, April 8, 2009.

Pacific Gas and Electric Company (PG&E) (1988). Final report of the Diablo Canyon long term seismic program, US Nuclear Regulatory Commission Enclosure 1, PG&E letter No. DCL-05-002, Docket No. 50-275 and No. 50-323.

Pacific Gas and Electric Company (PG&E) (1989a). Long term seismic program: Plate Q43i-2-1, Geologic map of coastal California from Morrow Bay to the Santa Maria Valley, south-central California. US Nuclear Regulatory Commission Docket No. 50-275 and No. 50-323.

Pacific Gas and Electric Company (PG&E) (1989b). Long term seismic program: Plate Q43i-2-4, Model B longitudinal profile of marine terrace shoreline angles from Morrow Bay to the Santa Maria Valley, south-central California. US Nuclear Regulatory Commission, Docket No. 50-275 and No. 50-323.

Pacific Gas and Electric Company (PG&E) (1990). Long term seismic program: Plate Q16-1B: Onshore-offshore geologic correlation map of the southwestern boundary of the San Luis/Pismo structural block, north sheet. US Nuclear Regulatory Commission Docket No. 50-275 and No. 50-323.

Pacific Gas and Electric Company (PG&E) (2004). Final safety analysis report of the Diablo Canyon independent spent fuel storage installation, figure 2-6.6, US Nuclear Regulatory Commission Docket No. 72-26.

Pacific Gas and Electric Company (PG&E) (2008). Email, Subject: Preliminary data for seismic discussion, To: Alan Wang, Vincent Gaddy (NRC), From: Bill Guldemond (PG&E) with attachment, DCPP_Nov 20-2008_v2 (3).ppt.

Petersen, M., Cao, T., Dawson, T., Frankel, A., Wills, C. and Schwartz, D. (2004). Evaluation fault rupture hazard for strike-slip earthquakes, proceedings from GeoTrans, p 787-796.

Sharpless, S.W. and Walter, A.W. (1988). Data report for the 1986 San Luis Obispo, California, seismic refraction survey, U.S. Geol. Surv. Open File Rep., 88-0035, 48 pp.

Sliter, R.W., Triezenberg, P.J., Hart, P.E., Watt, J.T., Johnson, S.Y., and Scheirer, D.S. (2009). High-resolution seismic reflection and marine magnetic data along the Hosgri fault zone, Central California, USGS Open File Report 2009-1100. http://pubs.usgs.gov/of/2009/1100

Thurber, C. H. (2009). Central California Offshore Earthquake Assessment, August 18, 2009.

Waldhauser, F., and Ellsworth, W.L. (2000), A double-difference earthquake location algorithm; method and application to the northern Hayward Fault, California, Bull. Seis. Soc. Am., 90, 1353-1368.

Watt, J.T., Johnson, S.Y., Langenheim, V.E., Scheirer, D.S., Rosenberg, L.I., Graymer, R.W., and Kvitek, R. (2009). Geologic mapping in the Central California coastal zone: integrating geology, geophysics, and geomorphology: Geological Society of America Abstracts with Programs, v. 41, n. 7, p. 283.

Zhang, H. and Thurber, C.H. (2003). Double-difference tomography: the method and its application to the Hayward fault, California, Bull. Seis. Soc. Am. 93, 1875-1889.

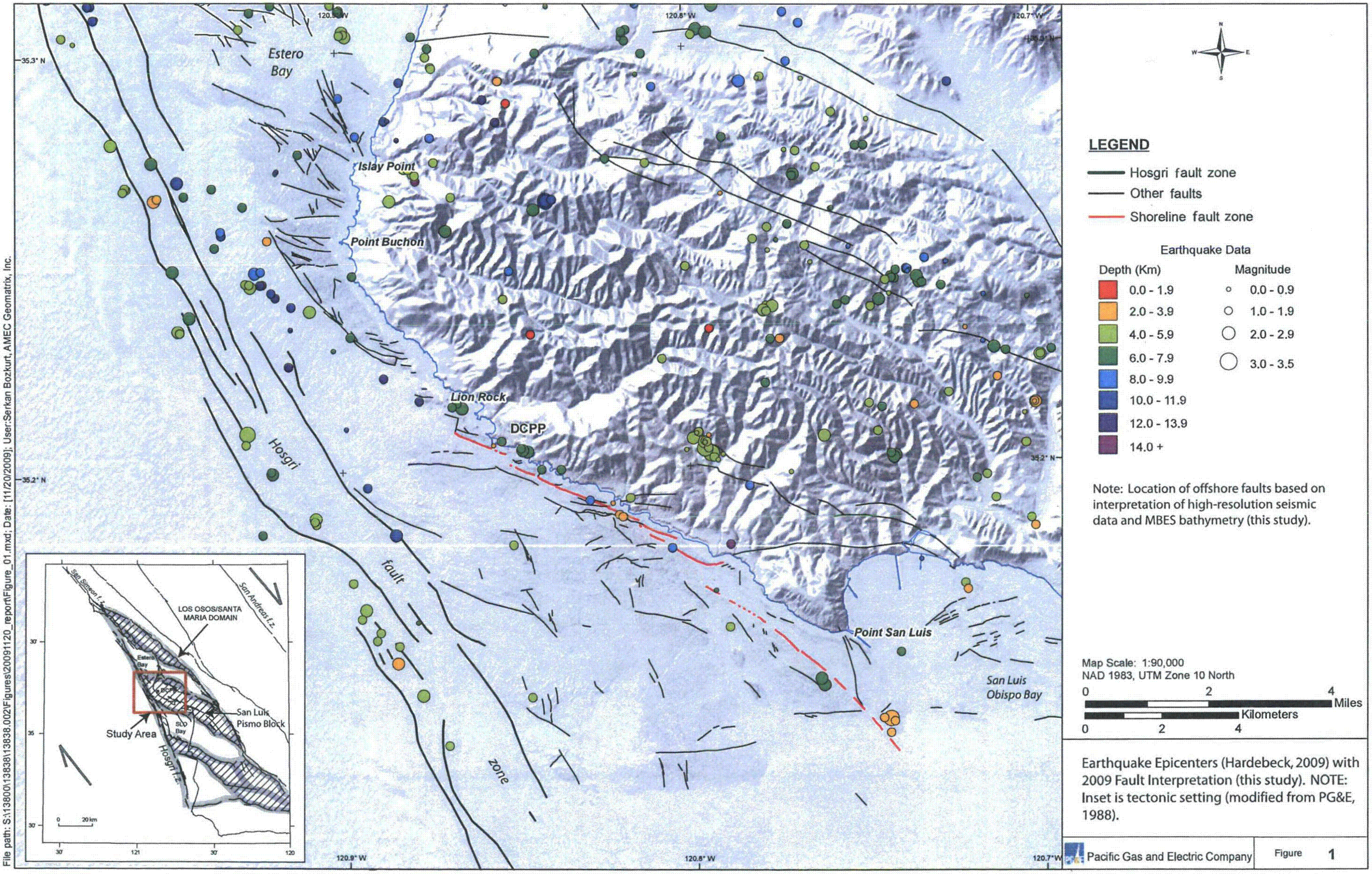

Earthquake Epicenters (Hardebeck, 2009) with 2009 Fault Interpretation (this study). NOTE: Inset is tectonic setting (modified from PG&E, 1988).

Pacific Gas and Electric Company | Figure 1

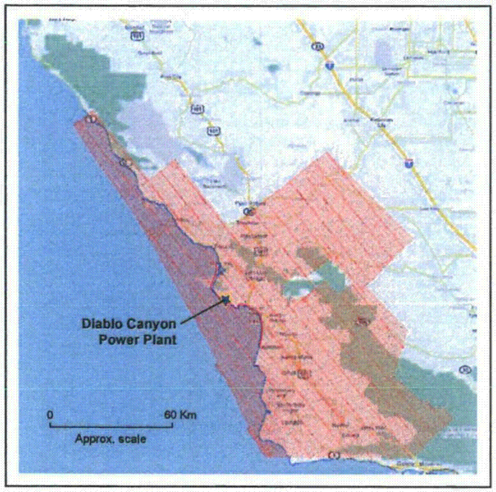

a. Aeromagnetic Survey Area 2008

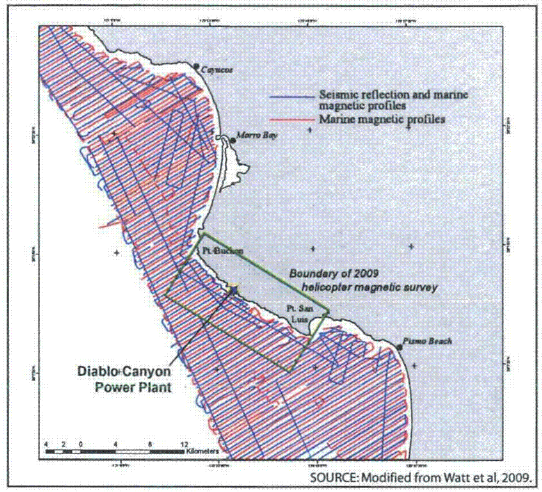

b. New Marine Geophysical Data Collected in 2008-2009

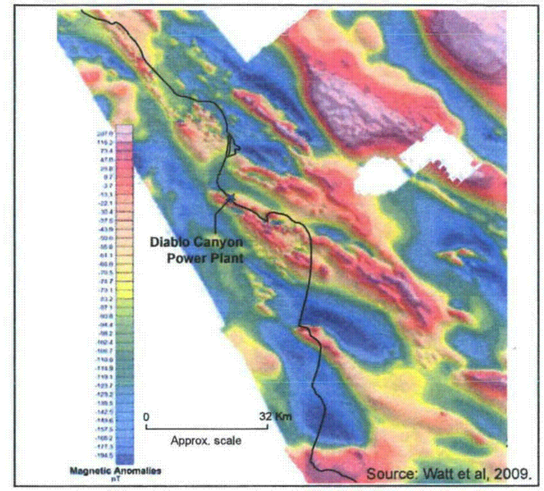

c. Regional Magnetic Anomalies

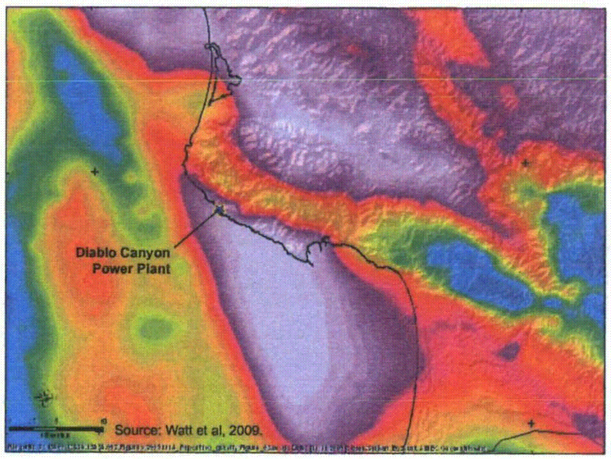

d. Regional Isostatic Gravity Anomalies

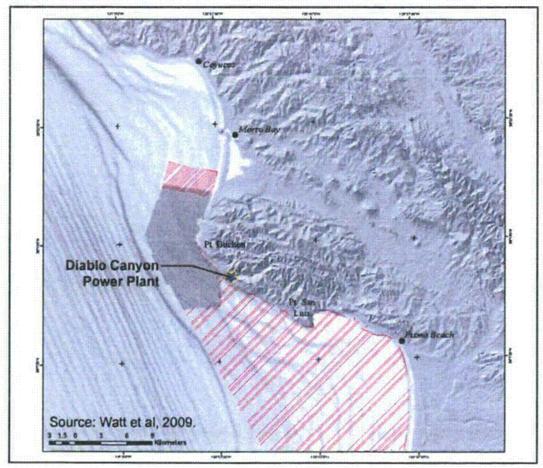

e. Multibeam Echo Sounding Bathymetry Data Coverage 2006 and 2009

Maps Showing Aeromagnetic, Gravity, Seismic Reflection, and Bathymetry Survey Areas and Data Examples

NOTE: See next page for 2f.

Pacific Gas and Electric Company | Figure 2

File path: S:\13800\13838\13838.002\Figures\20091120_report\Figure_02.ai; Date: [12/07/2009]; User:Serkan Bozkurt, AMEC Geomatrix, Inc.

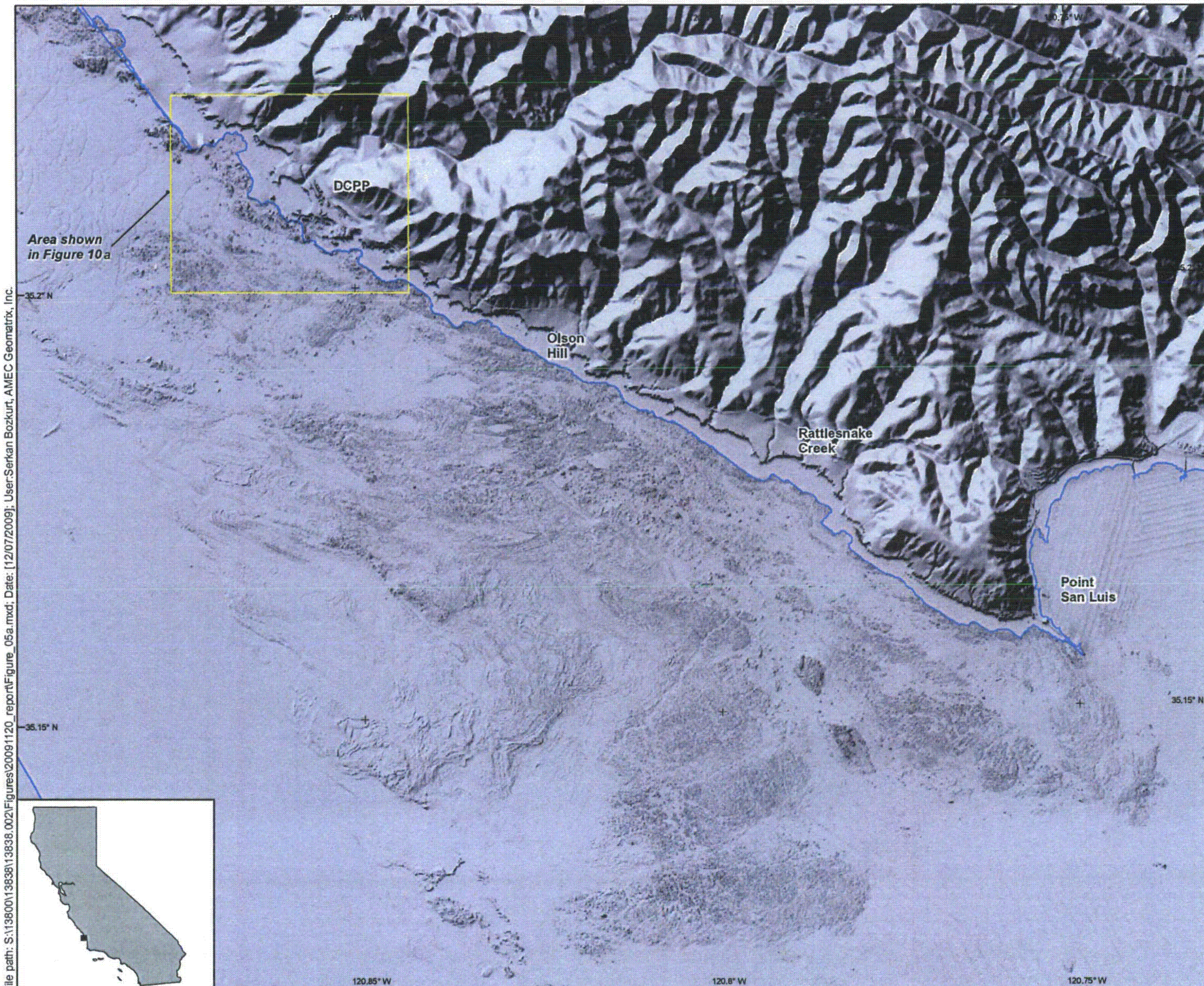

N
W E
S

LEGEND

Limits of MBES data

Map Scale: 1:50,000
NAD 1983, UTM Zone 10 North

0 1 2 Miles
0 1 2 3 Kilometers

Multibeam (MBES) Bathymetry Image Obtained for Analysis of Offshore Geology within the Shoreline Fault Zone Area

Pacific Gas and Electric Company | Figure 2f

File path: S:\13800\13838\13838.002\Figures\20091120_report\Figure_05a.mxd; Date: [12/07/2009]; User:Serkan Bozkurt, AMEC Geomatrix, Inc.

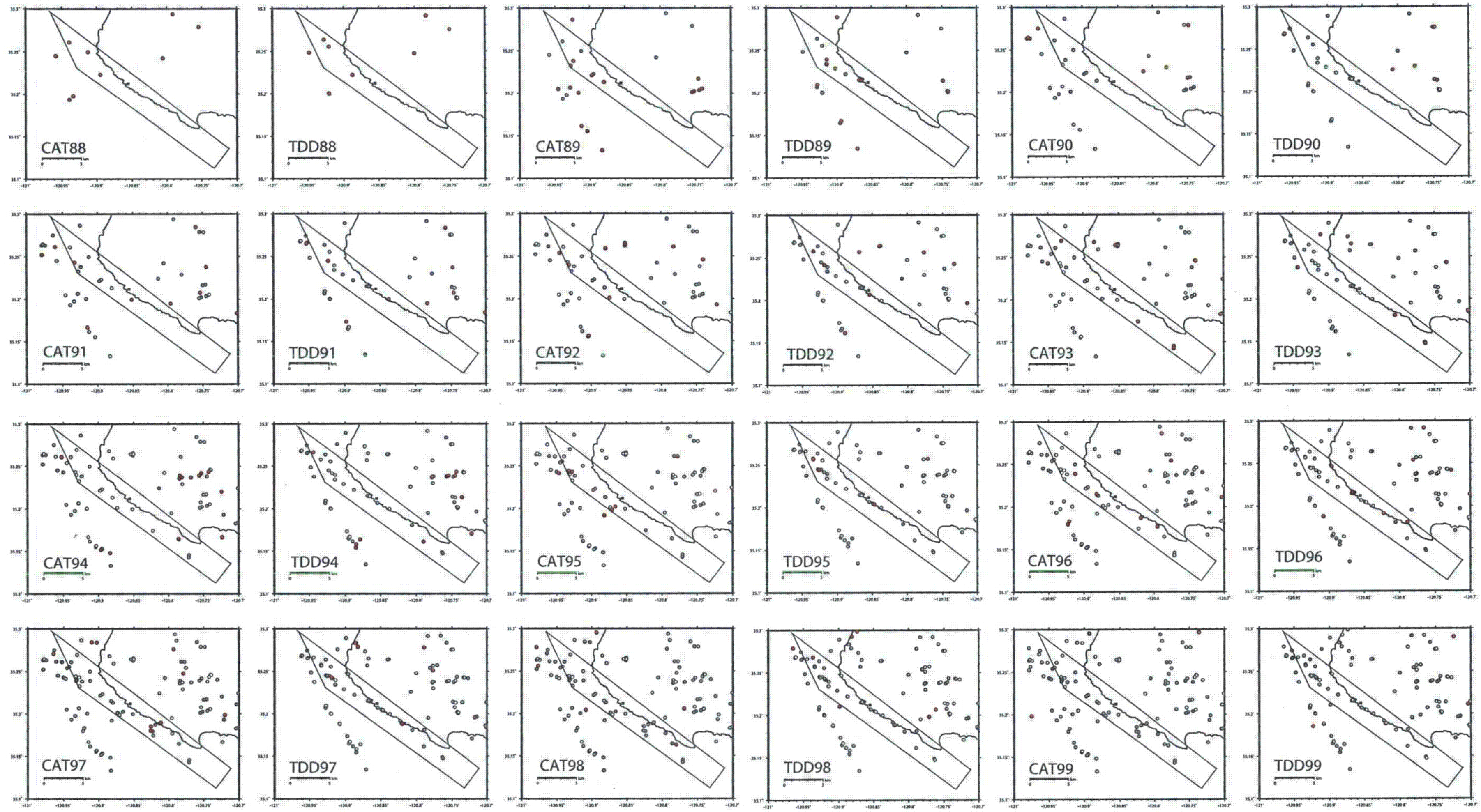

Current year earthquake locations
Previous year(s) earthquake locations

Yearly Seismicity Plots from 1988 to1999, Comparing USGS/PGE Catalog (CAT) Locations to Hardebeck tomoDD (TDD) Locations.

NOTE: Polygon encloses general area of the Shoreline fault zone. See Figure 3b for plots from 2000 to 2008.

Pacific Gas and Electric Company | Figure **3a**

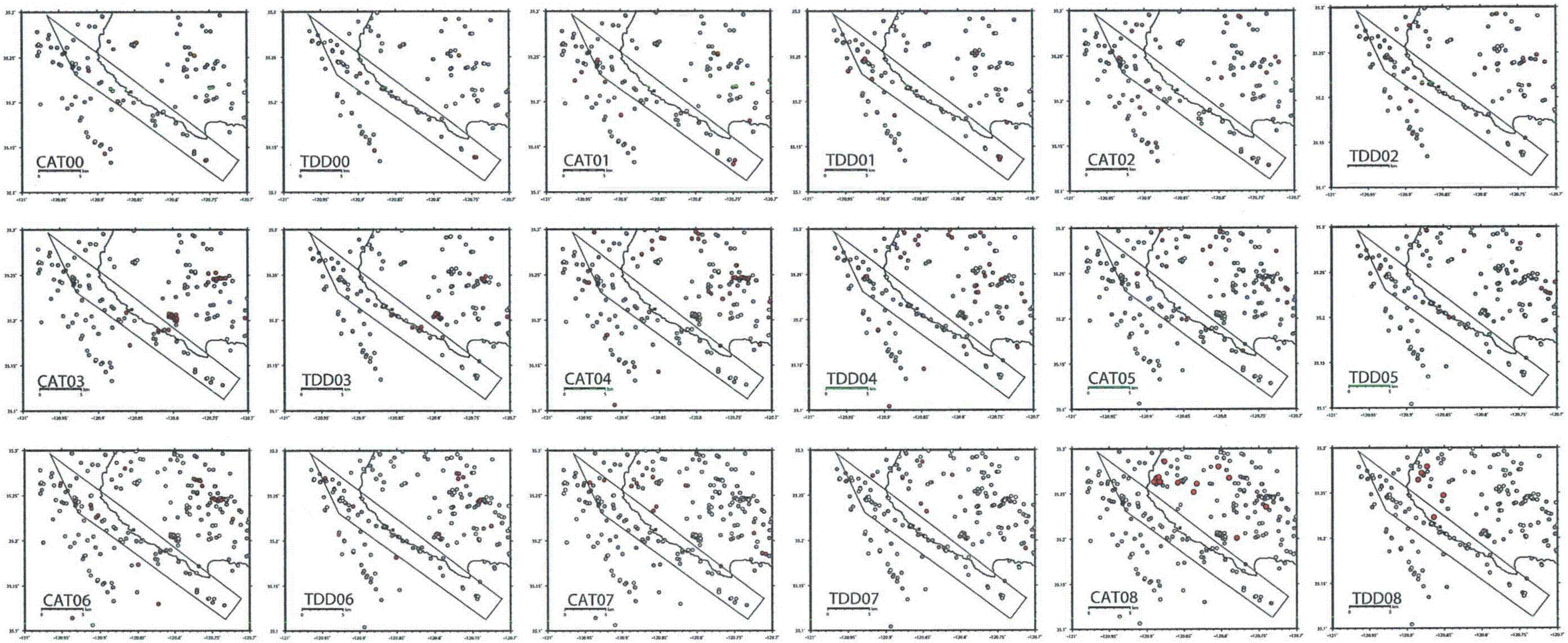

Current year earthquake locations
Previous year(s) earthquake locations

Yearly Seismicity Plots from 2000 to 2008, Comparing USGS/PGE Catalog (CAT) Locations to Hardebeck tomoDD (TDD) Locations.

NOTE: Polygon encloses general area of the Shoreline fault zone. See Figure 3a for plots from 1988 to 1999.

Pacific Gas and Electric Company	Figure **3b**

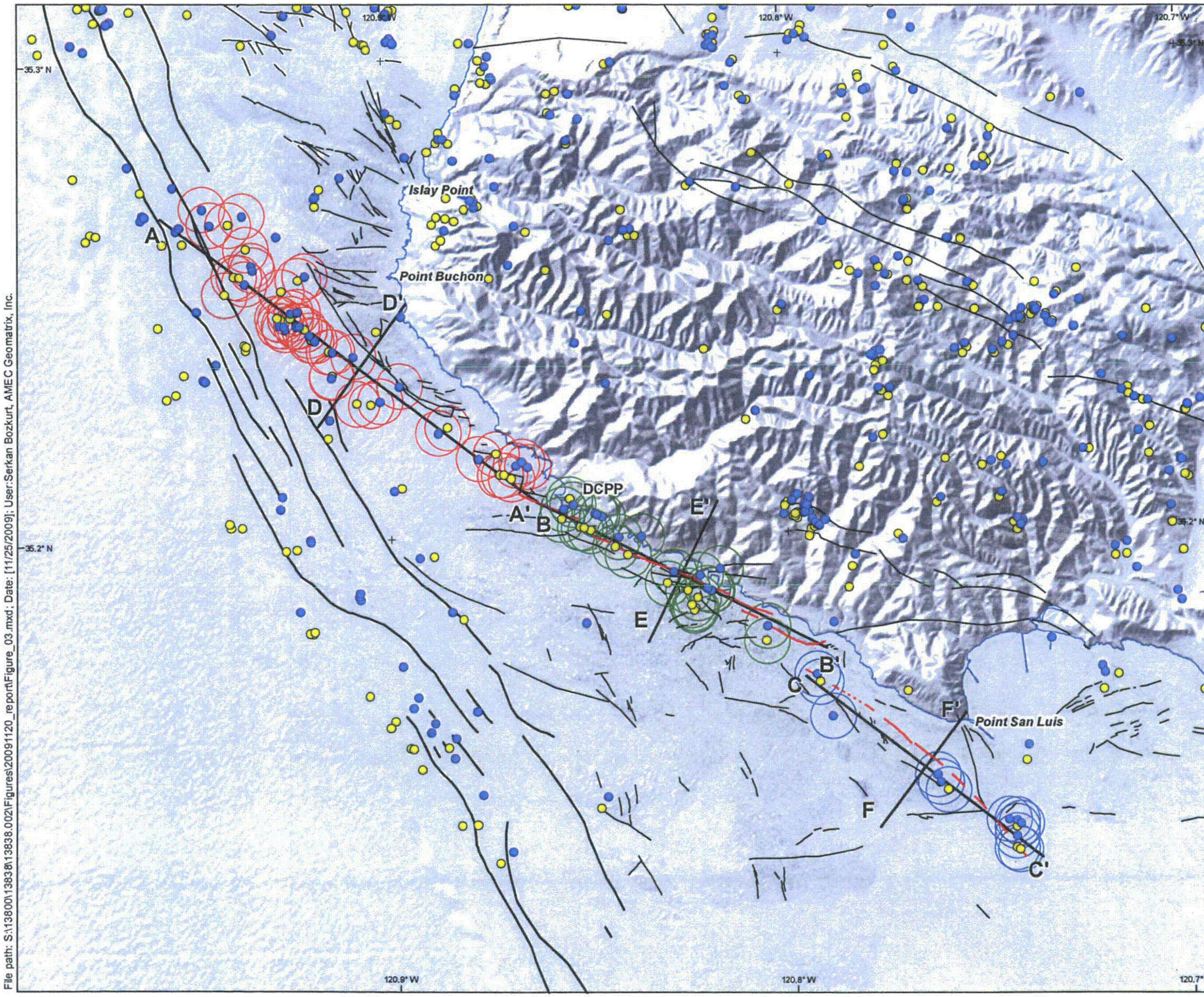

Earthquake Epicenters from Hardebeck and Thurber tomoDD Inversions with 2009 Fault Interpretation and 2009 MBES data.

Pacific Gas and Electric Company

Figure 4

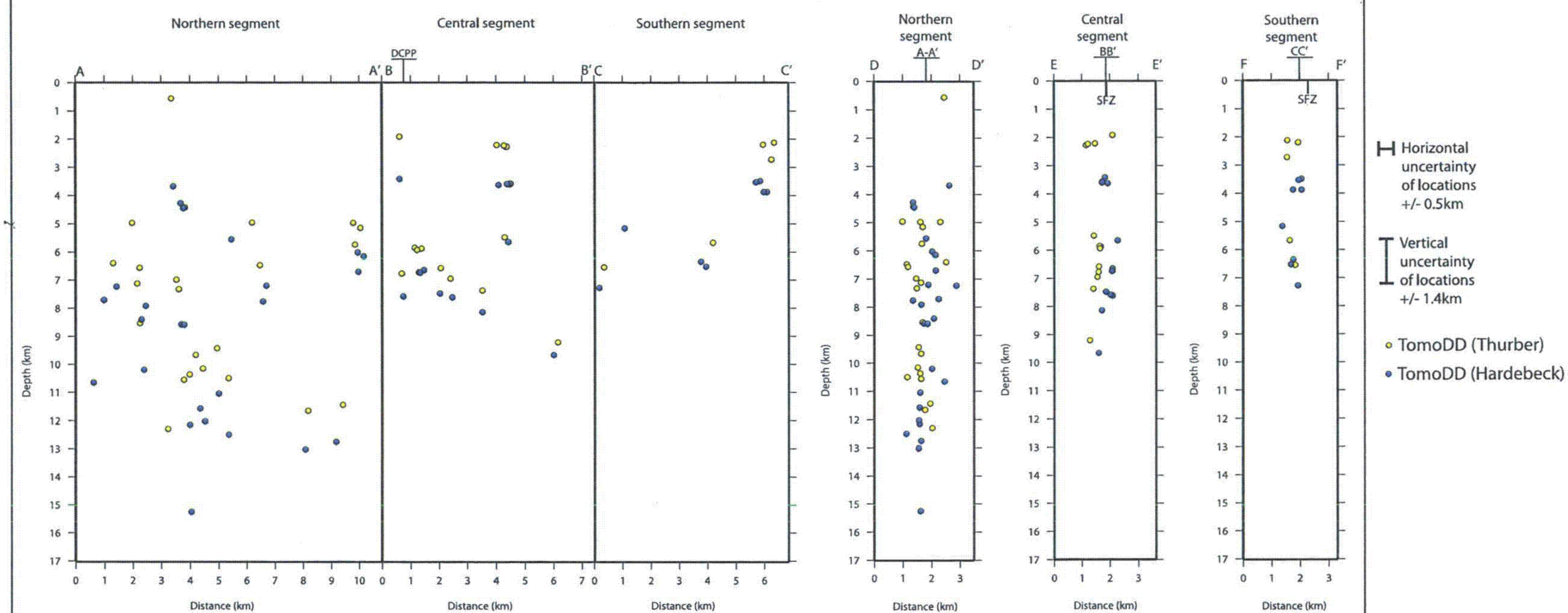

Seismicity Cross Sections Projecting Hardebeck and Thurber Locations.

NOTE: Cross sections AA', BB' and CC' are seamed together. See Figure 4 for cross section locations. SFZ=Shoreline fault zone.

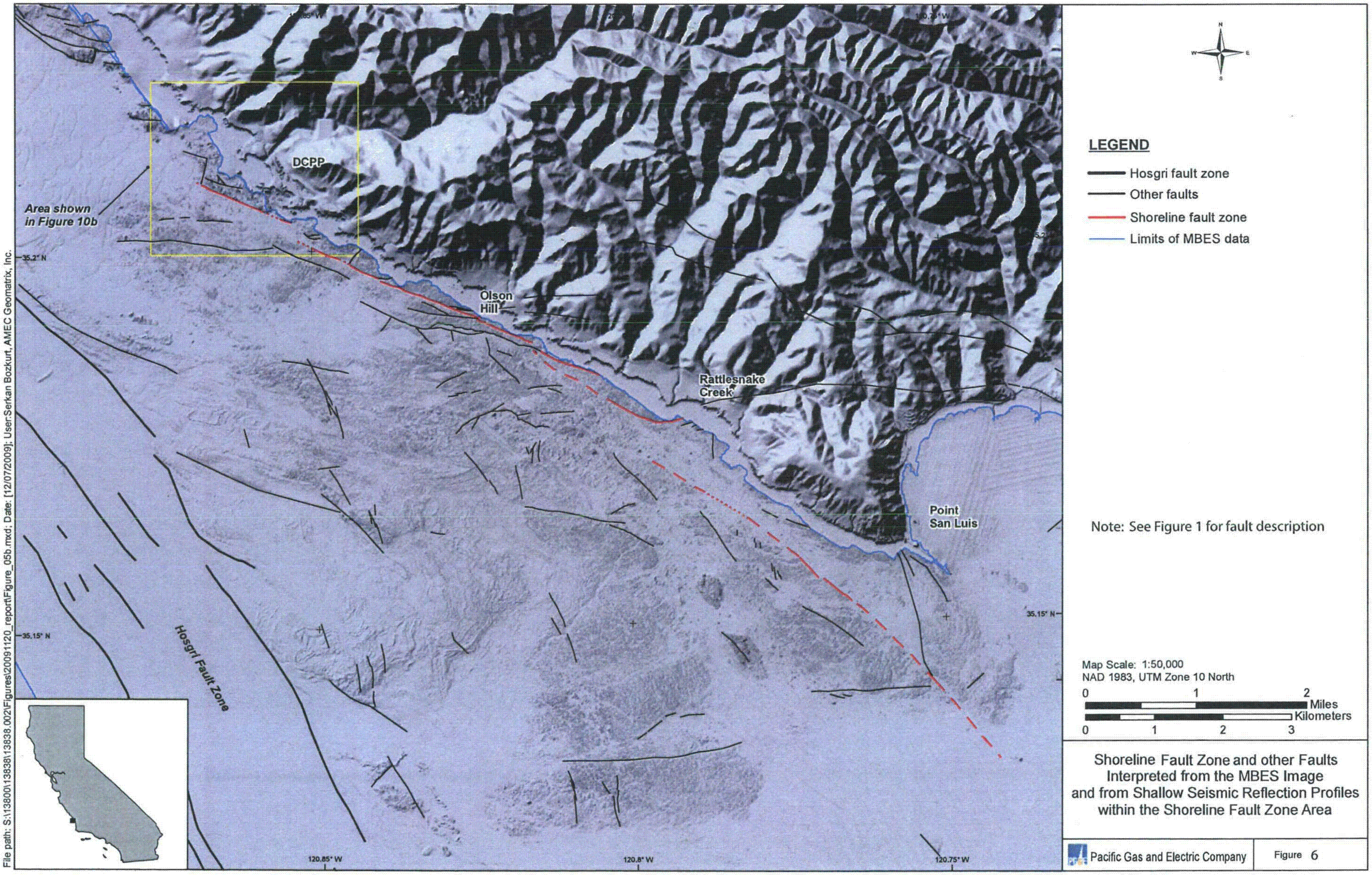

Shoreline Fault Zone and other Faults Interpreted from the MBES Image and from Shallow Seismic Reflection Profiles within the Shoreline Fault Zone Area

Pacific Gas and Electric Company | Figure 6

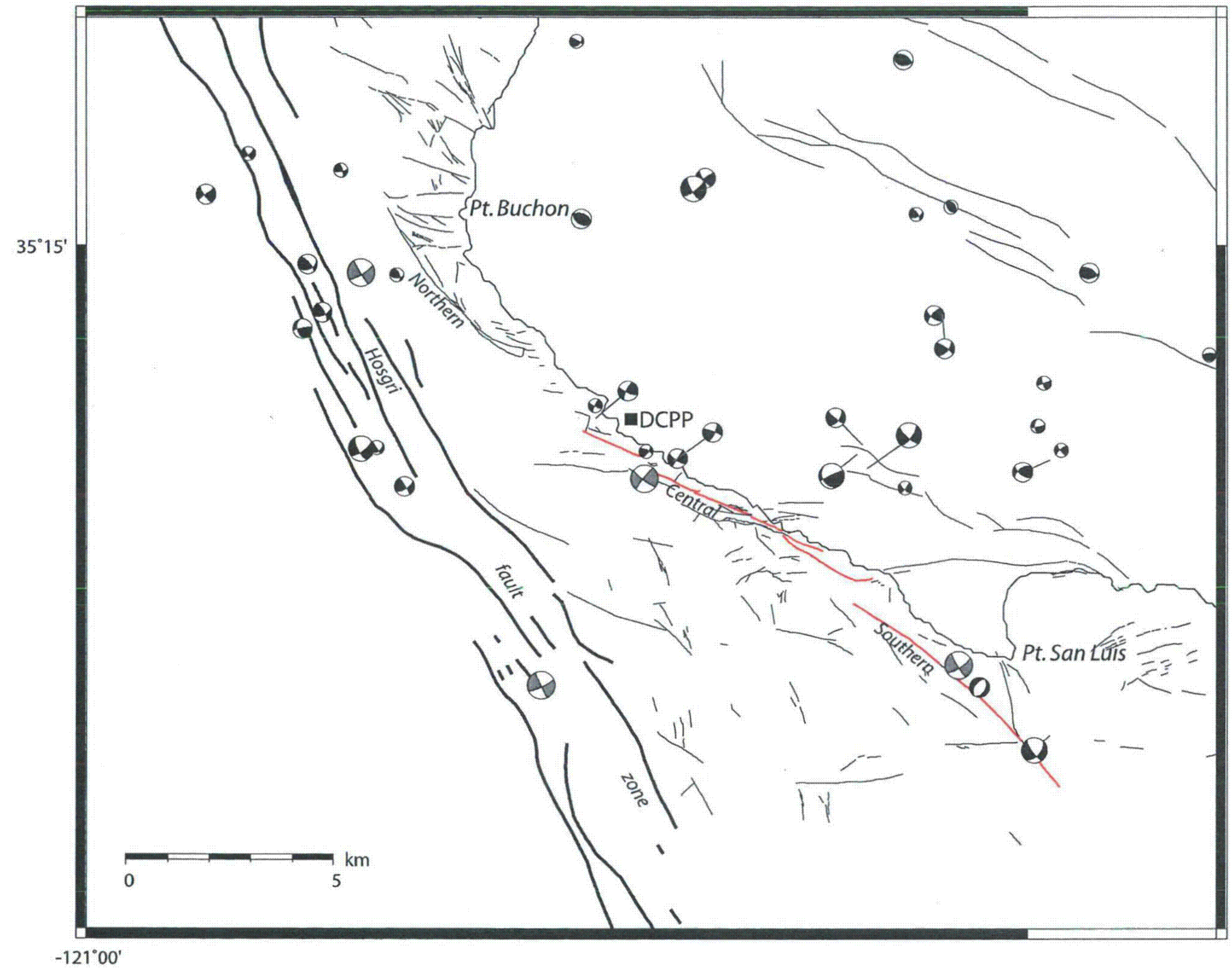

LEGEND

Focal Mechanisms

- M1-1.99
- M2-2.99
- M3-3.99
- Composite Focal Mechanisms

See Figure 1 for fault desriptions.

Focal Mechanisms from Hardebeck (2009)

NOTE: Shoreline fault zone segments are labeled.

Pacific Gas and Electric Company | Figure 7

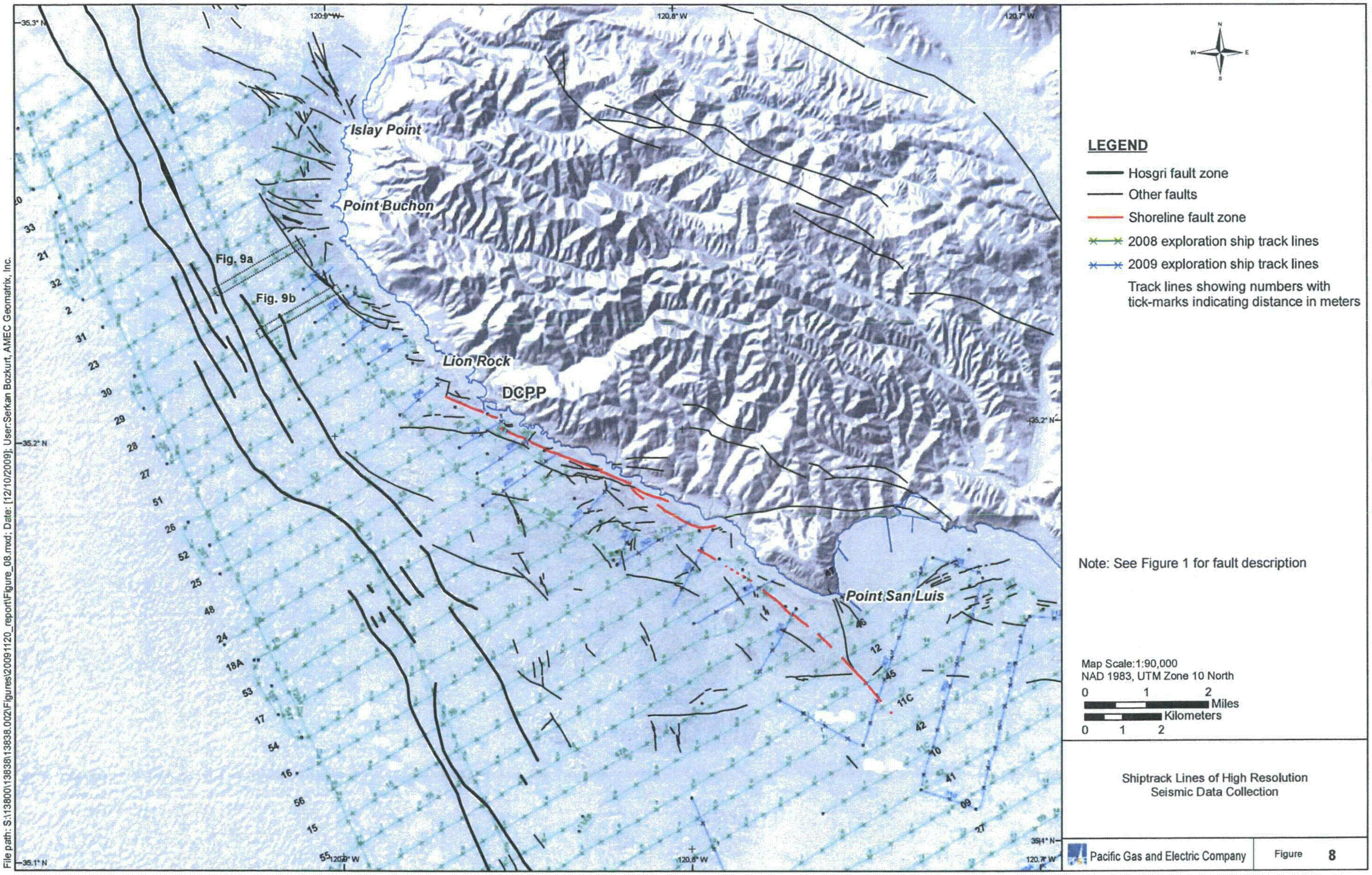

Islay Point
Point Buchon
Lion Rock
DCPP
Point San Luis
Fig. 9a
Fig. 9b
120.9° W
120.8° W
120.7° W
35.3° N
35.2° N
35.1° N
LEGEND
Hosgri fault zone
Other faults
Shoreline fault zone
2008 exploration ship track lines
2009 exploration ship track lines
Track lines showing numbers with tick-marks indicating distance in meters
Note: See Figure 1 for fault description
Map Scale:1:90,000
NAD 1983, UTM Zone 10 North
0 1 2 Miles
0 1 2 Kilometers
Shiptrack Lines of High Resolution Seismic Data Collection
Pacific Gas and Electric Company
Figure 8
File path: S:\13800\13838\13838.002\Figures\20091120_report\Figure_08.mxd; Date: [12/10/2009]; User:Serkan Bozkurt, AMEC Geomatrix, Inc.

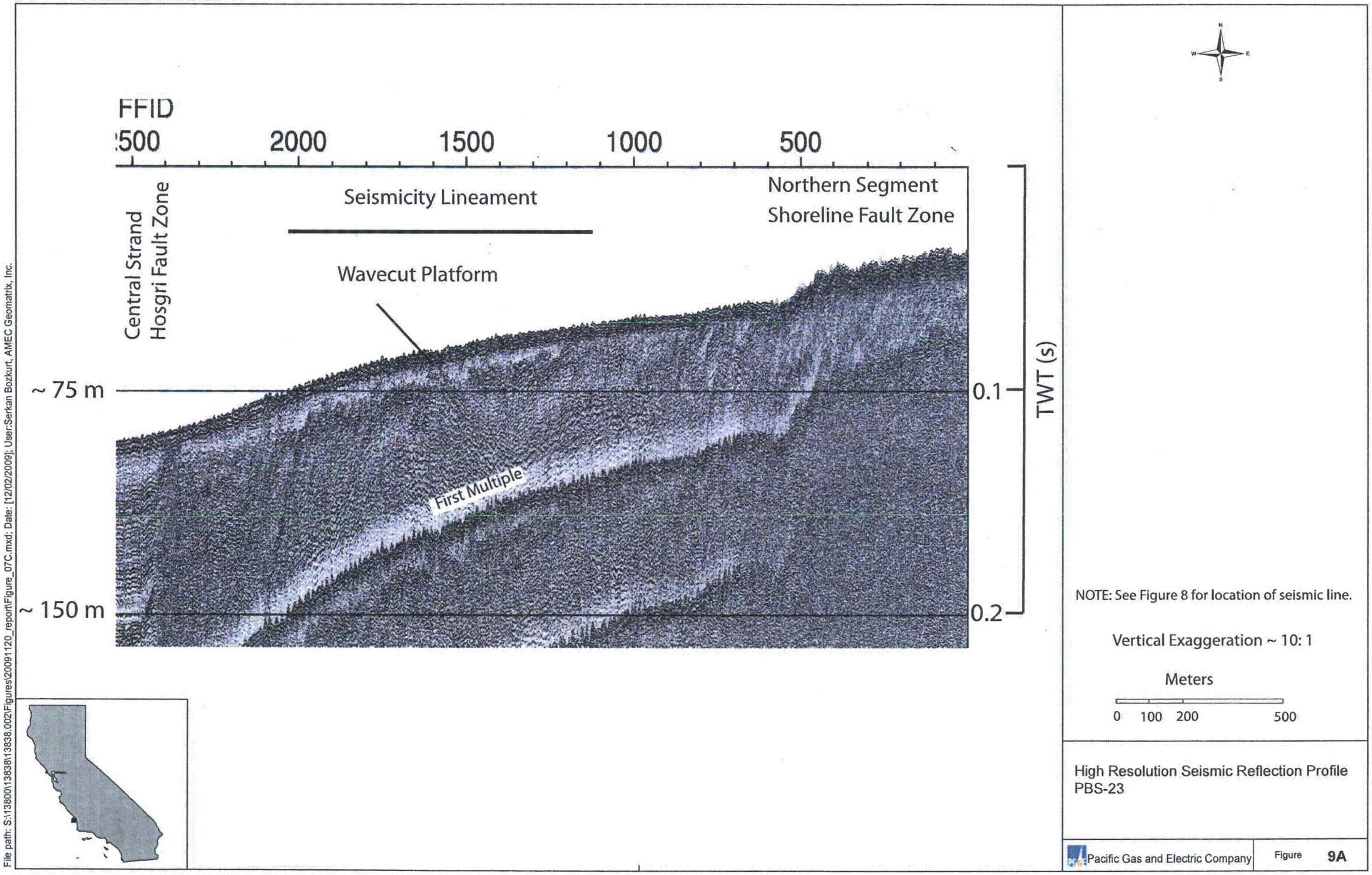

High Resolution Seismic Reflection Profile PBS-23

Pacific Gas and Electric Company | Figure 9A

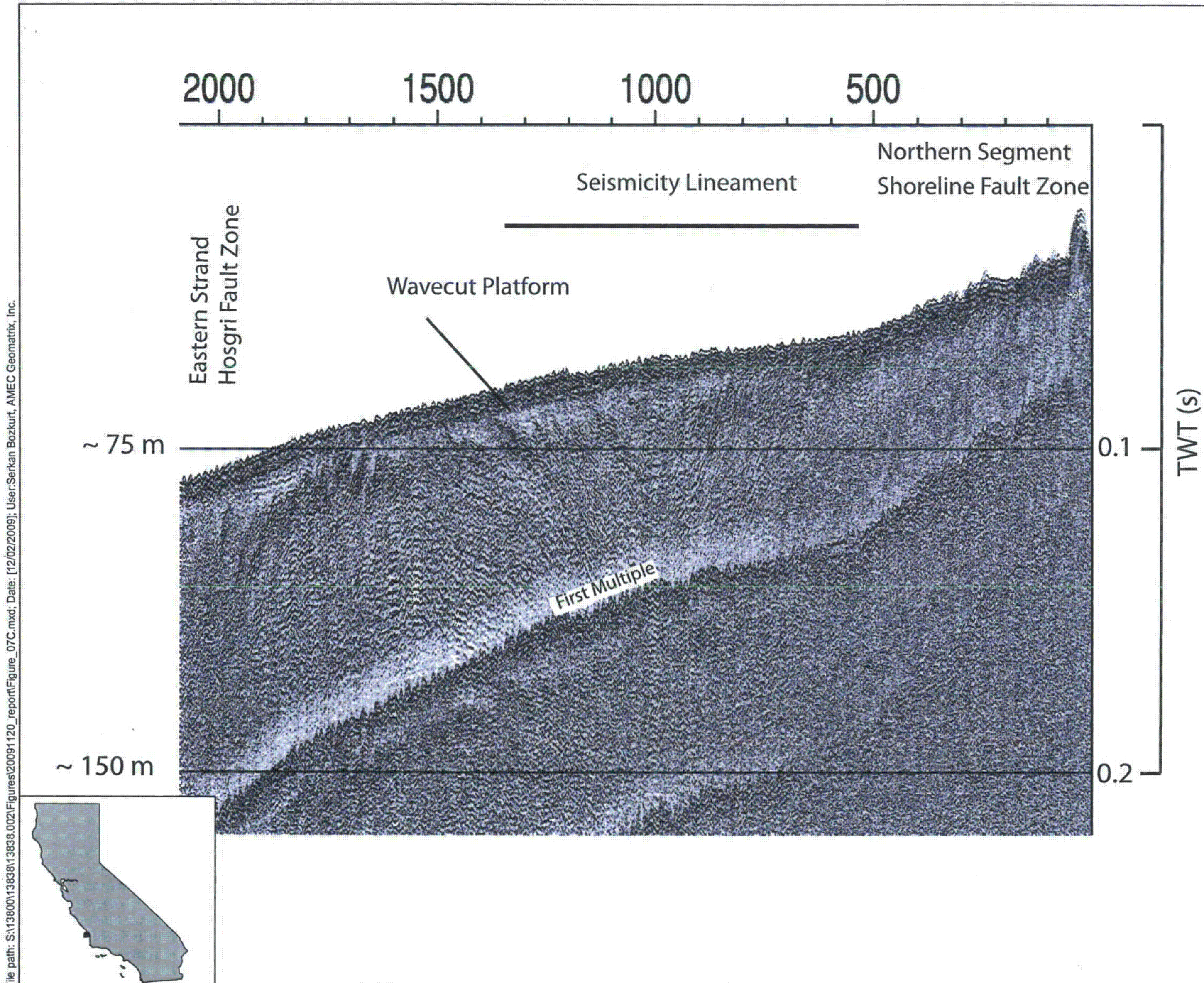

NOTE: See Figure 8 for location of seismic line.

Vertical Exaggeration ~ 10: 1

Meters

0 100 200 500

High Resolution Seismic Reflection Profile PBS-29

Pacific Gas and Electric Company | Figure 9B

File path: S:\13800\13838\13838.002\Figures\20091120_report\Figure_07C.mxd; Date: [12/02/2009]; User:Serkan Bozkurt, AMEC Geomatrix, Inc.

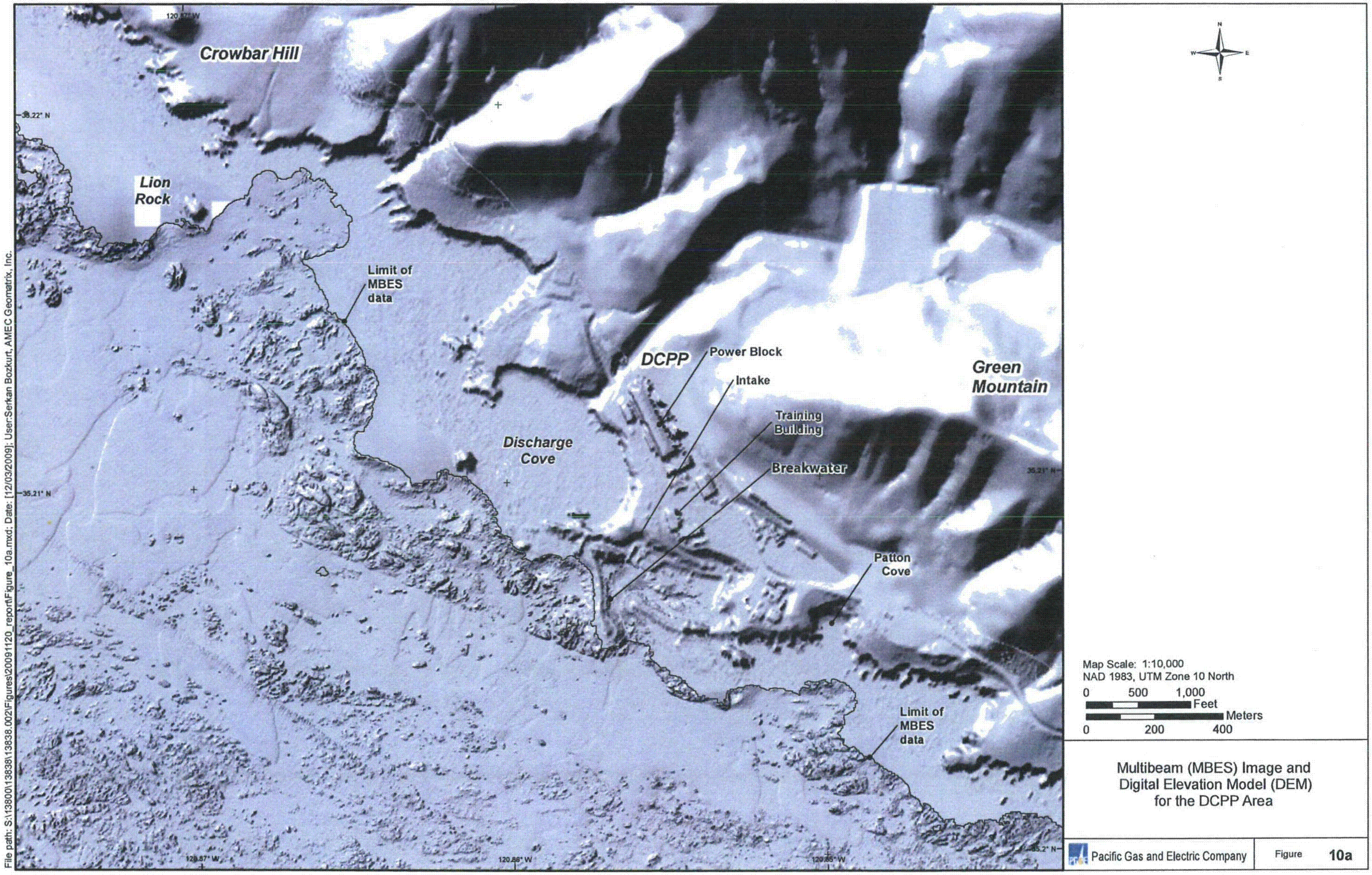
Crowbar Hill
Lion Rock
Limit of MBES data
DCPP
Power Block
Intake
Training Building
Breakwater
Discharge Cove
Green Mountain
Patton Cove
Limit of MBES data
35.22° N
35.21° N
35.21° N
35.2° N
120.87° W
120.86° W
120.85° W
Map Scale: 1:10,000
NAD 1983, UTM Zone 10 North
0 500 1,000 Feet
0 200 400 Meters
Multibeam (MBES) Image and Digital Elevation Model (DEM) for the DCPP Area
Pacific Gas and Electric Company
Figure 10a
File path: S:\13800\13838\13838.002\Figures\20091120_report\Figure_10a.mxd; Date: [12/03/2009]; User:Serkan Bozkurt, AMEC Geomatrix, Inc.

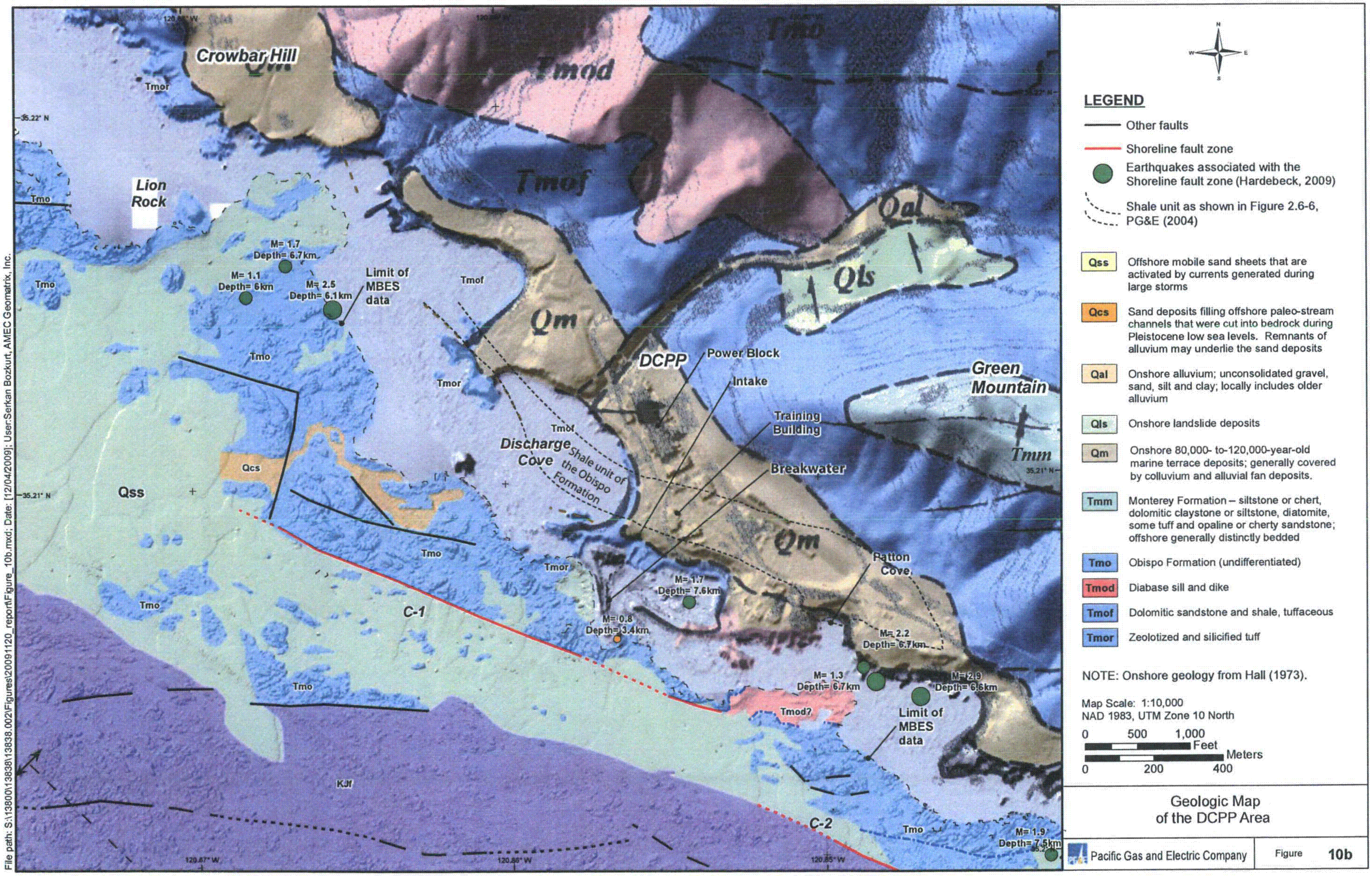

Crowbar Hill
Qm
Tmod
Tmo
Tmof
Qal
Qls
Lion Rock
Tmor
M= 1.7 Depth= 6.7km
M= 1.1 Depth= 6km
M= 2.5 Depth= 6.1km
Limit of MBES data
Qm
DCPP
Power Block
Intake
Training Building
Breakwater
Green Mountain
Tmm
Discharge Cove
Shale unit of the Obispo Formation
Qcs
Qss
C-1
M= 1.7 Depth= 7.6km
M= 0.8 Depth= 3.4km
Patton Cove
M= 2.2 Depth= 6.7km
M= 1.3 Depth= 6.7km
M= 2.9 Depth= 6.6km
Tmod?
Limit of MBES data
KJf
C-2
M= 1.9 Depth= 7.5km
File path: S:\13800\13838\13838.002\Figures\20091120_report\Figure_10b.mxd; Date: [12/04/2009]; User:Serkan Bozkurt, AMEC Geomatrix, Inc.
LEGEND
Other faults
Shoreline fault zone
Earthquakes associated with the Shoreline fault zone (Hardebeck, 2009)
Shale unit as shown in Figure 2.6-6, PG&E (2004)
Qss Offshore mobile sand sheets that are activated by currents generated during large storms
Qcs Sand deposits filling offshore paleo-stream channels that were cut into bedrock during Pleistocene low sea levels. Remnants of alluvium may underlie the sand deposits
Qal Onshore alluvium; unconsolidated gravel, sand, silt and clay; locally includes older alluvium
Qls Onshore landslide deposits
Qm Onshore 80,000- to-120,000-year-old marine terrace deposits; generally covered by colluvium and alluvial fan deposits.
Tmm Monterey Formation – siltstone or chert, dolomitic claystone or siltstone, diatomite, some tuff and opaline or cherty sandstone; offshore generally distinctly bedded
Tmo Obispo Formation (undifferentiated)
Tmod Diabase sill and dike
Tmof Dolomitic sandstone and shale, tuffaceous
Tmor Zeolotized and silicified tuff
NOTE: Onshore geology from Hall (1973).
Map Scale: 1:10,000
NAD 1983, UTM Zone 10 North
0 500 1,000 Feet
0 200 400 Meters
Geologic Map of the DCPP Area
Pacific Gas and Electric Company
Figure 10b

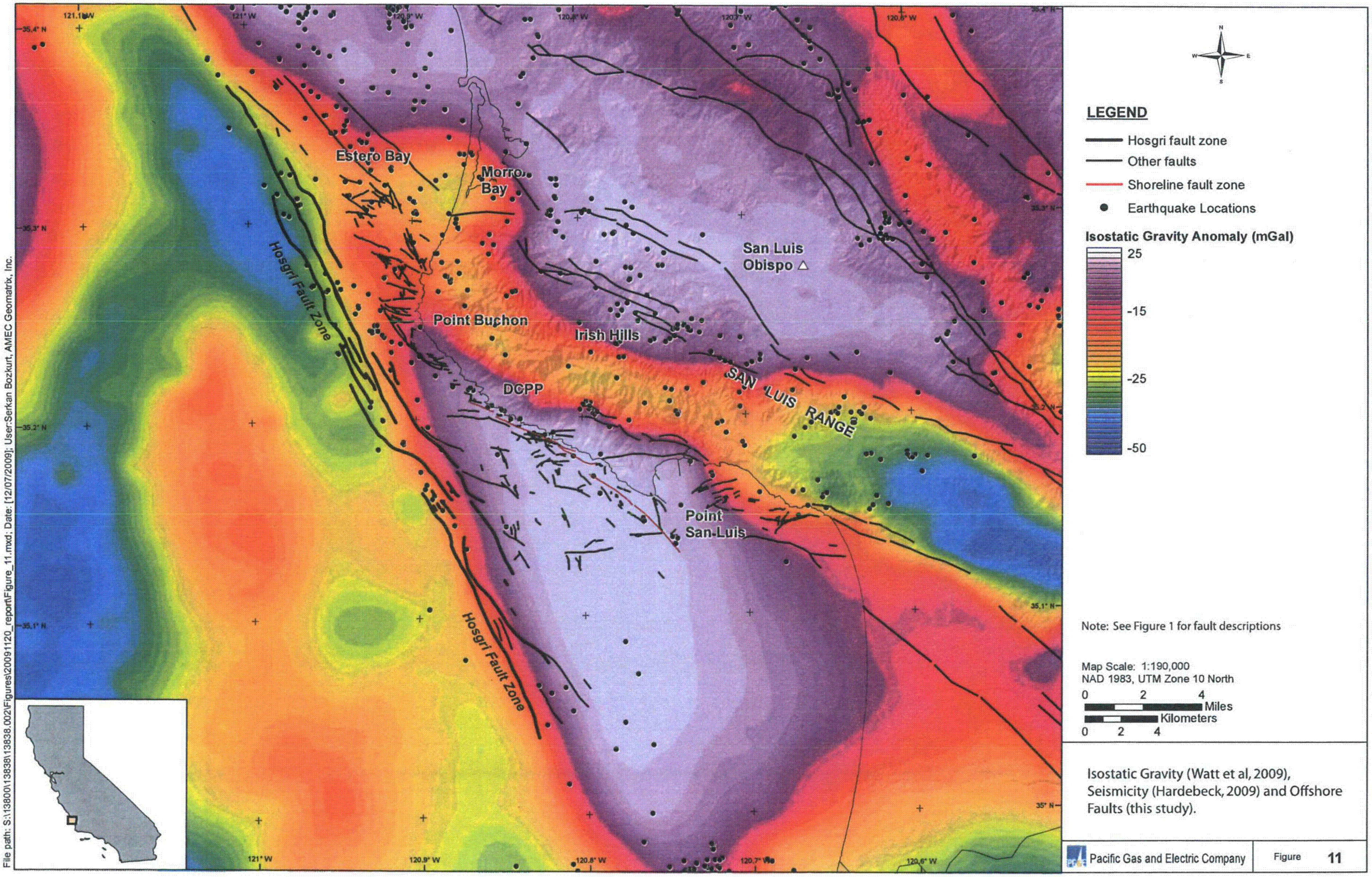

Isostatic Gravity (Watt et al, 2009), Seismicity (Hardebeck, 2009) and Offshore Faults (this study).

Pacific Gas and Electric Company | Figure 11

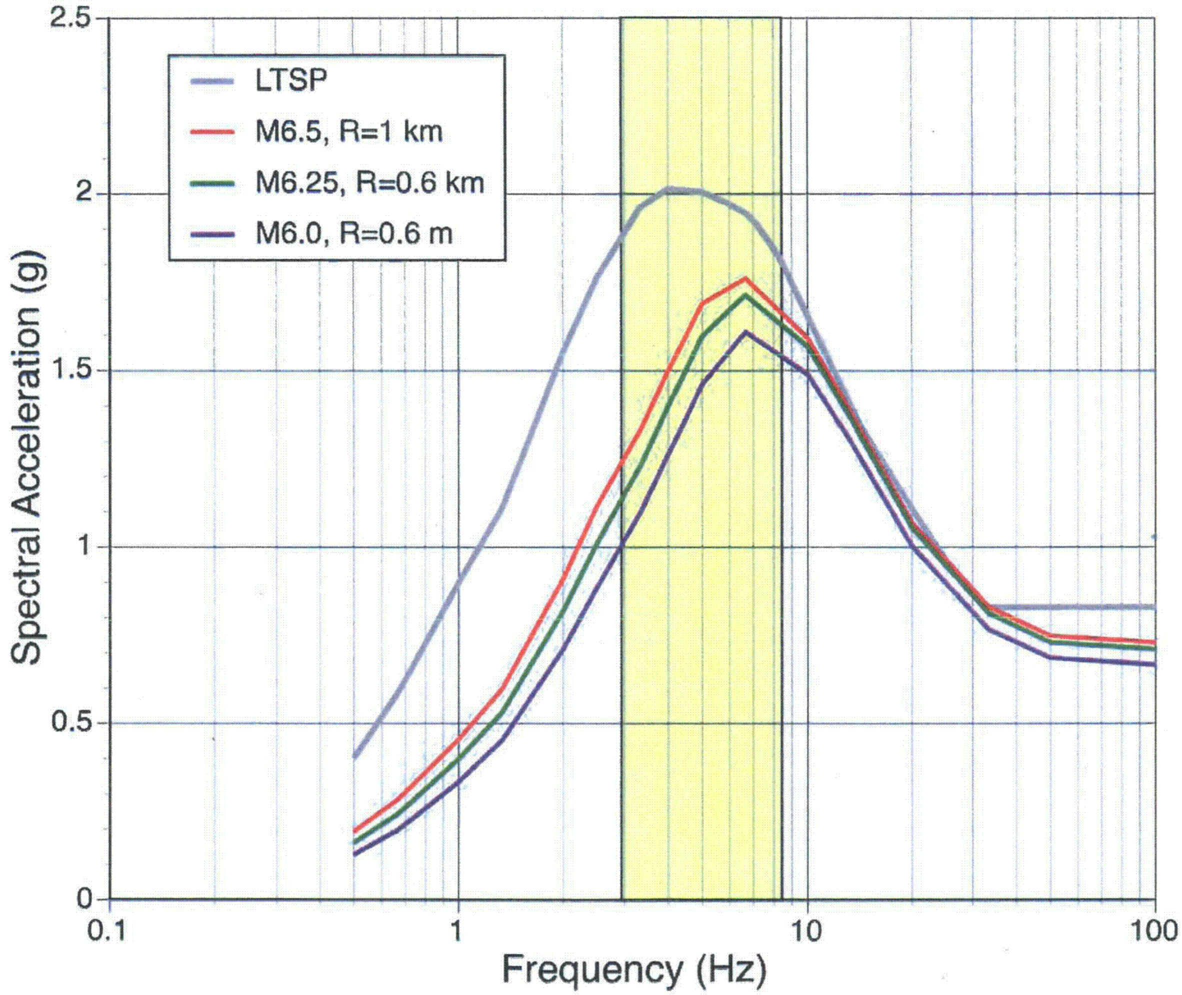

NOTE: The red curve shows the spectrum from a M6.5 earthquake at a distance of 1 km assumed in the 2008 evaluation. The green and purple curves show the spectra used the updated values for either the central segment (M6.0) or the central and southern segments together (M6.25) and with the shorter distance of 0.6 km.

Comparison of the 84th Percentile Ground Motion Spectra from the Shoreline fault zone with the LTSP Spectrum.

Pacific Gas and Electric Company | Figure 12

Appendix A-3

REVISED ACTION PLAN FOR THE STUDY OF THE SHORELINE FAULT

PG&E Geosciences Department

April 17, 2009

COVER LETTER

April 17, 2009

This Revised Action Plan for the study of the Shoreline Fault Zone is based on updated information and planning since the original Action Plan was submitted in December 2008.

Significant changes include

Geophysical Studies (GP)

- Tasks GP-2 and GP-4.

Tasks GP-2 and GP-4 were combined into one task - Task GP-2. Further evaluation of the airborne bathymetric LiDAR methodology to map the surf zone indicated that environmental conditions (water turbidity, wave action and kelp growth) would significantly interfere with the quality of the data collected. A side scan interferometric sonar technique was identified as a more promising alternative for mapping close to the shore line.

- Tasks GP-5 and GP-6

Tasks GP-5 and GP-6 were combined into a single task – GP-4. Both tasks addressed the need to conduct very high resolution studies of specific target areas identified by other geophysical mapping programs (e.g. multibeam, seismic, magnetics). These target area studies would be used to further constrain the style and rate of faulting for both the Hosgri and +Shoreline Fault Zones.

REVISED ACTION PLAN FOR THE STUDY OF THE SHORELINE FAULT ZONE

I. INTRODUCTION

Recent processing of seismic recordings from small earthquakes (1987-2007, magnitudes <1 to 3.5) using improved earthquake location computer programs shows an alignment of epicenters along the coast offshore, approximately one km from DCPP that is suggestive of a vertical strike-slip fault at depth (~3-11 km). The seismicity alignment has a length of 15 km. If it is extended to the intersection with the Hosgri fault, the length is 24 km. In addition to the seismicity data, raw (unprocessed) aero-magnetic and marine-magnetic data that were recently collected by the USGS show a magnetic anomaly with a trend that is consistent with the seismicity alignment. Although the geophysical survey results are preliminary, taken together, the available seismicity and geophysical data suggest that there is an active fault located offshore DCPP which we call the Shoreline fault.

Based on this preliminary data, PG&E estimated magnitudes of 6.25 and 6.5 for the Shoreline fault based on rupture lengths of 15 and 24 km, respectively, and an average rupture depth of 12 km. The potential ground motion at DCPP from these two events was evaluated and was found to be lower than the current design ground motions based on a larger earthquake on the more distant Hosgri fault.

The Action Plan below is designed to collect data and conduct analyses to better constrain the characteristics of the Shoreline fault and the potential ground motions at DCPP and ground deformation west of the power block. The Plan has three objectives. The first objective is to characterize the Shoreline fault in terms of its location, geometry, activity rate, rupture characteristics, and relation to the Hosgri fault zone. The second objective is to evaluate the ancient (Tertiary) shear zone west of the power block structure for evidence of secondary deformation that may have been associated with the Shoreline fault. The third objective is to estimate potential ground motions from the Shoreline fault, including both independent rupture of the Shoreline fault and possible synchronous rupture with the Hosgri fault.

This Action Plan describes the geology, seismology, geophysics, and ground motions studies to be performed over the next 2 years to achieve the above objectives. Results from these new studies will be integrated with results from the PG&E/USGS CRADA which is developing new regional tectonic models. An updated evaluation of the seismic hazard at DCPP will be conducted by PG&E Geosciences as part of the Long Term Seismic Program (LTSP) hazard update, which is scheduled to be completed in 2011. PG&E Geosciences and their consultants will perform the majority of the work; as part of the CRADA, the USGS will perform the balance of their marine magnetic survey and evaluate additional seismicity data in the region.

II. GEOLOGIC STUDIES (G)

Purpose: Locate, if possible, the surface expression of the Shoreline fault through geologic mapping and geophysical surveys (as described in Section IV). If located, then assess the last displacements for timing and amount of displacement. In addition, evaluate whether or not the shear zone has experienced secondary ground deformation related to the Shoreline fault. The shear zone is considered in this context as the shears in the shale unit of the Obispo Formation that crops out west of the power block.

Task G-1 Geologic mapping between Montana del Oro and Point San Luis

This Task will update existing knowledge of the geology along the coast between Montana del Oro and Point San Luis to provide the geologic framework for interpretation of the geologic setting of the Shoreline fault.

Subtask G-1A - Review and compile the 1988-1991 LTSP and other data concerning the geology of the coast, including diver geology cores, videos and notes.

Subtask G-1B – Map geologic contacts and faults along the coast; inspect the coast in detail for exposures of the Olson and Rattle Snake faults where recent erosion may have exposed them. Use the offshore geophysics information (Task GP-2) as a guide to where the Shoreline fault may come onshore and be exposed in the sea cliffs. This Subtask includes detailed geologic mapping to improve existing geological maps at the DCPP site, including mapping the wave-cut platforms in Diablo Cove and elsewhere.

Subtask G-1C - Use divers and/or remotely operated vehicles (ROV) to extend mapping offshore at sites identified by offshore geophysics (Task GP-2) and onshore mapping. This Subtask is focused on extending mapped geologic contacts and/or strata offshore to document fault offsets, if any.

Subtask G-1D - Profile selected streams that discharge from the Irish Hills to identify breaks in slope and channel offsets related to faulting. The multibeam bathymetry (Task GP-2) and other pertinent data from the offshore geophysics will be used in this analysis.

Task G-2 - Evaluation of secondary deformation in the Obispo Fm. shale unit This Task will improve the location of the shear zone as mapped for the ISFSI FSAR and will evaluate the amount of secondary ground deformation that may have been associated with earthquakes on the Shoreline fault.

Subtask G-2A - This Subtask will evaluate the potential for secondary deformation using the methodology of Peterson et al (2004) to calculate the probabilistic fault rupture hazard for strike-slip faults and will compare these results with geologic analogs.

Subtask G-2B - This Subtask will conduct detailed field investigations to improve the location of the shear zone and evaluate the amount of secondary deformation that may have been associated with the Shoreline fault. This Subtask has several elements:

a. Clean the cliffs at Diablo Cove to expose the 120,000-year-old wave-cut contact at top of rock over bedrock shears and faults in order to look for evidence of past secondary deformation.

b. Conduct local shallow seismic reflection surveys (and/or Ground Penetrating Radar) to improve the location of the shear zone and the depth of the wave-cut platforms in the area.

c. Based on the shallow seismic reflection data (from element b), drill borings to better define the depths of the wave-cut platforms, find the depths of colluvium and marine deposits over the wave-cut platform to help locate trench sites, and delineate the extent of the shear zone south of the plant where it is covered by colluvium.

d. Excavate trenches to measure the orientation of the shears and to confirm the location of the shear zone and evidence for recent deformation (or lack thereof) observed in the cleaned cliff exposures.

III. SEISMICITY STUDIES (S)

Purpose: Analyze and document the earthquakes that make up the seismicity alignment. Studies will include quantifying uncertainties of the hypocentral locations and focal mechanisms, and studying the depth distribution and activity rate.

Task S-1: Expand the time period covered by the data set used by the USGS in their analysis of the regional seismicity and determine the locations and focal mechanisms. This Task will add earthquakes that occurred from 1980 to 1987 and from Mar 2007 to Dec 2008 to the original data set and will estimate their location and focal mechanisms using the TomoDD and HASH computer programs. This work will be performed by the USGS as part of the CRADA.

Task S-2: Provide independent reviews of USGS data analyses described in Task S-1.

Task S-3: Analyze and document the expanded data set for the Shoreline fault. After completion of Tasks S-1 and S-2, this Task will address the following parameters:

a. Hypocentral and focal mechanism uncertainties

b. Differences between 1D, 3D, hypoDD and tomoDD locations

c. Temporal and spatial development of the lineament

d. Magnitude recurrence model for the Shoreline fault based on historical seismicity

Task S-4: Evaluate the feasibility of offshore seismic stations

This Task will evaluate the feasibility of installing ocean bottom seismometers (OBS) offshore from DCPP, west of the Hosgri fault zone to improve the accuracy of past and future earthquake locations and focal mechanisms in the offshore DCPP region. Earthquakes that occur offshore, outside the PG&E and USGS seismographic on-land networks, have inherent location errors, particularly depth errors. OBSs would improve the azimuthal coverage, resulting in more accurate locations.

IV. GEOPHYSICAL STUDIES (GP)

Purpose: Conduct additional offshore geophysical studies to improve characterization of the Shoreline fault and its relation to the Hosgri fault. High priority tasks will build on the marine work done by the USGS in 2008. These tasks include GP-1 (high resolution marine magnetics), GP- 2 (nearshore geophysics), and GP-3 (scoping study for a 3-D seismic survey). Supplemental tasks (GP-4 through GP-6) will be considered as collaborative opportunities present themselves or the need arises.

Task GP-1: High Resolution Marine Magnetics.

Subtask GP-1A: High Resolution Marine Magnetics Data Collection: This Subtask will complete the USGS marine field work that was delayed due to equipment malfunction in 2008.

Subtask GP-1B: Marine Magnetics Data Integration and Interpretation: This Subtask will provide support for the interpretation of the high resolution marine magnetic data and integration of these data with the regional aeromagnetic survey data.

Task GP-2: Multi beam Bathymetry

This Task will provide uniform, high-resolution bathymetric coverage from Montana del Oro to south of Point San Luis to define the extent and character of the Shoreline fault to support Task G-1. Shallow water depths necessitate the use of various geophysical techniques to complete this Task. Mapping wil extend from the shoreline (surf zone) west to the Hosgri fault zone

Task GP-3: 3-D Seismic Survey Scoping Study

This Task will develop a scope and cost estimate for conducting a 3-D Seismic Survey within approximately 5 km of DCPP. The scope of the survey will include both onshore and offshore seismic reflection and refraction from the offshore Hosgri to the onshore Los Osos fault zone. Part of this scope will include preliminary 2-D seismic surveys to optimize the later full scale 3-D seismic survey. This Task will also include support for PG&E consultants to familiarize themselves with the LTSP and USGS CRADA datasets to develop data collection strategies that will complement and leverage previously collected information.

Supplemental Geophysical Tasks (as needed)

Task GP-4: 2D High Resolution seismic survey and age dating

This Task would conduct additional high resolution seismic reflection studies and coring for age dating to augment already collected USGS marine data and to improve the resolution of marine structures in critical target areas as identified.

V. SOURCE CHARACTERIZATION OF THE SHORELINE FAULT

Purpose: Integrate of all the data from the G, S, and GP tasks and develop a set of alternative models for the characterization of the Shoreline fault in terms of its location, geometry, activity rate, rupture characteristics, and relation to the Hosgri fault zone

Task SC-1: Compile existing data on geology into a GIS data base

Create a GIS data-base for the coast and plant site that will include existing topographic maps, orthophotos, LiDAR, as well as LTSP and more recent geologic maps.

Task SC-2: Characterize the Shoreline fault

Using the GIS database, integrate the various data layers and interpret the results. Build alternative models of the location, geometry, activity rate, rupture characteristics of the Shoreline fault, and its relation to the Hosgri fault zone. Develop a logic tree structure and assign weights for the Shoreline fault characterization.

VI. GROUND MOTION STUDIES (GM)

Purpose: Evaluate the ground motions at DCPP for the case with synchronous rupture of the Hosgri and Shoreline faults using numerical simulation methods. Ground motions from independent ruptures of the Shoreline fault are adequately characterized by the existing models. These tasks will include defining the rupture characteristics for the case in which there is synchronous rupture on the Hosgri and Shoreline faults and computing the resulting ground motions at the DCPP site.

Task GM-1: This Task will use dynamic rupture models to evaluate the rupture characteristic for the generic problem of a vertical strike-slip fault with a splay fault.

Subtask GM-1A: Validate dynamic rupture models for a vertical strike-slip fault with a vertical splay fault.

The SCEC working group on dynamic rupture model code validation will add an additional validation case for a vertical strike-slip earthquake with a vertical splay fault. The working group will identify which dynamic rupture computer programs are applicable for this case.

Subtask GM-1B: Simulate a suite of ruptures on a vertical strike-slip fault with a vertical splay with a strike that is 30 degrees from the strike of the main fault.

Based on the results of Subtask GM-1A, two different computer programs will be selected and used to simulate the rupture characteristics (slip distribution, rise time, rupture velocity, and hypocenter location) for the main fault and the splay fault. This Task will also provide information on the relative rates of independent verses synchronous rupture of the main trace and the splay fault.

Subtask GM-1C: Develop kinematic source inputs.

The dynamic rupture sources from Subtask GM-1B will be converted to kinematic source models so that they can be used to simulate broadband ground motions (Task GM-2).

Task GM-2. Compute site-specific ground motions at the DCPP site using the generic kinematic sources developed in Subtask GM-1C.

The SCEC broadband simulation platform will be used to simulate the ground motions at the DCPP site from a suite of representative rupture scenarios that were developed in Subtask GM-1C.

Task GM-3. Parameterize the site-specific ground motions into a fault-specific attenuation relation for the synchronous rupture case.

The ground motion response spectra from the kinematic simulations (Task GM-2) will be parameterized into a set of attenuation equations and will be incorporated into the seismic hazard computer program.

VII. REPORT

The above results will be summarized in a report to be completed by 4th quarter 2010.

The report will address the issues investigated in this study:

- Characterization of the Shoreline fault in terms of its location, geometry, activity rate, rupture characteristics, and relation to the Hosgri fault zone.
- Evaluation of the ancient (Tertiary) shear zone west of the power block structure for evidence of secondary deformation that may have been associated with the Shoreline fault and estimate potential amount of ground deformation in the shear zone.
- Estimation of potential ground motions from the Shoreline fault, including both the independent rupture of the Shoreline fault and its synchronous rupture with the Hosgri fault.
- Summary of the feasibility studies of the Ocean-Bottom Seismometers and a 3-D seismic survey.